ISSN 1349-1113
JAXA-RR-08-007E

JAXA Research and Development Report

Experimental and Numerical Research on Boundary Layer Transition Analysis at Supersonic Speed: JAXA-ONERA cooperative research project

Kenji YOSHIDA, Hiroki SUGIURA, Yoshine UEDA, Hiroaki ISHIKAWA
Naoko TOKUGAWA, Takashi ATOBE, Shohei TAKAGI
Daniel ARNAL, Jean-Pierre ARCHAMBAUD and Alain SÉRAUDIE

March 2009

Japan Aerospace Exploration Agency

Contents

Experimental and Numerical Research on Boundary Layer Transition Analysis at Supersonic Speed: JAXA-ONERA cooperative research project*

Kenji YOSHIDA*1, Hiroki SUGIURA*2, Yoshine UEDA*1, Hiroaki ISHIKAWA*1, Naoko TOKUGAWA*1, Takashi ATOBE*2, Shohei TAKAGI*2, Daniel ARNAL*3, Jean-Pierre ARCHAMBAUD*3 and Alain SÉRAUDIE*3

Abstract

In the aerodynamic design of the National EXperimental Supersonic Transport (NEXST) program, a supersonic natural laminar flow (NLF) wing design concept was originally developed. Before the flight test of the NEXST-1 airplane, more detailed transition analysis should be performed in order to validate the NLF wing effect. Therefore, the JAXA-ONERA cooperative research project started in April 2000, because ONERA had great ability of analyzing transition phenomena and JAXA had some experimental transition data in supersonic flow. In the transition analysis on the sharp cone with a half angle of 5 degrees, the nose cone, and the NLF wing of the NEXST-1 airplane, good cross validation of both ONERA's and JAXA 's e^N codes was obtained. There was also high correlation between the experimental results in ONERA's continuous circuit-flow type supersonic wind tunnel and both laboratories' predictions under the assumption of a critical transition N value of 6. In addition, a risk of transition due to attachment-line contamination was predicted at inner wing, using the well-known Poll's criterion.

Keywords: boundary layer transition, supersonic flow, linear stability analysis, e^N method, natural laminar flow, transition measurement

1. Introduction

(1) Background

Drag reduction by delaying boundary layer transition is effective for improving the lift-to-drag ratio of next generation supersonic transport (SST) aircraft[1)] and thus remains an attractive measure for realizing an economically-viable SST. Achievement of laminar flow up to 60% of wing chord for a real size SST configuration has been estimated to produce a total-aircraft drag reduction of about 7% and its acoustic noise could also be reduced.

However, flowfield over supersonic aircraft is generally fully three-dimensional (3-D) and understanding of 3-D boundary layer transition mechanism is critical for delaying the transition. Moreover, compressibility adds further complexity to the problem. Adding to that, few experimental transition data exist for supersonic flow conditions and hardly any detailed transition results at flight condition has been published.

For these reasons, although many issues remain unsettled in incompressible 3-D boundary layer

* Received 16 February 2009（平成 21 年 2 月 16 日受付）
*1: Supersonic Transport Team, Aviation Program Group
（航空プログラムグループ　超音速機チーム）
*2: Fluid Dynamics Group, Aerospace Research and Development Directorate
（研究開発本部　流体グループ）
*3: Department of Aerodynamics and Energetics Modeling, ONERA /DMAE
（フランス航空宇宙研究所　空力／エネルギーモデル部）

transition, ONERA and JAXA started a cooperative research project on supersonic boundary layer transition, which are the most relevant to supersonic flight. The JAXA-ONERA research project, "Experimental and Numerical Research on Boundary Layer Transition Analysis at Supersonic Speed" inaugurated in April 17th, 2000 and lasted for seven years till March 31st in 2008.

(2) Motivations

ONERA has been tackling the subject of boundary layer transition prediction for long periods of time and has developed a number of effective transition prediction methods[2)]. One of the methods is an e^N method. The method consists of boundary layer stability computations and estimation of so-called N factor. The N factor is defined by the integration of amplification rates of small disturbances along a path where disturbances propagate. The amplification rates correspond to the eigenvalues of stability equations. The method is fully validated at both low and transonic speeds by means of comparing predictions with numerous experiments[2)]. Its validity at supersonic speed was sought after as the next target.

On the other hand, JAXA had been promoting the National EXperimental Supersonic Transport (NEXST) program from 1996 to 2006 in Japan[3), 39)]. JAXA had designed and developed an unmanned, scaled supersonic experimental airplane called NEXST-1 using an original CFD-based aerodynamic design method in the program. JAXA independently developed supersonic natural laminar flow (NLF) wing design concept and applied it to the NEXST-1 design[32)] (See Appendix A).

There were two features in the NLF wing design procedure. First, it involved stability analysis of 3-D boundary layer on highly-swept wings[4)]. Last, it centered on a CFD-based inverse-design methodology[5)] and one of the primary objectives of the program was to develop an effective inverse-design methodology.

The prediction of boundary layer transition is one of the most difficult problems in modern aerodynamics. The e^N method is regarded as the first choice for predicting transition location qualitatively. The SALLY code[6)], one of the most popular e^N codes, was used in the design phase of the NEXST-1 airplane[7-8)]. The SALLY code, however, was based on an incompressible stability theory. Apparently a compressible stability analysis is mandatory before the flight test. Thus, JAXA developed a compressible transition prediction tool[9)]. But it has not yet been sufficiently verified nor validated at supersonic speed[9)]. Moreover JAXA had already carried out a number of transition measurements in supersonic flow in order to validate the effect of the NLF wing design concept[10)].

(3) Objectives

Therefore, the present cooperative research project started in April 2000 under the framework of fundamental research activities in the NEXST program. The research project had two objectives. The first was to develop a reliable database of N values regarding boundary layer transition in supersonic flow. The last was to develop a reliable and effective transition prediction method useful and practical for aircraft designs.

(4) Approaches

In order to achieve those objectives, JAXA carried out boundary layer transition measurement experiments on several chosen configurations. ONERA and JAXA carried out transition analysis on the configurations and cross-verified their e^N codes. Then ONERA and JAXA tried to validate their codes through comparisons with the experimental data.

ONERA and JAXA tried to verify and validate their own respective stability analysis codes for cases of boundary layer in supersonic flow with increasing degree of complexity, from one of the simplest configurations with 2-D boundary layer to complex one with full 3-D boundary layer. Both laboratories also tried to verify their own respective attachment-line contamination (ALC) analysis methods for the case of the highly-swept wing at supersonic speed.

Three typical configurations were chosen for the boundary layer transition analyses in the cooperative research project. The first configuration was a sharp cone with a half angle of 5 degrees, called 5-degree half-angle sharp cone. It is one of the simplest configurations with two-dimensional (2-D) boundary layer at zero angle of attack (AOA) in supersonic flow, with a wealth of reliable experimental transition data already accumulated. The second configuration was a nose cone of the NEXST-1 airplane. It is also an axisymmetric body with 2-D boundary layer at zero AOA. It has a favorable pressure gradient but few reliable experimental transition data exists on the effect of pressure gradient. The third configuration was the natural laminar flow (NLF) wing of the NEXST-1 airplane. It has a complicated shape and the transition analysis of the wing involves a couple of issues that are a selection of an effective path for integrating amplification rates and an attachment-line contamination problem.

In order to perform a thorough comparison of the analytical results between ONERA and JAXA, a step-by-step approach was adopted in all the cases in order to sort out which part of the analytical procedure causes the difference in the results. As a starting point, both laboratories shared an identical pressure distribution around a configuration in each case. Then, derivatives of velocity and temperature boundary layer profiles, boundary layer thickness, integral path, and growth rate of disturbance with various frequencies were compared step-by-step and matched after investigating causes of any small difference at every step. If required, eigenvalue plots or propagation direction of disturbances with different frequencies were also compared and matched. Any kind of approximation or smoothing such as in the treatment of flow around leading edge or a bow shock was discussed thoroughly between the two laboratories before any of them was adopted.

(5) Schedule

From April 2000 till March 2002, ONERA and JAXA carried out the studies on the boundary layer transition of the 5-degree half-angle sharp cone and the NEXST-1 nose cones at zero AOA. During this period, we also studied the transition on the NEXST-1 NLF wing at ONERA-S2MA test condition. During the period of April 2002 -March 2005, we studied the transition on the NEXST-1 nose cone at nonzero AOA. The next period of April 2005- March 2008 was devoted for detailed comparisons of transition prediction with the NEXST-1 flight-test results. The present report was summarized during the period of March 2008 –February 2009.

(6) Research Plan

Table 1 shows a brief summary of our research plan.

Table 1. Research Plan

	Task	JAXA	ONERA
1	**10° Sharp cone** 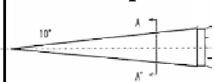	**[W/T test]** ①$x_{onset, end, Tr.}$, Transition map ②Condition: M=2.0, α=0, ≠0 **[Analysis]** ①Cp: Analytic, Euler, NS ②LBL: BL(α=0), NS(α≠0) ③ e^N: Linear (α=0, α≠0) ④Condition: W/T, Flight	**[Analysis]** ①e^N: Linear(α=0, ≠0) ②PSE (α=0) ③Condition: W/T, Flight
2	**Nose cone of NEXST-1** 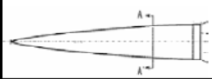		
3	**NLF wing of NEXST-1** 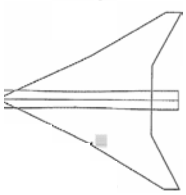	**[W/T test]** ①$(x/c)_{Tr.}$ @y/s, Transition map ②Condition: M=2.0, α-sweep **[Analysis]** ①Cp: NS(TBL, LBL, Exp.) ②LBL: BL, NS(α-sweep) ③e^N: Linear (α-sweep) ④Condition: W/T, Flight ⑤ALC: Poll method	**[Analysis]** ①LBL: 3-D BL code ② e^N: Linear (α_{Design}) ③Condition: W/T, Flight ④ALC: Poll method

(7) Members

The members of the cooperative research team are all of the authors of the present paper. The members from ONERA are: D. Arnal, J.-P. Archambaud and A. Séraudie. The members from JAXA are: K. Yoshida, H. Sugiura, Y. Ueda, H. Ishikawa, N. Tokugawa, T. Atobe and S. Takagi.

(8) Contents of the present paper

The objective of present paper is to summarize the results obtained in the cooperative research activity. The present paper particularly focused on the in-depth comparisons of stability analysis results carried out individually by ONERA and JAXA with different stability codes.

The present paper consists of three parts. The first part is a fundamental transition analysis on the 5-degree half-angle sharp cone. It describes cross-verification of both e^N codes and a validation through comparisons with transition measurement results. The second part is transition analyses on the NEXST-1 nose cone at both wind tunnel and flight test conditions. The third part is a transition analysis on the NEXST-1 NLF wing at both wind tunnel and flight test conditions. The third part also includes comparisons between the estimated and measured transition data in the flight test. The estimated transition characteristics on the NLF wing including the attachment-line contamination subject are summarized.

Finally, JAXA was renamed from National Aerospace Laboratory (NAL) in October, 2003 during the cooperative research project and therefore, JAXA is referred as NAL in some figures below.

2. Fundamental transition analysis on the 5-degree half-angle sharp cone

(1) Objectives

Since there is no streamwise pressure gradient on sharp cones at zero AOA, self-similar solutions exist for their laminar boundary layers that are able to be solved analytically. The accuracy of boundary layer stability analyses strongly depends on the accuracy of the calculated boundary layer velocity and temperature profiles. Thus, sharp cones that have analytical laminar boundary layer profiles are the most suitable for verifying the accuracy of stability analysis.

There are a number of wind tunnel and flight test data regarding boundary layer transition on sharp cones at supersonic speed, particularly for the sharp cone with a half angle of 5 degrees called "5-degree half-angle sharp cone", which makes it furthermore suitable for validations of the stability analyses. The transition data realizes a database regarding N values for boundary layer transition criteria, which is particularly useful for e^N methods. Numerous examples of wind tunnel and flight test data of the transition on the 5-degree half-angle sharp cone are summarized in Ref.11.

Thus, the 5-degree half-angle sharp cone was chosen as the subject for the first cross verification and validation study of transition prediction tools of ONERA and JAXA. The transition analysis was carried out at flight condition at Mach 2, unit Reynolds number of 9 millions, total temperature T_0=300K and total pressure P_0=73.58 kPa along an adiabatic wall, as one of the representative conditions.

(2) Laminar boundary layer profiles

In order to analyze transition characteristics, velocity and temperature profiles of the laminar boundary layer were estimated under the condition of a constant Mach number 1.941 along the cone surface. The Mach number was reduced from the freestream value of 2.0 according to the estimation using the conical shock theory. While ONERA adopted the analytical self-similar solution for the boundary layer profiles, JAXA calculated the profiles by solving the compressible laminar boundary layer equation using a finite difference method, called TUF code[12)] developed by Herring and Mellor. Here, δ is boundary layer thickness where the flow velocity reaches 99.8% of the freestream velocity; δ^* is displacement thickness and is defined as:

$$\delta^* = \int_0^\infty \left(1 - \frac{\rho u}{\rho_e u_e}\right) dy$$

Figure 1(a) shows a comparison of the calculated laminar boundary layer profiles between ONERA and JAXA (NAL). Here, y is a coordinate in the direction of boundary layer thickness and u means local velocity in the direction parallel to the surface of the cone within the boundary layer. Prandtl number (Pr) for ONERA's result is 0.72 and those for JAXA are 0.72 and 1.0. A comparison of JAXA's results between Pr=0.72 and Pr=1.0 shows that Prandtl number has nonnegligible effect on determining temperature profiles i.e. Prandtl number controls the recovery temperature at wall.

Figures 1(b) and 1(c) show comparisons of the derivatives of the velocity and temperature profiles, respectively. Both zero and first order derivatives exhibit very good agreement between ONERA's and JAXA's results qualitatively and quantitatively. Second order derivatives have fairly good agreement; their difference is assumed to be due to errors caused by numerical differentiation. As a whole, very good agreement was obtained for velocity and temperature profiles at the condition of Pr=0.72.

(3) Principal results of stability analysis

JAXA's e^N code called LSTAB is used throughout this paper. Its formulation is given in Ref. 9.

Figures 2(a) and 2(b) show N characteristic curves computed by ONERA and JAXA, respectively. Horizontal axes indicate Reynolds numbers based on displacement thickness. Each N curve corresponds to the streamwise integration of amplification rates of the small disturbance at constant physical frequency. Both laboratories applied the envelope strategy[2)] in estimating N factors. As for laminar boundary layer (LBL) profiles, while ONERA adopted the analytical solution, JAXA adopted the numerical solution.

As shown in the figures, ONERA and JAXA obtained a fairly good agreement, with less than 5% difference for the N curves. Dotted-dashed lines in the figures show that at $Re_{\delta *}$=3000 and f=29kHz, N is 4.5 for ONERA and 4.6 for JAXA while at $Re_{\delta *}$=5000 and f=15kHz, N is 9.6 for ONERA and 10.1 for JAXA. Accordingly, both laboratories' stability analysis methods based on boundary layer stability theory were confirmed to be mathematically equivalent although they have different details regarding their analytical methods.

(4) Comparison of N curves with JAXA's instability measurements

As a case for validation, JAXA compared the predicted unstable wave characteristics with experimental results[13)]. The experiment was conducted in JAXA's small supersonic wind tunnel (JAXA-SWT2, described in Ref. 14) under the conditions of Mach 2, P_0=55kPa, and low freestream turbulence level. Unstable wave characteristics were measured using a flush-mount unstable pressure transducer on a 330mm-long, 5-degree half-angle sharp cone model made of stainless steel SUS-303. (The static pressure fluctuation of the tunnel normalized by dynamic pressure is Cp_{rms}=0.1%.) One of the comparisons is shown in Figure 3. The experimental results are shown as sound pressure levels (SPL) at two different test conditions, namely, natural transition on smooth and rough surface conditions. On the other hand, the predicted result is shown as N values at several frequency conditions. Each vertical axis was adjusted for the purpose of the comparison. As shown in Figure 3, the predicted unstable wave characteristics are in fairly good agreement with those of the experiments, having less than 10% difference.

(5) Comparison of N curves with JAXA's transition location measurements

In the light of the fact that both laboratories' methods produced similar and valid results at Mach 2, JAXA concluded that JAXA's numerical methodology and prediction code were verified and validated for computations of the N characteristics of the cone also at the other flight Mach numbers than 2. Figure 4 shows two critical N values estimated by JAXA. Red circles correspond to the onset of transition and blue squares correspond to the end of transition. The N factors are estimated by comparing the predicted N characteristics with the transition Reynolds numbers based on the actual flight test data[11)]. The actual flight conditions

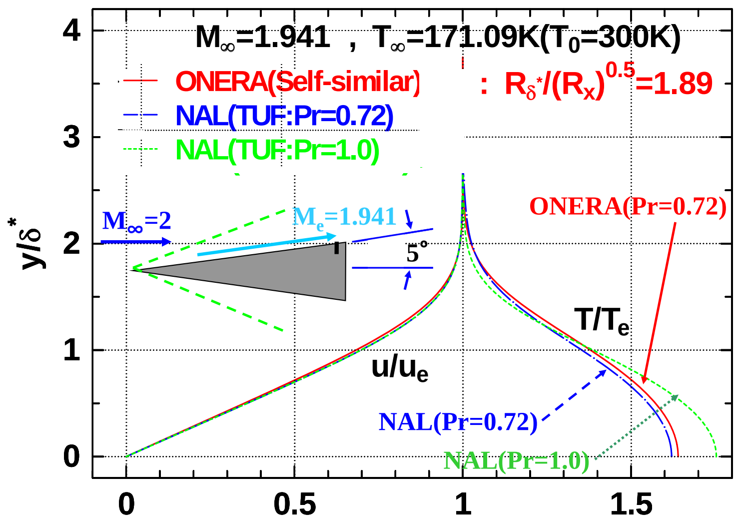

(a) Velocity & Temperature profiles
Figure 1. Laminar boundary layer profiles on 5-degree half-angle sharp cone

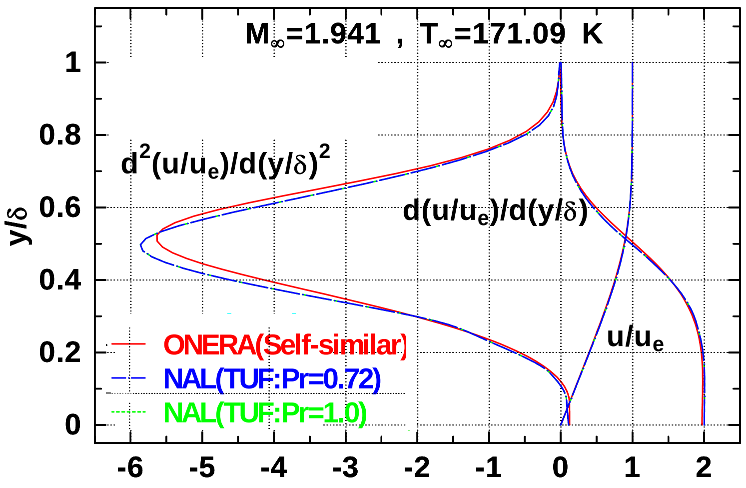

(b) Derivatives of velocity profile
Figure 1. Laminar boundary layer profiles on 5-degree half-angle sharp cone

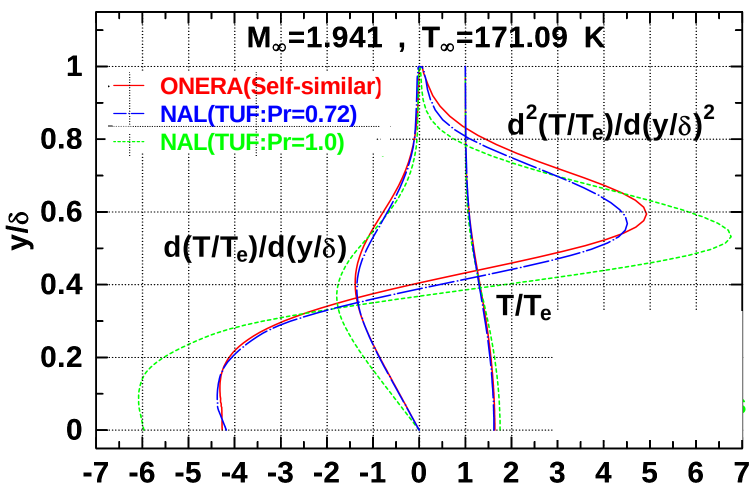

(c) Derivatives of temperature profile
Figure 1. Laminar boundary layer profiles on 5-degree half-angle sharp cone

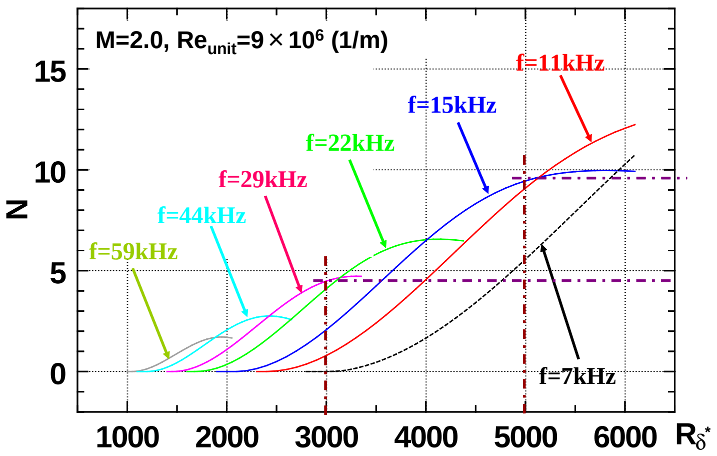

(a) ONERA's computations

Figure 2. Comparison of estimated N-factors on 5-degree half-angle sharp cone

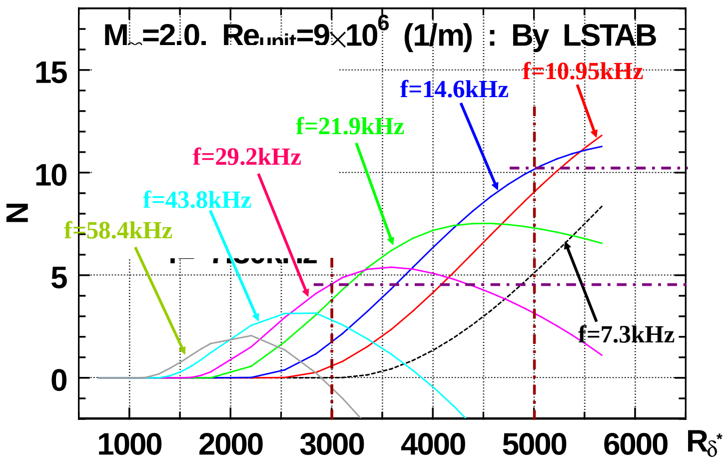

(b) NAL's computations

Figure 2. Comparison of estimated N-factors on 5-degree half-angle sharp cone

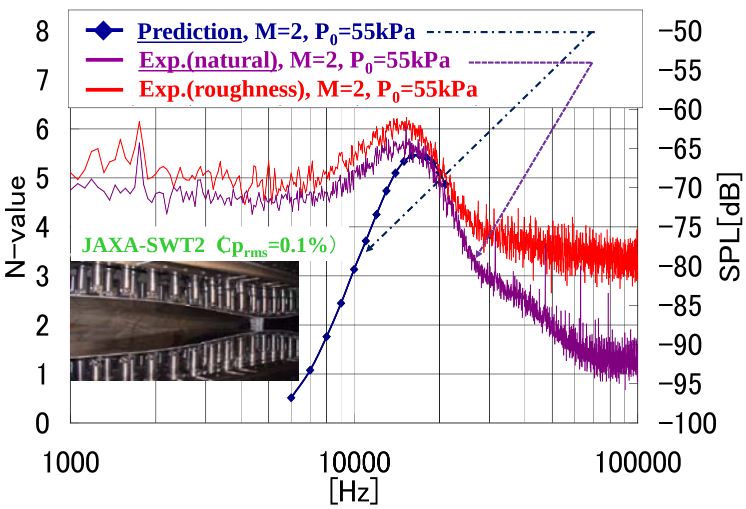

Figure 3. Unstable wave characteristics on 5-degree half-angle sharp cone

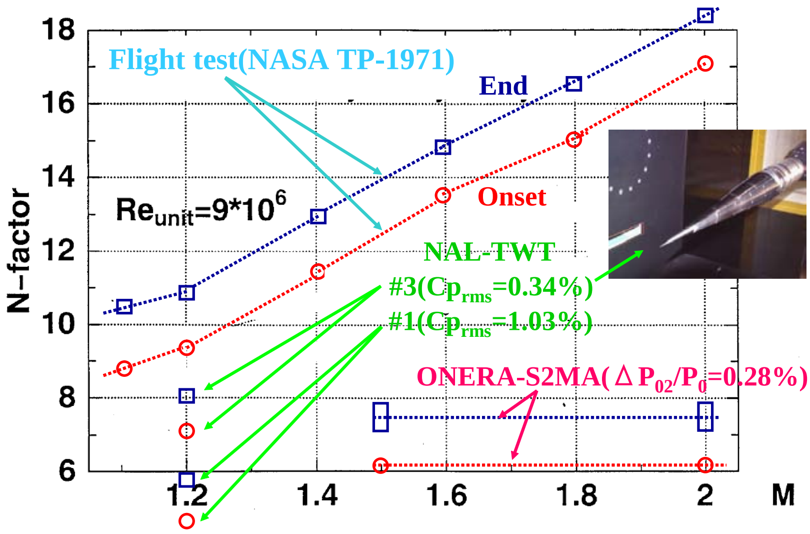

Figure 4. Transition N-criterion on 5-degree half-angle sharp cone, based on JAXA's e^N code except the ONERA-S2MA case

were measured under an extremely small freestream turbulence level. The N curves serve as useful criteria to predict natural onset and end of transition at flight test conditions.

In addition, ONERA and JAXA possess some wind tunnel test data on the 5-degree half-angle sharp cone. ONERA has independently found the onset of transition N value of about 6 in the continuous circuit-flow type supersonic wind tunnel in Modane (ONERA-S2MA), by comparing predicted N characteristics with measured transition locations. Transition was detected using infra-red thermography. The transition-onset N value in S2MA calculated by JAXA was in strict correspondence with the ONERA's value of N=6. Thus, the N value corresponding to the transition onset was concluded to be N=6.

JAXA independently carried out transition measurements at Mach 1.2 using JAXA's continuous circuit-flow type transonic wind tunnel (JAXA-TWT1). The tunnel has two different test sections (#1 and #3) each with different freestream turbulence level. The #1 test section has perforated walls and thus has a relatively high freestream turbulence level of Cp_{rms}=1.03%. The #3 test section has slotted walls and thus has a relatively low freestream turbulence level of Cp_{rms}=0.34%. Transition locations were measured using Preston tube technique. By comparing the predicted and measured results at the #3 section condition, JAXA independently found that N=7 and 8 correspond to the onset and end of transition, respectively, in the #3 test section as shown in Figure 4.

Therefore, the Figure 4 constitutes a database of transition criterion for axisymmetric bodies in supersonic flow, both in flight and in W/T conditions.

(6) Summary

The present study on the 5-degree half-angle sharp cone confirmed that both transition prediction tools of ONERA and JAXA yielded nearly identical results and their unstable wave characteristics also showed good agreements with experimental results.

3. Transition analysis on NEXST-1 nose cone

ONERA and JAXA investigated transition characteristics of the nose cone of the NEXST-1 airplane in detail because the configuration was chosen as a standard model to study the relation between the transition Reynolds number and freestream turbulence level. The NEXST-1 nose cone was designed by applying the forward part of a Sears-Haack (S-H) body to a straight fuselage in order to reduce wave drag due to volume of the NEXST-1; the S-H body is defined to have minimum wave drag caused by volume at zero

AOA under the slender body theory. It is described by the following expression:

$$r = A\left[\frac{x}{l}\left(1-\frac{x}{l}\right)\right]^{\frac{3}{4}} \quad , \quad 0 \le x \le l_w \qquad (1)$$

When x and r are expressed in meters, $l = 11.5$, $l_w = 2.9$ and $A = 0.92942$. The S-H body serves as a guideline reference for designing fuselages of supersonic aircraft[7, 32].

3.1. Analysis at zero angle of attack condition

3.1.1. Analysis at S2MA test condition

(1) Estimation of Cp distribution

In order to calculate laminar boundary layer (LBL) characteristics of the NEXST-1 nose cone, since there is no such analytical solution as for the 5-degree half-angle sharp cone, JAXA solved it numerically. ONERA and JAXA used the same Cp distribution calculated by JAXA. Since the code required input of pressure distributions of the flowfield, JAXA used JAXA's axisymmetric Euler code (described in Ref. 15) in order to calculate the surface pressure distribution on the nose.

Figure 5(a) shows calculated pressure distribution in the vicinity of the apex of the NEXST-1 nose cone. Here x is a coordinate of the axis of the NEXST-1 nose cone and l is defined in equation (1). The figure shows that there is a typical pressure rise due to a slightly detached shock wave in front of the apex. Particularly, the pressure distribution calculated at M=1.2 condition as a reference brings out the influence of the detached shock wave. In the actual flow, after the rapid pressure rise due to a shock in the vicinity of the apex, the pressure decreases monotonically (i.e. the flow accelerated) from the maximum value

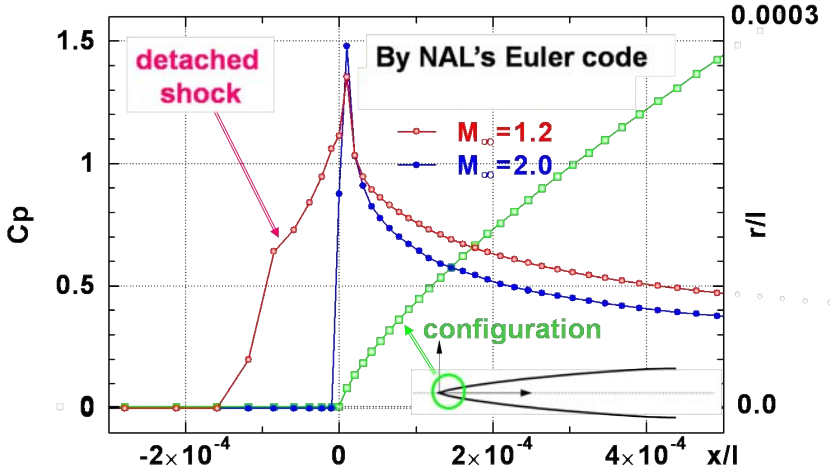

(a) Euler solution
Figure 5. Cp distributions near the NEXST-1 nose cone

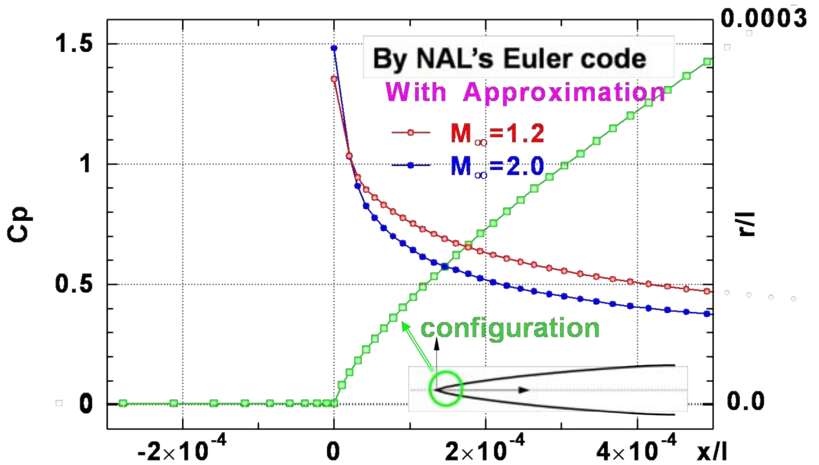

(b) Approximation of neglecting detached shock
Figure 5. Cp distributions near the NEXST-1 nose cone

at the apex. However, in the figure, the next node to the apex (x=0) instead of the apex shows the highest pressure rise. This is because by the use of a difference scheme the rapid pressure rise was smeared out to adjacent nodes.

It is impossible to treat such rapid pressure rise when calculating boundary layer profiles. Thus, we skipped the next node to the apex in the calculated pressure distribution and replaced with the apex. In the resulting approximate pressure distribution shown in Figure 5(b), the pressure decreases monotonically from the maximum value at the apex.

(2) Laminar boundary layer calculation

Mach- and Reynolds-number conditions are required for boundary layer calculation. Freestream characteristics downstream of a detached shock change discontinuously from those upstream according to normal shock wave relation. Thus, it is, first of all, important to specify the upstream conditions carefully, taking account of the influence of the detached shock wave.

Figure 6 shows flow conditions before and after the detached shock. Both freestream Mach number and total pressure decrease after the shock wave, and the unit Reynolds number based on the freestream condition decreases as a result.

Both ONERA and JAXA calculated laminar boundary layer characteristics assuming adiabatic wall and using the approximated pressure distributions and those upstream conditions. JAXA applied the TUF code[12] that was validated for the 5-degree half-angle sharp cone. ONERA applied its in-house boundary layer code called 3C3D. Figures 7(a) and 7(b) show displacement thickness and Reynolds number distributions based on them, respectively. Both distributions by ONERA and NAL (JAXA) agree very well. Here X is a coordinate along the body axis of the NEXST-1 nose cone, and L is 11.5 m which is the body length of the NEXST-1 airplane. The nose part was defined by the part of the fuselage from 0 to 2.99 m from the apex where the diameter of the fuselage is maximum. Therefore, the end of the nose part is expressed by X/L=0.26.

Figure 7(c) shows a comparison of incompressible shape factor distributions. The distributions by ONERA and NAL (JAXA) agree fairly well. Small difference of the magnitude is possibly due to the difference in definitions of the edge of boundary layers. JAXA assumed boundary layer edge as a position where local velocity within the boundary layer reached 99.8% of the maximum velocity. ONERA used a generally-used value of about 99.5% which was automatically defined in the 3C3D code.

Figure 7(d) shows calculated velocity profiles of

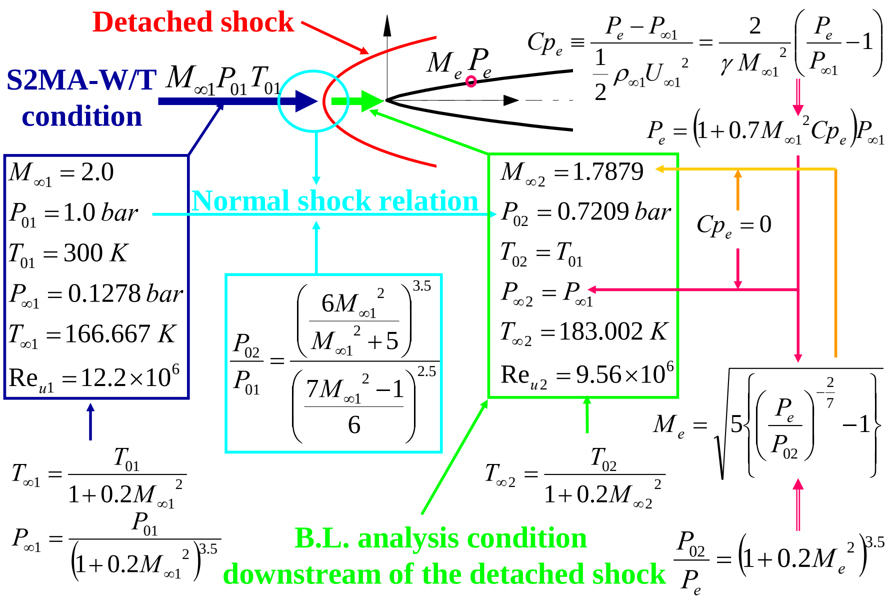

Figure 6. Approximated analysis condition on laminar boundary layer profiles at zero angle of attack

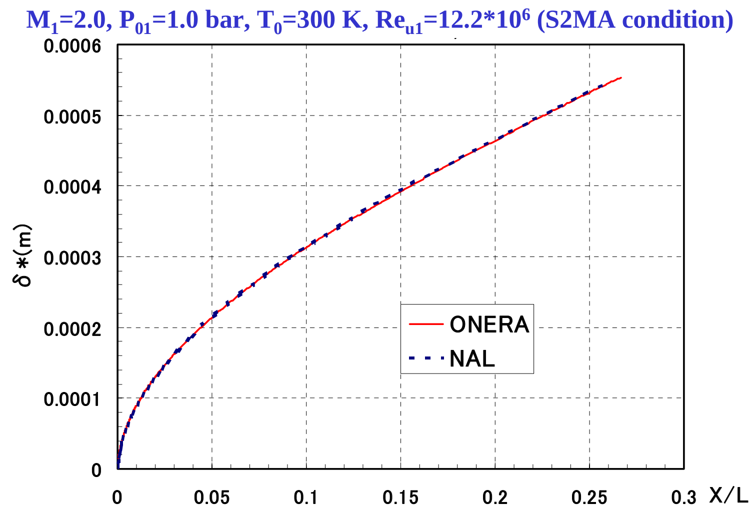

(a) Displacement thickness distribution
Figure 7. Estimated B.L. characteristics at zero angle of attack

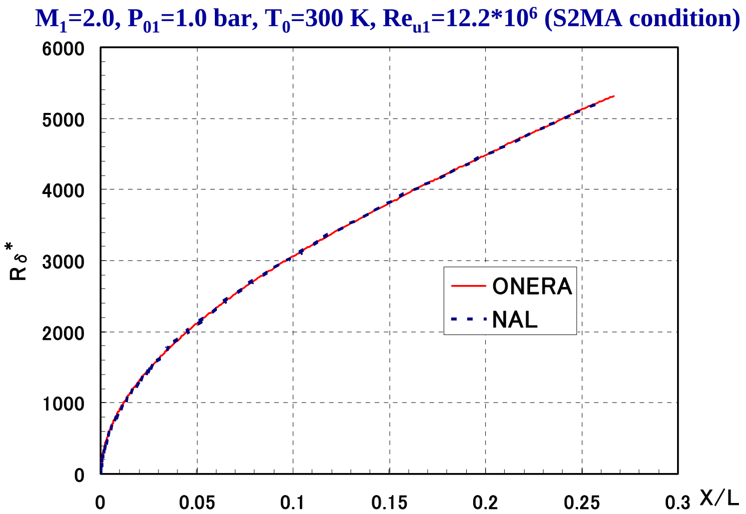

(b) Reynolds number based on displacement thickness
Figure 7. Estimated B.L. characteristics at zero angle of attack

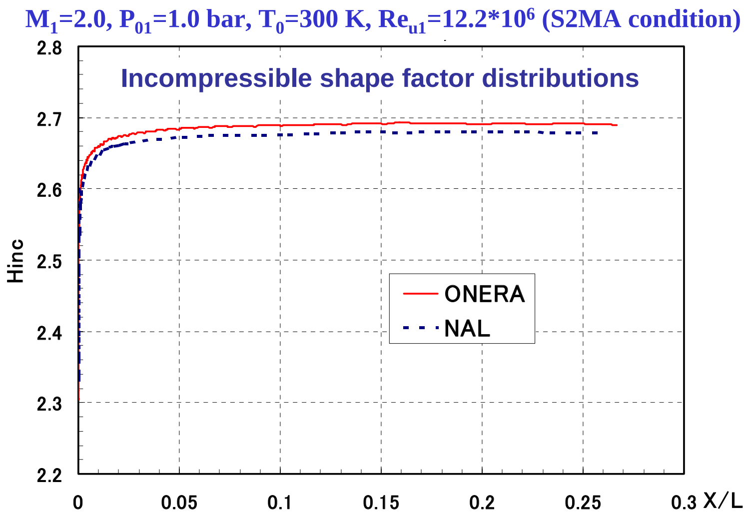

(c) Incompressible shape factor distribution
Figure 7. Estimated B.L. characteristics at zero angle of attack

the boundary layer by ONERA and NAL (JAXA). Both zero and first order derivatives are in very good agreement qualitatively and quantitatively. There are some differences in second order derivatives. This is because the second order derivatives are very sensitive to the precision and number of grid points in the boundary layer. It was very difficult for us to eliminate this difference. In order to cross verify both transition analysis methods of ONERA and JAXA, we decided that it was important to know the overall difference between the methods including the difference in the boundary layer profiles. Thus, ONERA and JAXA each calculated stability characteristics based on one's respective boundary layer profiles. Figure 7(e) shows calculated temperature profiles by ONERA and NAL (JAXA), which also agree well.

Figure 7(f) shows generalized inflection points (GIP) of compressible laminar boundary layer profile. Although there are a few differences in the profiles of d(du/dy/T)/dy (probably due to the difference in the second derivatives of the velocity and temperature profiles described in the previous paragraph), the locations of GIP (i.e. the heights in the boundary layer) agree very well. This good agreement imply that the above difference in the second derivatives of the profiles creates little difference in the stability analysis results, considering that GIP location is strongly related to the boundary layer instability .

(3) Stability analysis and comparison with transition measurements

Figures 8(a) and 8(b) show N characteristic curves computed by ONERA and JAXA, respectively, at the ONERA-S2MA test condition of Mach 2. Horizontal axes indicate nondimensionalized chordwise lengths. Red lines are the envelope curves of all the N curves.

There is very good agreement between both N characteristics calculated by both laboratories. An N=6 line is shown as a dotted line in each figure as a reference. N=6 corresponds to the transition onset criterion independently estimated by ONERA by means of comparing the calculated N characteristics with the transition measurement on the 5-degree half-angle sharp cone. The estimated chordwise onset locations using the N=6 criterion in both computations agree very well.

Onset and peak locations shown in the figures were estimated from transition measurement by JAXA on the wind-tunnel model of the NEXST-1 nose cone with a 23.3% scale of the NEXST-1 airplane at M=2.0 in the continuous circuit-flow type supersonic wind tunnel, ONERA-S2MA. The transition locations were detected using hot-film (HF) sensors. The test model has a NEXST-1 wing-body configuration with 4 HF sensors in its nose part. The onset and peak locations in the figures were determined as follows: a) JAXA measured HF signals during total pressure (P_0) sweep; b) HF signal data show a curve rising from the laminar to the turbulent value with an intermediate peak; c) this curve was approximately fitted by a quadratic function, as shown in Figure C-1 of Appendix C.; d) both peak and onset locations were determined using an approximate curve of least squares, as shown in Figure C-2 of Appendix C. It has been established by Owen[16)] that the peak location coincides with the maximum surface-temperature location and the maximum burst-frequency location, i.e. with the middle of the transition region.

As a result, the transition onset on the nose corresponds to N=4.5 and is quite different from the N=6 criterion for the transition onset on 5-degree half-angle sharp cone. Since the NEXST-1 nose cone has a favorable pressure gradient i.e. accelerating flow and a continuous change in surface curvature, this may imply that the difference in the N values is due to either pressure gradient, streamwise curvature, or due to a different receptivity of surface roughness or freestream turbulence.

(4) PSE computation: N curves

To clarify that point, ONERA carried out more elaborate stability analysis using parabolic stability equations (PSE). PSE includes streamwise curvature and non-parallelism terms which the classical (i.e. parallel) e^N method lacks. Here ONERA also used an e^N method called “fixed beta method”. The method is different from the

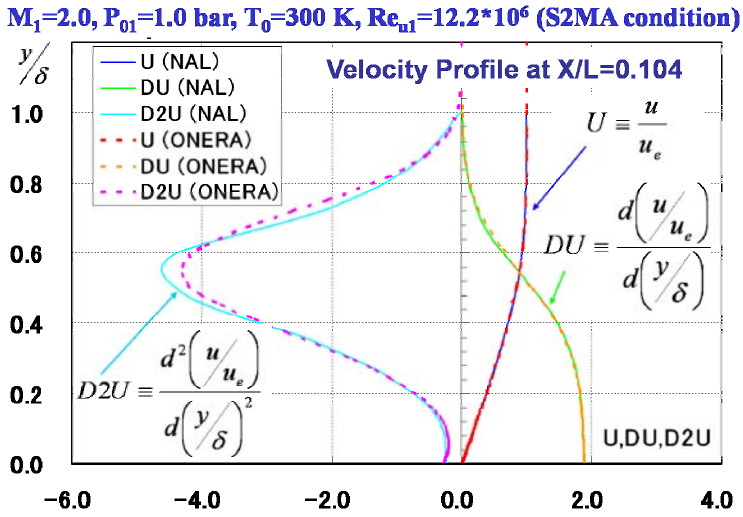

(d) Velocity profiles

Figure 7. Estimated B.L. characteristics at zero angle of attack

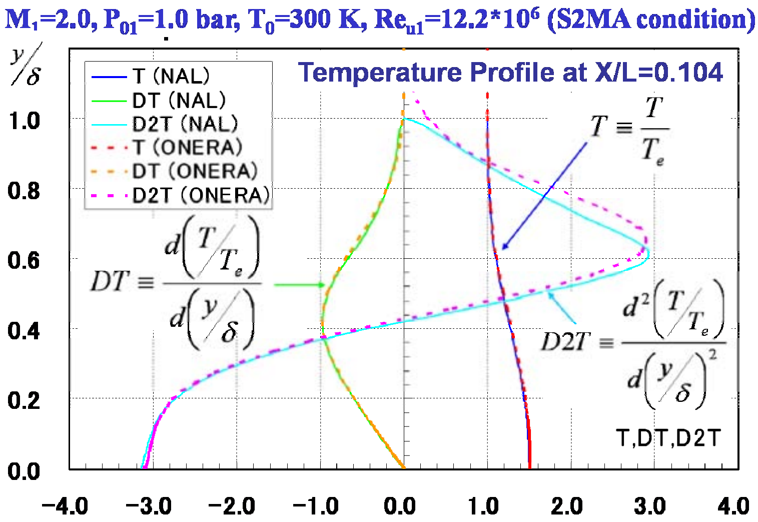

(e) Temperature profiles

Figure 7. Estimated B.L. characteristics at zero angle of attack

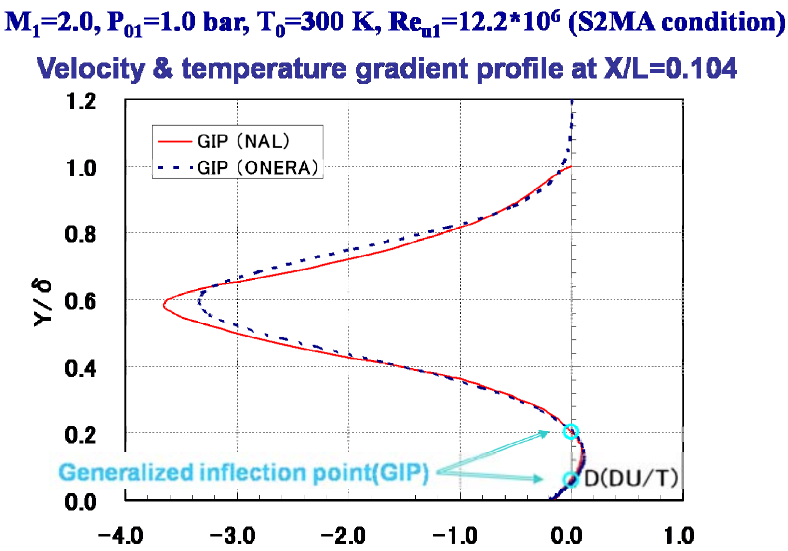

(f) Generalized inflection point

Figure 7. Estimated B.L. characteristics at zero angle of attack

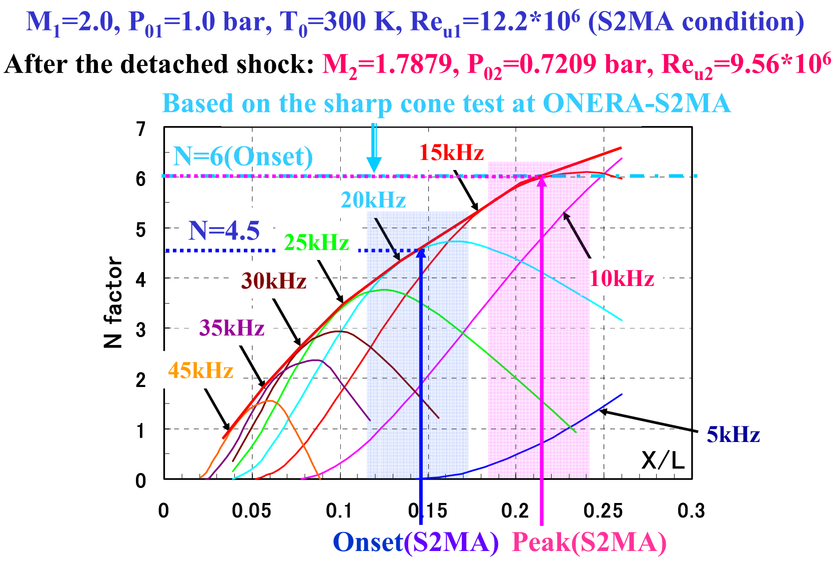

(a) NAL's computation

Figure 8. N-factors of NEXST-1 nose cone at M=2.0 & $\alpha=0^{\circ}$

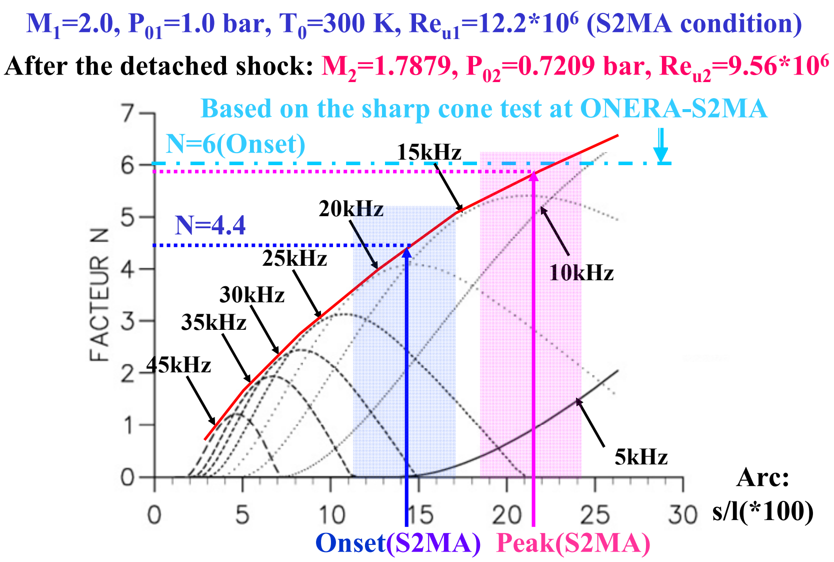

(b) ONERA's computation: Fixed Beta Method

Figure 8. N-factors of NEXST-1 nose cone at M=2.0 & $\alpha=0^{\circ}$

envelope method in that the propagation direction $\psi \equiv \tan^{-1}[\alpha_r/\beta_r]$ of disturbance is fixed in the method. The use of the fixed beta method clarifies the effect of the propagation direction on the growth of the most unstable mode. ONERA have recently applied the method to fully 3-D flows with a view to understand the physics of transition mechanism. But in the cases when the propagation direction selected in the envelope method is constant, β_r is constant along the streamline and the two methods yield same results. The same thing occurs in the present case of the nose cone at zero angle of attack and also in other 2-D flow cases. Therefore, in the present case, the PSE results were compared with the results using the fixed beta method instead of ones using the envelope method.

The PSE method includes the influence of upstream region of the body both in the calculations of disturbance growth rates and boundary layer profiles while the classical e^N method includes the influence just in boundary layer profile calculation. Figure 9 shows a comparison between the fixed beta method and PSE computations by ONERA. Figure 9 shows that the N factors are increased by using PSE method instead of the fixed beta method. Compared to the transition measurement results in S2MA, the transition onset location corresponds to N=5.8, which is very close to N=6. This suggests that at least consistency is retained by using PSE in both cases for the NEXST-1 nose cone and the 5-degree half-angle sharp cone. This may imply that the lack of either the curvature and non-parallelism effects or the influence of the upstream region of the body in the calculation of disturbance growth rate explains the N-value discrepancy in the e^N method calculations. However, a certain amount of errors exist in the present e^N method of transition location determination in the S2MA experimental data and further investigation is required for its justification.

3.1.2. Analysis at NEXST-1 flight test condition

ONERA and JAXA conducted similar stability analyses as the previous S2MA test case at the NEXST-1 flight test condition. The freestream conditions at flight altitude of 15km are estimated in the same manner as for the S2MA case and are summarized in Figure 10. Results are shown below.

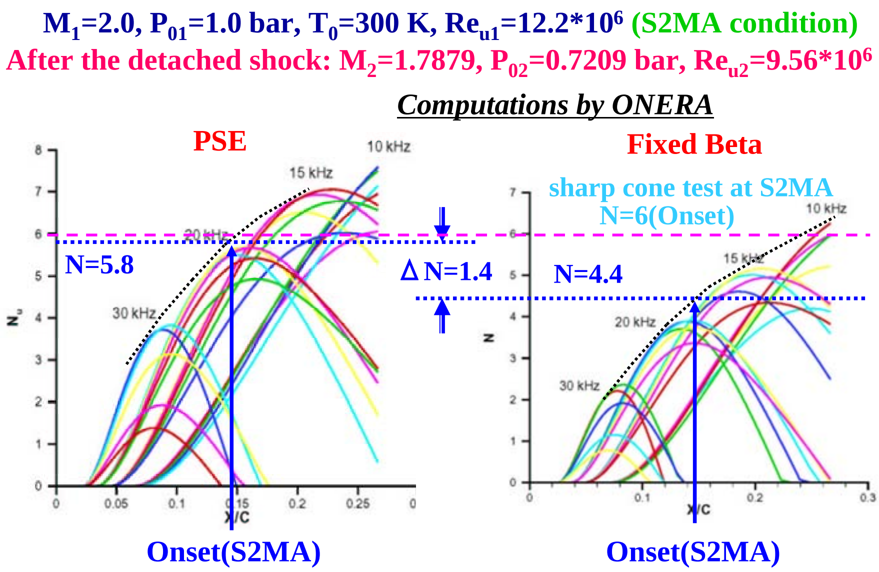

Figure 9. Comparison of N-factors by fixed beta method & PSE

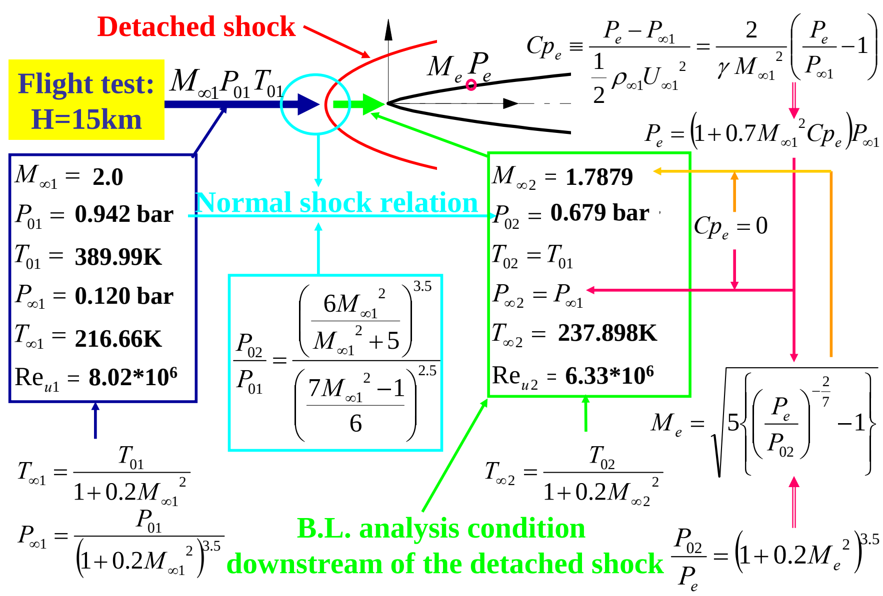

Figure 10. Boundary layer analysis condition at zero angle of attack in flight test

(1) Stability analysis: N curves

As shown in Figure 11, very good agreement between both N characteristics computed by both laboratories was confirmed also at the flight test condition.

(2) PSE computation: N curves

As shown in Figure 12, PSE computation showed similarly larger N values as in the previous case. These data constitute a database for future comparisons with the flight test results.

3.2. Analysis at nonzero angle of attack

The gap between relatively simple 2-D boundary layer transition and very complex fully 3-D one is very large. Thus, to bridge this gap, ONERA and JAXA compared their analysis results on the axisymmetric NEXST-1 nose cone with small angle of attack. Throughout this section, all the calculations and measurements were carried out at AOA of 2 degrees.

3.2.1. Analysis at S2MA test condition

(1) Estimation of flowfield

The NEXST-1 nose cone at nonzero AOA has

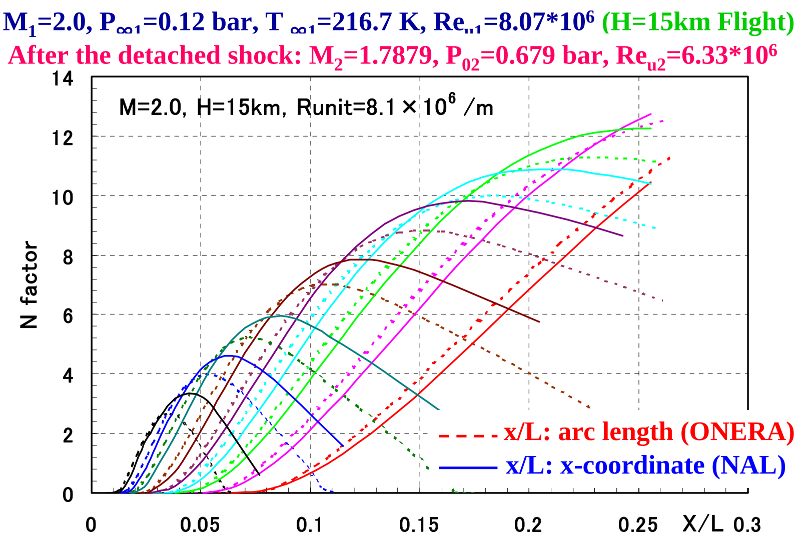

Figure 11. N-factors of NEXST-1 nose cone in flight test

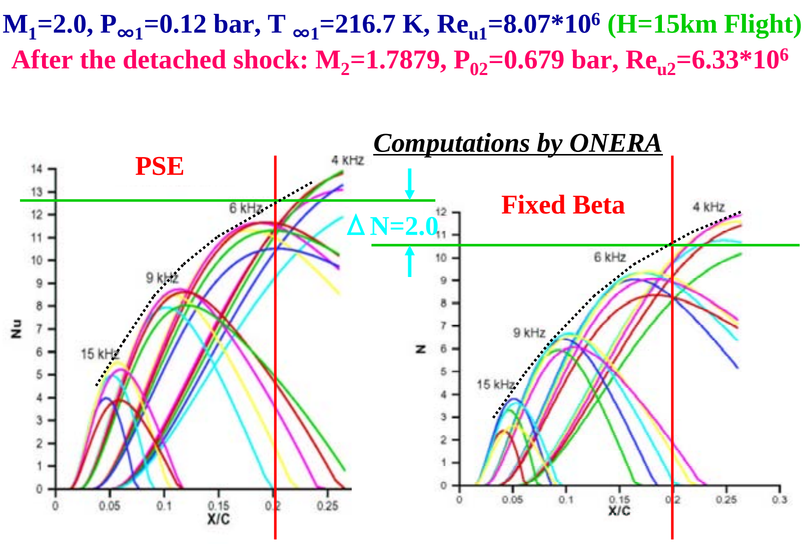

Figure 12. Comparison of N-factors by fixed beta method & PSE

complex flowfield. The flowfield and the boundary layer become fully three-dimensional. Thus, JAXA figured that it is more efficient to solve both flowfield and the laminar boundary layer profiles at the same time rather than solving them separately. Accordingly, JAXA tried to calculate them using a Navier-Stokes (NS) code at full laminar conditions.

JAXA used the 3-D NS code called UPACS independently developed by JAXA. In order to precisely estimate the pressure distributions, at least 70 grid points were placed in boundary layers, which were about three times as many as in usual cases[37]. As for convergence tests of the solutions, while one usually focuses attention on the time history of either pressure or force, JAXA focused on wall temperature that changed slowest. JAXA set the convergence time three times as long as the usual cases and calculated until boundary layer temperature profiles were converged. On the other hand, ONERA calculated boundary layer profile using ONERA's boundary layer code 3C3D from the pressure distribution computed by JAXA.

Figure 13(a) shows fine pressure distribution near the apex of the NEXST-1 nose cone calculated using the UPACS (NS) code. Here, X is a coordinate along the body axis of the NEXST-1

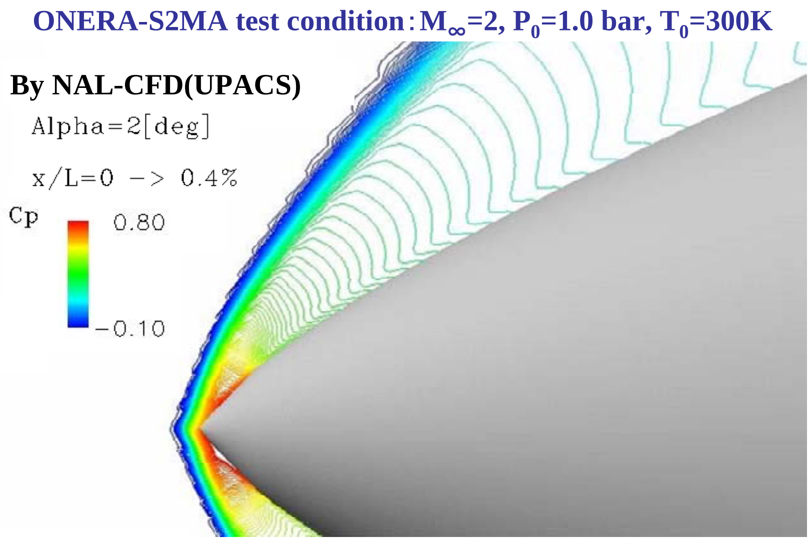

(a) Cp contours near nose
Figure 13. NS analysis of NEXST-1 nose cone at M=2.0, $\alpha=2^\circ$

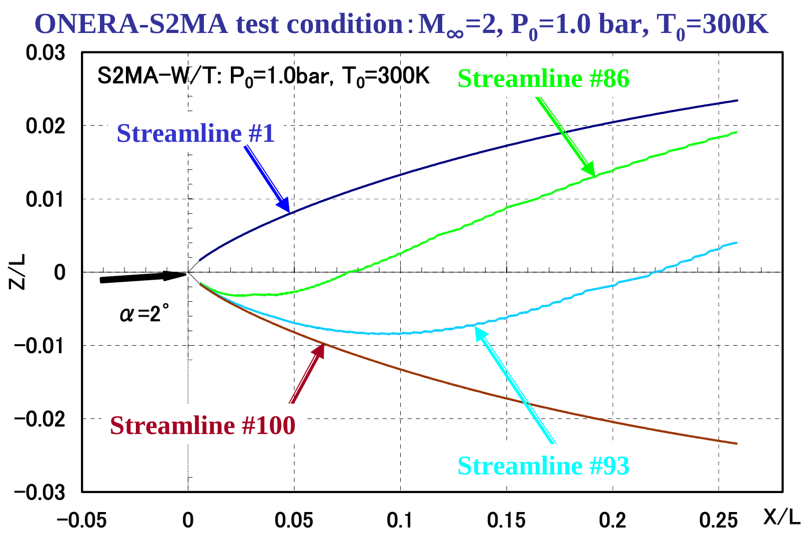

(b) External Streamlines
Figure 13. NS analysis of NEXST-1 nose cone at M=2.0, $\alpha=2^\circ$

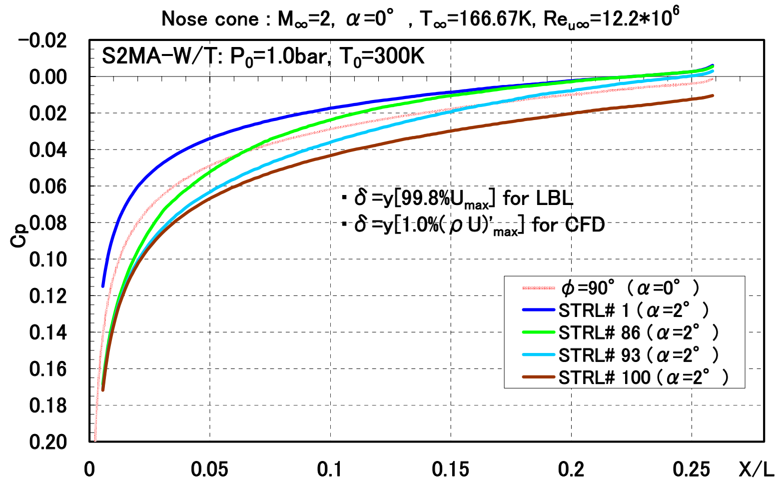

(c) Cp distributions

Figure 13. NS analysis of NEXST-1 nose cone at M=2.0, $\alpha=2^{\circ}$

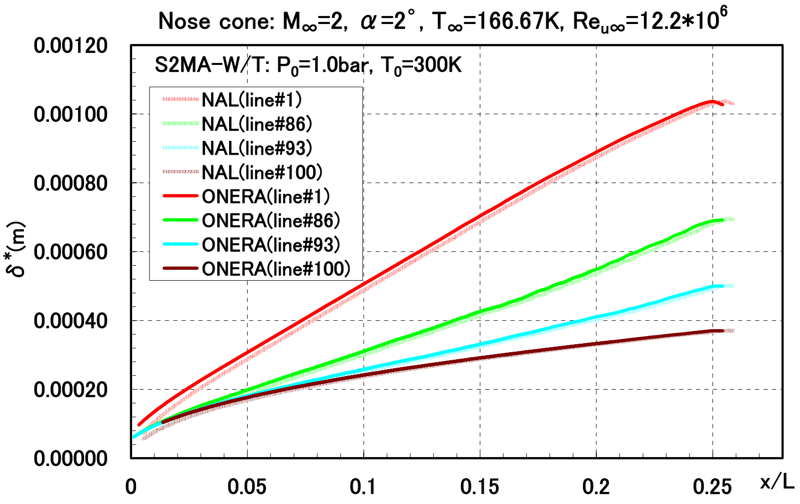

(d) Displacement thickness distributions

Figure 13. NS analysis of NEXST-1 nose cone at M=2.0, $\alpha=2^{\circ}$

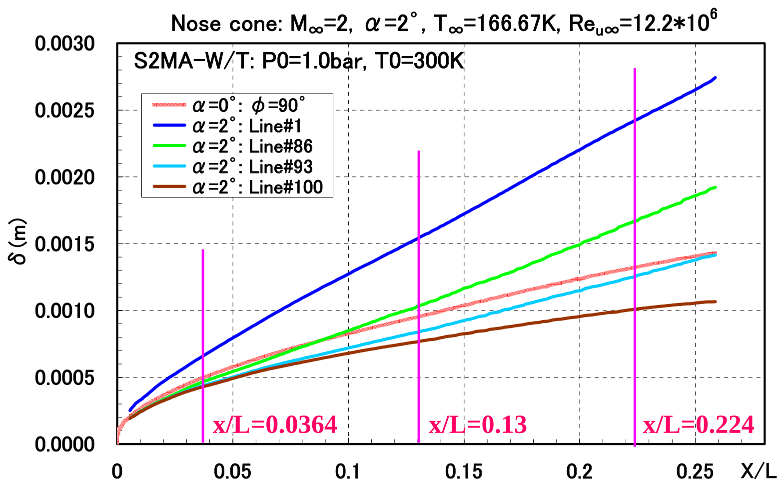

(e) Boundary layer thickness distributions

Figure 13. NS analysis of NEXST-1 nose cone at M=2.0, $\alpha=2^{\circ}$

nose cone and (X, Y, Z) are independent variables of the body axis coordinate system. Figure 13(b) shows four typical streamlines on the side of NEXST-1 nose cone; Figures 13(c), 13(d) and 13(e) show pressure coefficient, displacement thickness and boundary layer thickness distributions along the streamlines, respectively. In the Figure 13(d), displacement thickness distributions calculated by ONERA are also shown and they agree very well with JAXA's results. Figures 14(a)~14(c) show external streamwise and crossflow-wise velocity profiles (U and V ,respectively) of the laminar boundary layers at three chordwise stations, respectively, which are described in Figure 13(e).

(2) Linear stability analysis: iso-N contours

Stability analysis based on linear stability equation was carried out along each external streamline in order to calculate an N factor curve. Figures 15(a), 15(b) and 15(c) show the N-factor envelopes along the three respective external streamlines shown in Figure 13(b) at 2-deg. AOA. ONERA's and JAXA's N curves have fairly good agreement with a small difference of 0.01-0.02 in nondimensionalized length of X/L (L: total fuselage length). However, at the same streamwise positions, N values of ONERA are about 1 larger than those of JAXA.

Figures 16(a), 16(b) and 16(c) respectively show side, top and bottom view for a comparison of iso-N contours between ONERA and JAXA. However, ONERA's N contours are always a little upstream of the JAXA's contours; i.e. ONERA's N values are a little greater than those of JAXA. The cause of this is not yet clear but since the similar tendency also appeared at zero AOA as shown in Figure 11, it implies that the tendency became more distinguished with increasing the AOA.

Just for references, Figures D-11 (a)~ 11(d) and D-12 (a)~ 12(d) of Appendix D respectively show propagation directions and amplification rates of the small disturbances along the four typical streamlines, compared with the results for the cases at zero AOA.

(3) Summary of sections from 3.1 to 3.2.1

In summary, ONERA and JAXA had a very good agreement at 0-deg AOA and fairly good agreement at 2-deg AOA. Thus, we conclude that both codes by ONERA and JAXA were qualitatively verified through those comparisons.

3.2.2. Analysis at FHI-W/T transition test condition

The significance of the above comparison lies in the fact that the computational tools of ONERA and JAXA were cross-verified for the cases when the e^N method based on the stability theory was applied to the transition characteristic analyses in a very complex flowfield around an axisymmetric body at an incidence. The calculated results obtained by both laboratories agreed very well at least qualitatively and there were quantitatively consistent discrepancy between them throughout all the cases. These facts suggest that the main cause of the discrepancy does not have any essential effect for estimating quantitative differences between cases analyzed by one of the two codes.

Accordingly, as a next step, JAXA tried to verify the present stability analysis through comparison between the calculated iso-N contours and measured surface transition location distributions. JAXA independently measured the transition distributions in wind tunnel tests conducted in an in-draft type high-speed wind tunnel with a 0.61m-square test section of Fuji Heavy Industries (FHI). In-draft type wind tunnel has fairly low freestream fluctuation, compared to other conventional tunnels that have the test section downstream of disturbance sources such as pressure valves and blowers[17]. Without tunnel-wall suction, boundary layer on the tunnel wall is apparently turbulent and the flow in the tunnel is not free from the influence of its sound radiations, such as in so-called “quiet” supersonic tunnels[18]. However, a quite low C_{Prms}, static pressure fluctuation normalized by dynamic pressure, of 0.10% has been reported in the FHI tunnel (FHI-W/T) [13]. The tunnel was a supersonic tunnel with the lowest turbulence tunnel available to JAXA and JAXA decided that it was sufficient as a first step.

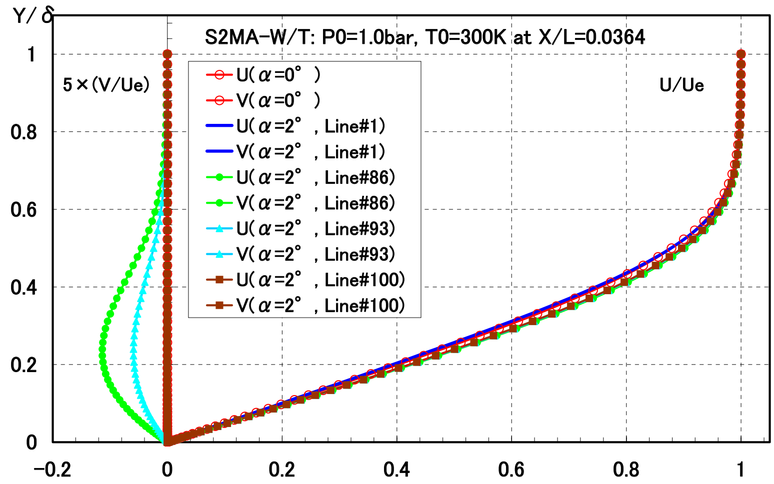

(a) x/L=0.0364

Figure 14. Velocity profiles of laminar boundary layer on NEXST-1 nose cone

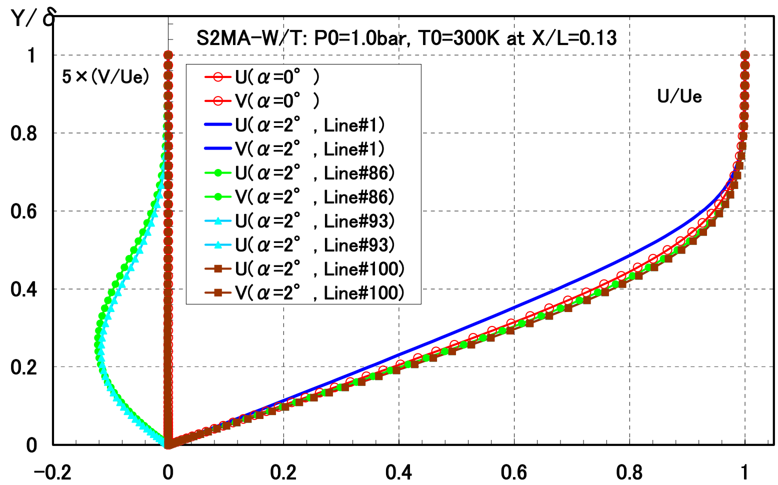

(b) x/L=0.13

Figure 14. Velocity profiles of laminar boundary layer on NEXST-1 nose cone

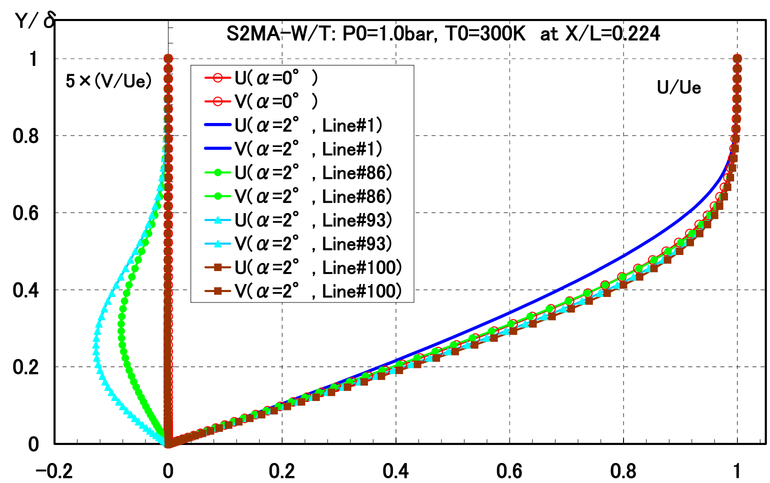

(c) x/L=0.224

Figure 14. Velocity profiles of laminar boundary layer on NEXST-1 nose cone

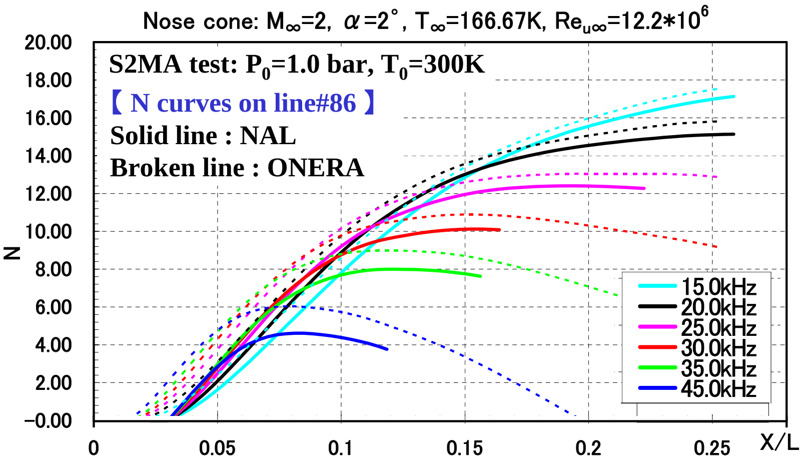

(a) Sreamline #86

Figure 15. N curves of NEXST-1 nose cone at M=2.0, $\alpha=2°$

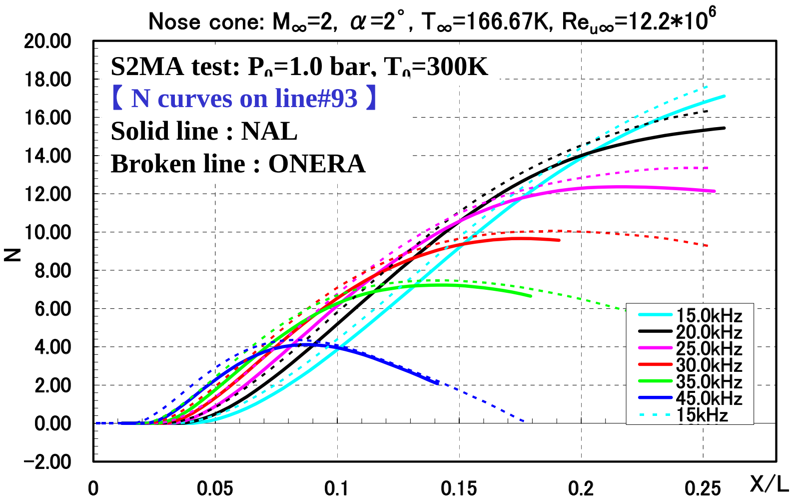

(b) Sreamline #93

Figure 15. N curves of NEXST-1 nose cone at M=2.0, $\alpha=2°$

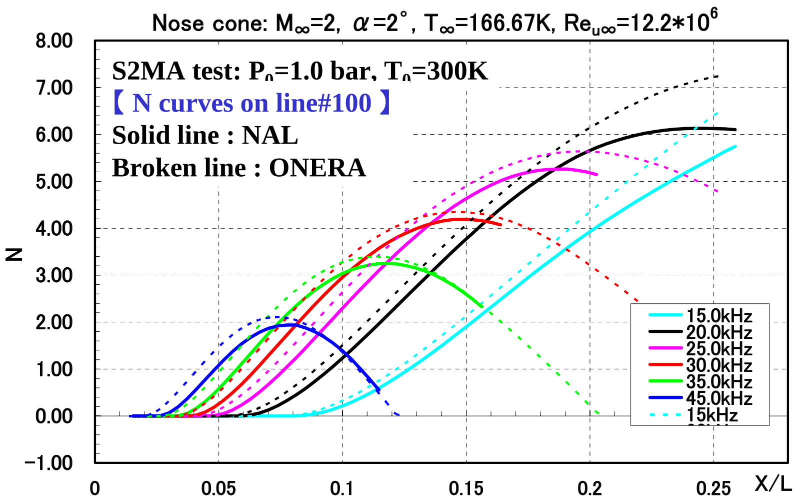

(c) Sreamline #100

Figure 15. N curves of NEXST-1 nose cone at M=2.0, $\alpha=2°$

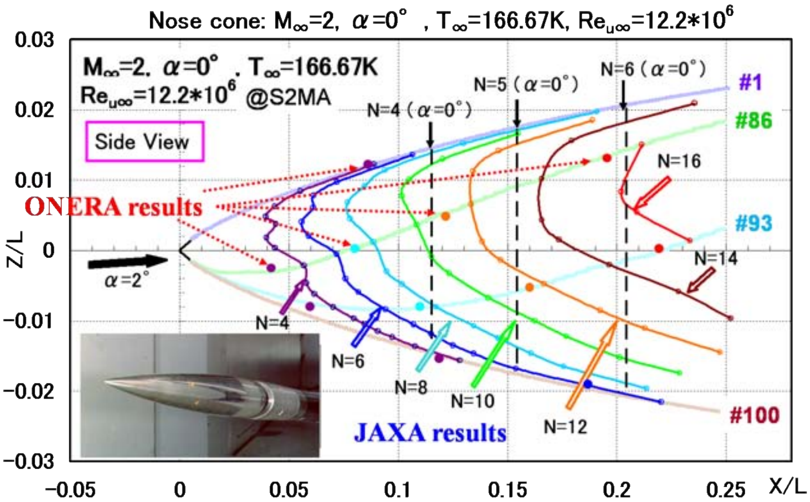

(a) Side view

Figure 16. N-contours of NEXST-1 nose cone at M=2.0, α =2°

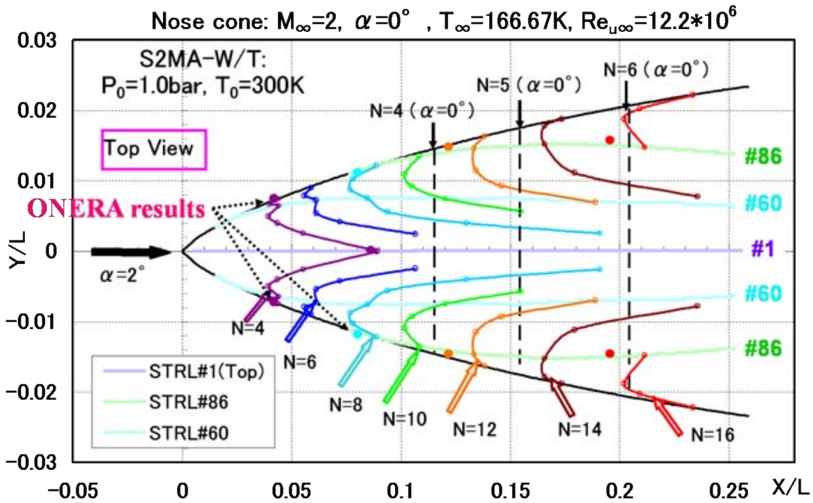

(b) Top view

Figure 16. N-contours of NEXST-1 nose cone at M=2.0, α =2°

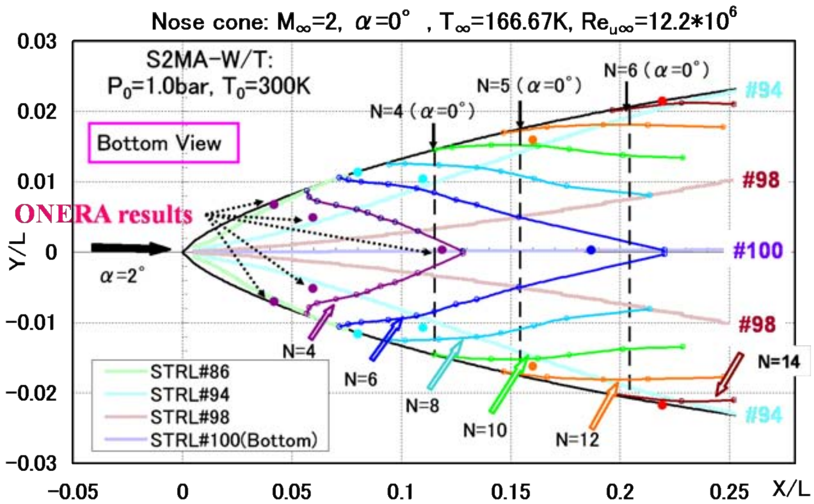

(c) Bottom view

Figure 16. N-contours of NEXST-1 nose cone at M=2.0, α =2°

(1) Linear stability analysis: iso-N contours

The analytical method used here is identical to the one used in the section 3.1; only the Reynolds number condition is different.

(2) Comparison of JAXA's results with transition test

The transition location distributions were acquired using an infrared (IR) thermography, which enabled both high data productivity and little surface roughness influence at the same time. The test model was made of insulated material so that surface temperature distribution can be acquired by the IR camera, which usually requires the use of adiabatic material to maintain the differences in surface wall temperature. The use of resin with high processability allowed JAXA to attain the transition front with little influence of surface roughness; the rms amplitude of the roughness was 0.22 μm. Further detail of the test model is described in Ref. 19.

The IR camera technique is based on measurements detecting variable wall temperatures in the transition region as a result of different heat transfer coefficients of laminar and turbulent flows. Figure C-3 of Appendix C shows a typical temperature profile along a streamline as a jagged line; the streamline coincides with the leeward ray. The temperature remains constant when the flow is either laminar or turbulent and changes linearly with distance during the transition. Thus, the beginning of transition was defined as the location of the intersection point of two approximate lines of least squares respectively through the laminar and transitional region, according to Owen[16].

Figures 17, D-13(a), 13(b), and 13(c) of Appendix D show comparison of the iso-N contours of NEXST-1 nose cone calculated by JAXA with measurement results in the FHI wind tunnel, at 2-deg AOA, Mach 2, P_0=1.01 bar and T_0=288.16 K. N=6 criterion corresponds to the beginning of transition around the windward and leeward rays and N=8-8.5 criterion coincides well on the side. The above trend is consistent for the whole surface regardless of the directions of the views; the reason for the difference in the N values is to be sought out in the section (3).

(3) Investigation into physical mechanisms behind the transition pattern

To investigate the reason for the different N values for the side, leeward and windward regions, JAXA had to look into physical mechanisms behind the transition pattern.

As for boundary layer transition on axisymmetric bodies at AOA in supersonic flows, a number of experiments have been conducted to investigate the transition for cones at AOA because the cones are the simplest geometries that exhibit 3-D supersonic boundary layers[20-24]. The previous studies have

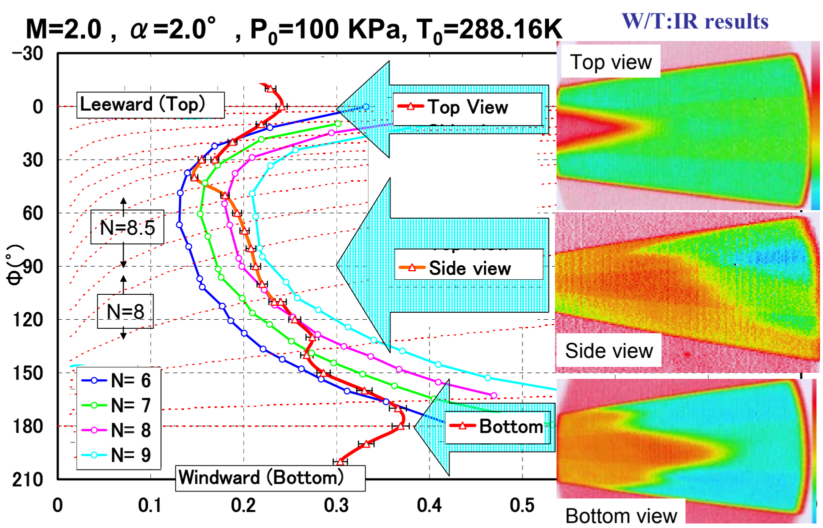

Figure 17. Comparison of N-contours of NEXST-1 nose cone by JAXA with measurement results at FHI-W/T test conditions

consistently found that as the AOA is increased transition moves rearward on the windward ray and forward on the side[20-22]. The same observation has been made on the present NEXST-1 nose cone as shown in Figure 17. Stability experiments[23-24] showed that Tollmien-Schlichting (T-S) instability dominated the transition process on the windward ray. Observations of streamwise vortices[20, 25-26] revealed that crossflow (C-F) instability dominated the transition process on the side. Since the difference between those sharp cones and the present nose cone is just a presence of favorable pressure gradient, it implies that C-F instability must be dominant on the side and T-S instability must be dominant on the windward rays.

Further, Sugiura et al.[19] studied the transition on the same nose cone model at a different Mach number of 1.2 in the JAXA-TWT1 (test section #3) in detail. Stationary C-F vortices evident in the surface temperature distribution revealed that C-F instability dominated on the side. Unsteady wave frequency measurement revealed that T-S instability dominated around the windward ray.

The above observation at Mach 1.2 is expected to have qualitatively similar trends as the Mach 2.0 case. Thus, the observations in the last two paragraphs suggest that C-F instability dominates on the side and T-S instability dominates around the windward ray.

The fact that the N=6 criterion coincided well around the windward and leeward rays and the N=8-8.5 corresponded to the transition onset on the side can be interpreted that the N value was 6 in the T-S dominated region and was 8-8.5 in the C-F dominated region. This means that N-factor is larger for stronger crossflow regions.

One of the explanations for the difference of N factors between the leeward/windward and the side regions is an effect of surface roughness. As shown in Figure 13(e), the boundary layer thickness increases both on the side and around the leeward ray and it decreases around the windward ray as AOA increases. Increase in the boundary layer thickness means a decrease in relative roughness height i.e. roughness sensitivity and this leads to increased N value around the windward ray. However, the present explanation fails to describe the increase in N values around the leeward ray. The receptivity of C-F instability to surface roughness is much larger than that of T-S instability. Thus, the different sensitivities of T-S and C-F instabilities to surface roughness are not likely cause of the different N values.

There is another possible explanation for the different N values for the side and windward regions. Freestream turbulence affects T-S instability more greatly than C-F instability, decreasing N-factor as a result. Similar conjecture was made for a sharp cone at M=7 by Arnal et al.[27, 28]; the N value was 3-4 for the T-S instability and was 10 for the C-F instability; Since the flow in the wind tunnel was highly turbulent, they conjectured that sensitivity to the turbulence was different for either instability.

To try to confirm the point, JAXA carried out the similar measurement on the 5-degree half-angle sharp cone at the same FHI-W/T test condition. Figures D-15(a)~15(d) of Appendix D show a comparison of iso-N contours (calculated by the same e^N code by JAXA) with the transition measurement results. The N-value was 5 around the leeward ray and was 7 on the side, which was qualitatively similar to the above tendency for the NEXST-1 nose cone. The reason of the difference in the magnitude of the N value than those for the NEXST-1 nose cone remains a future task.

(4) Summary

ONERA's and JAXA's stability analyses had good agreement. Respective N values were required for the T-S dominated region and for the C-F dominated region. The N=6 criterion coincided well with the beginning of transition around the windward and leeward rays, and the N=8-8.5 criterion coincided well on the side. The reason for the different N values for the side, leeward and windward regions was assumed to be different sensitivities between T-S and C-F instabilities to the influence of flow disturbance and surface roughness.

4. Transition analysis on the NEXST-1 NLF wing

One of JAXA's motivations behind the cooperative research project was to carry out a verified and validated compressible stability analysis on the NLF wing of the NEXST-1 airplane, since the incompressible stability analysis was only carried out in the NLF wing design phase described in Ref. 8. On highly swept wings, boundary layer transition generally occurs due to either attachment-line contamination or boundary layer instability. Therefore, in this chapter, we first discuss analyses of attachment-line contamination and then those of boundary layer instability.

4.1. Analysis of attachment-line contamination

(1) Outline of Poll method

In a swept wing, it is well known that there is another transition mechanism, other than the transition due to T-S and C-F instabilities. It is the transition due to attachment-line contamination originated in turbulent boundary layers on the fuselage surface[2]. The transition process cannot be analyzed theoretically and it is well known that Poll's criterion[29] based on an empirical database is very effective as a practical tool. Therefore ONERA and JAXA applied the criterion to the NEXST-1 NLF wing at the flight test condition.

According to Poll's criterion, when an attachment-line Reynolds number $\overline{R}^*$ called Poll's index is less than 245 ± 35, there is no risk of transition due to attachment-line contamination, as shown in Figure 18. In general, $\overline{R}^*$ is related to the boundary layer characteristics of attachment-line flow, compressibility effect and curvature radius of the leading edge as shown in Figure 19. This figure shows a summary of several practical relations in Poll's method. These relations are derived using compressible aerodynamic characteristics as described in Ref.38. As for nomenclatures, some of them are expressed in Figure 18, suffixes of "es" and "∞" indicate physical quantities along the attachment-line and at infinity, respectively and Λ indicates sweep angle of the leading edge.

The main purpose of the present section is to estimate $\overline{R}^*$ at the flight test condition. Both ONERA and JAXA used the exact definition of $\overline{R}^*$ shown in Figure 18, except in the section (3)-(A) where JAXA used a simpler definition based on cylindrical approximation as a preliminary analysis.

(2) Comparisons of different methods for calculating Poll's index

Poll's index requires the estimation of local velocity (U_e) gradient at the edge of laminar boundary layer in the vicinity of the stagnation point. First, JAXA calculated the pressure distribution (Cp distribution) using JAXA's NS solver at all-turbulent condition, in order to

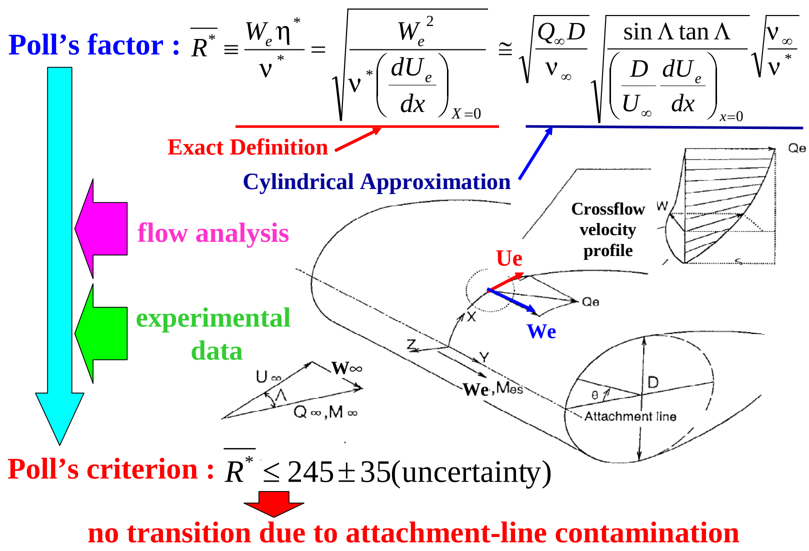

Figure 18. Poll's method for attachment-line contamination

suppress unexpected laminar separations in the flowfield which occurs when calculated at all-laminar condition around the NEXST-1 wing-body-tail configuration. Then, ONERA estimated edge velocity components (U_e and W_e) from the Cp distribution, using its own laminar boundary layer code and infinite swept wing approximation on inflow velocity condition. Finally, ONERA applied the exact definition of Poll's criterion to the present case. The present method of ONERA was verified by numerous flight and wind tunnel test results[30].

On the other hand, JAXA's analysis was a first trial for JAXA in this subject. Thus, JAXA considered ONERA's result as a reference in such analysis. The most difficult task of the analysis was to estimate edge velocity components as exact as possible. It was difficult to estimate the velocity components even with the use of CFD. Thus, JAXA also analyzed using two methods each of which based on a different assumption. Thus, ONERA's calculated result was compared with two results by JAXA in the following sections (A) and (B); JAXA used a different method in estimation of Poll's index in each section.

Poll Method: Formulation

$$\nu^* = \nu_{at\,T^*},\quad T^* = T_{es} + 0.1(T_w - T_{es}) + 0.6(T_r - T_{es})$$
$$T_r = T_{es}\left(1 + \sqrt{\Pr}\,\frac{\gamma-1}{2}M_{es}^2\right)$$

L.E. diameter

$$\overline{R^*} \equiv \frac{W_e\eta^*}{\nu^*} = \sqrt{\frac{W_e^2}{\nu^*\left(\frac{dU_e}{dx}\right)_{X=0}}} \cong \sqrt{\frac{Q_\infty D}{\nu_\infty}}\sqrt{\frac{\sin\Lambda\tan\Lambda}{\left(\frac{D}{U_\infty}\frac{dU_e}{dx}\right)_{x=0}}}\sqrt{\frac{\nu_\infty}{\nu^*}}$$

Exact Definition **Cylindrical Approximation**

$$\left(\frac{D}{U_\infty}\frac{du_e}{dx}\right)_{x=0} = \frac{2}{M_\infty\cos\Lambda}\sqrt{\frac{2}{\gamma}\frac{T_{es}}{T_\infty}\left(1-\frac{P_\infty}{P_{es}}\right)}$$

(Ref: AIAA J., Vol.34, No.4, p.649)

$$\frac{T_{es}}{T_\infty} = 1 + \frac{\gamma-1}{2}M_\infty^2\cos^2\Lambda \qquad \frac{P_{es}}{P_\infty} = \left[\frac{(\gamma+1)M_\infty^2\cos^2\Lambda}{2}\right]^{\frac{\gamma}{\gamma-1}}\left[\frac{\gamma+1}{2\gamma M_\infty^2\cos^2\Lambda-(\gamma-1)}\right]^{\frac{1}{\gamma-1}}$$

Figure 19. Several relations on Poll's method for attachment-line contamination

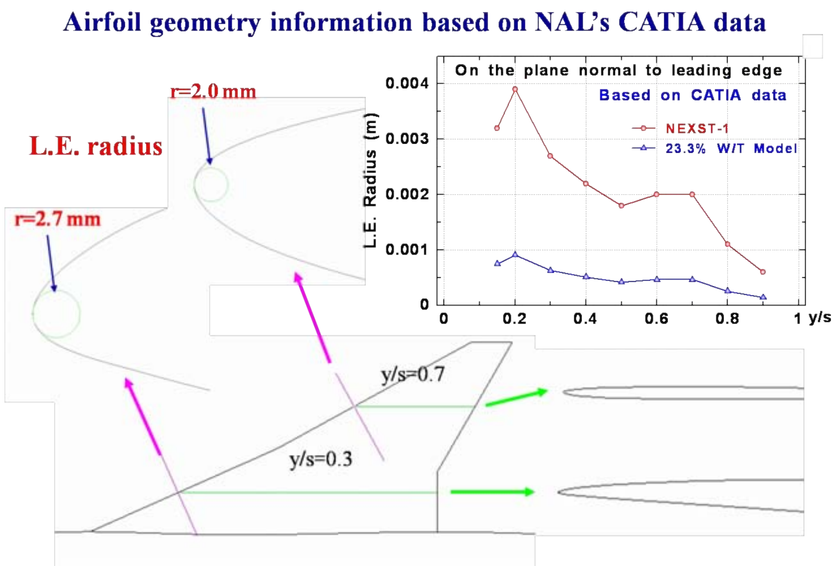

(a) Leading edge radius data

Figure 20. NAL's preliminary study by cylindrical approximation

(A) A preliminary analysis by JAXA

Here as a preliminary analysis, JAXA used a cylindrical approximation in calculating Poll's index. This method based on the cylindrical approximation is described in Figures 18 and 19. The main feature of this method is to replace dU_e/dx near stagnation of leading edge with dU_e/dx near stagnation of cylinder. The latter is easily estimated using an analytic formulation. This formulation is described in Figure 19. According to the relation described in Figure 19, the leading edge (L.E.) radius or diameter (as indicated by D) is the dominant factor in this analysis. The factor was estimated using the values of L.E. radius based on the CATIA data of the NEXST-1 airplane, as shown in Figure 20(a). Figure 20(b) shows comparisons of representative quantities calculated by ONERA and JAXA (NAL). JAXA estimated them using relations summarized in Figure 19. Figure 20(c) shows a comparison of Poll's indices between two laboratories. JAXA's $\overline{R}^*$ is 20-40 smaller than ONERA's. The difference mostly originates in difference in dU_e/dx. This is because when ONERA used JAXA's dU_e/dx instead of their original ones, both ONERA's curve indicated by “ONERA(approx. def.)” and JAXA's curve coincide, as clearly shown in Figure 20(d). This suggests that the cylindrical approximation should be limited to preliminary use only and the use of the exact definition is recommended for such complex configurations.

(B) A detailed analysis by JAXA (New approach)

Next, JAXA tried to apply the exact definition of Poll's index. JAXA calculated the edge velocity (U_e) distribution directly by JAXA's NS solver with laminar condition on the wing and all-turbulent condition on the body using the very fine grid system similar as in the section 3.1, in order to avoid unexpected laminar separations. JAXA calculated the velocity components of U_e and W_e by defining the condition of laminar boundary layer edge, as shown in Figure 21.

Figures 22(a) and 22(b) show comparisons of estimated velocity components normal to L.E. at two spanwise stations. ONERA's and JAXA's estimated velocity distributions are nearly identical. (Note that the horizontal axis in ONERA's computations is 0.233 times smaller than that in JAXA's ones. This difference was based on the scale between the real NEXST-1 airplane and the wind tunnel model used in the transition measurement test at ONERA-S2MA.) There were, however, numerical fluctuations around the stagnation point in the CFD calculation. They were unavoidable because they basically originated in a cell-centered algorism used in the formulation of CFD solver. Thus, JAXA approximated the velocity distribution by applying interpolations in order to smooth out the distribution in the vicinity of the stagnation point. This interpolation was made by combining both trend of pressure distribution on the wall near the stagnation and breakdown rule of velocity component due to infinite swept wing approximation. JAXA adopted an approximate quadratic polynomial of least squares for curve fitting in U_e distribution as shown in Figures 22(a) and (b). Furthermore, JAXA assumed isentropic changes in calculating W_e as shown in Figure 22(c).

Figure 22(d) shows a comparison of estimated $\overline{R}^*$, between ONERA and JAXA (NAL). The difference between two laboratories at H=15km condition got larger than the comparison of ONERA's result and JAXA's preliminary one. It is clear that the main reason depends on the difference of the estimated value of the dUe/dx. This might imply it is difficult to estimate the true value of the dUe/dx, even if CFD with fine grid system is applied. However, JAXA finally decided to use present new results to predict the transition due to attachment-line contamination according to the following reasons:

a) JAXA's new approach was the best way to estimate the Poll's index based on its exact definition, because JAXA and ONERA thought the way had higher accuracy numerically.

b) JAXA considered that larger $\overline{R}^*$ was better criterion to judge the transition due to attachment-line contamination.

This figure also shows Poll's index at three different altitudes. According to Poll's criterion, there is a possibility of transition due to attachment-line contamination for semi-spanwise location η <0.8 at 12km and in the inner wing (η <0.3~0.45)

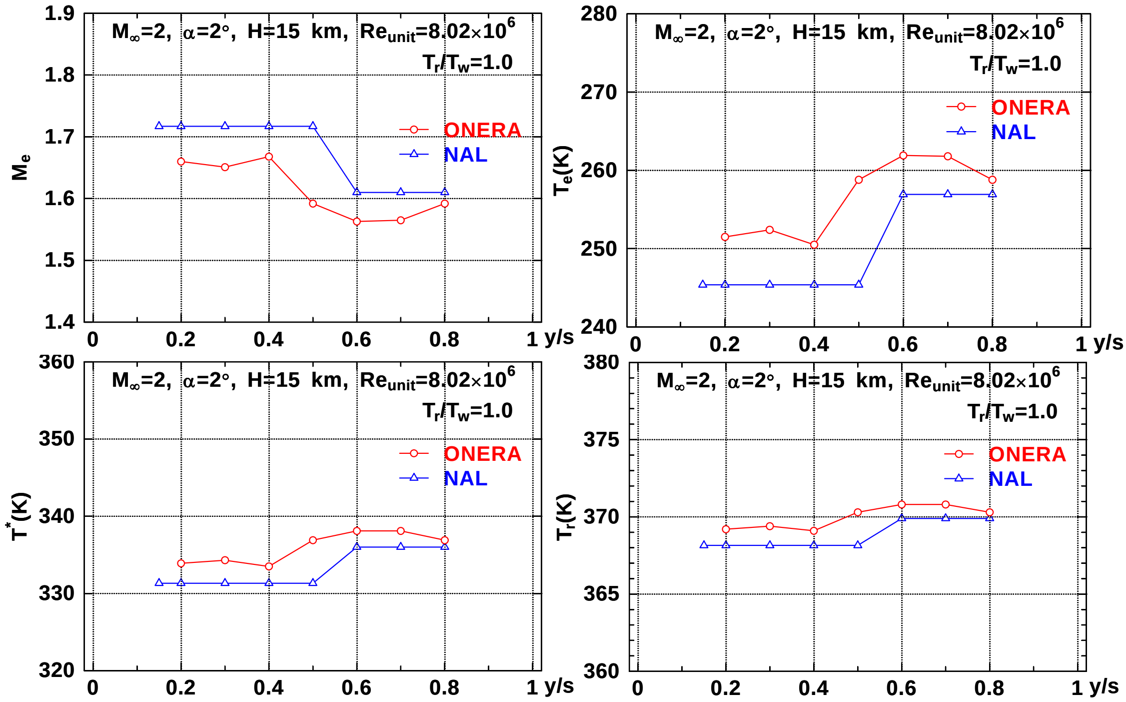

(b) Comparison of representative quantities

Figure 20. NAL's preliminary study by cylindrical approximation

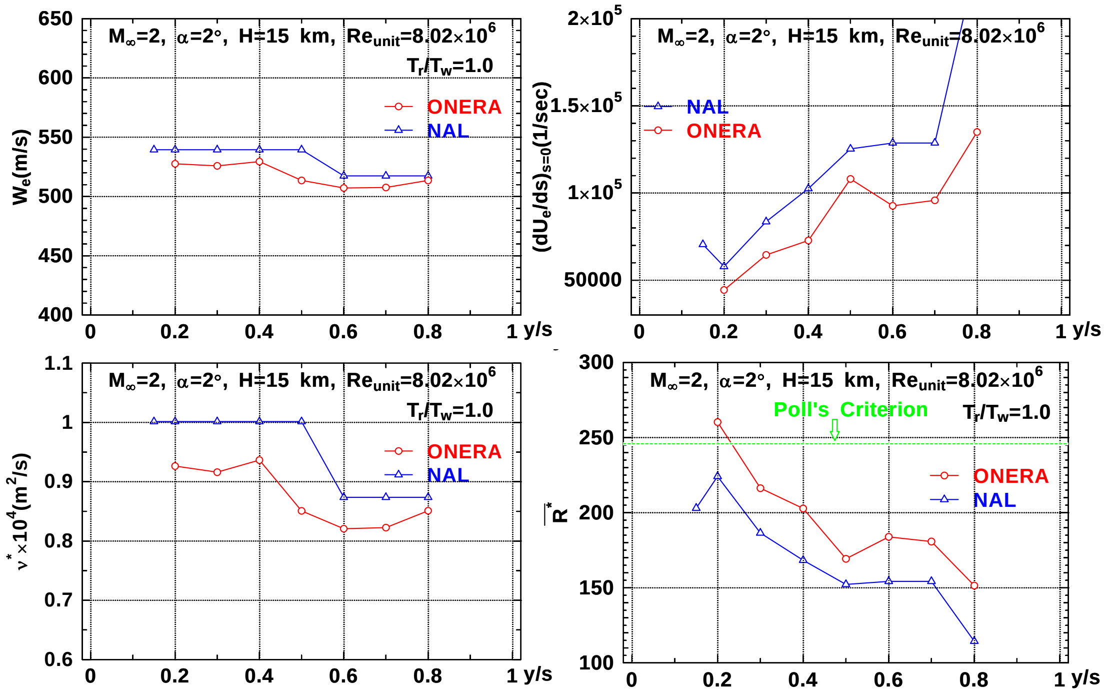

(c) Comparison of Poll's index

Figure 20. NAL's preliminary study by cylindrical approximation

at 15km. However, there is little possibility of transition due to contamination at 18km. Of course, the validity of present analysis is expected to be confirmed by the flight test results of the NEXST-1 airplane.

4.2. Analysis of boundary layer instability and “natural” transition prediction

4.2.1. Analysis at S2MA test conditions

Before mentioning the present transition analysis

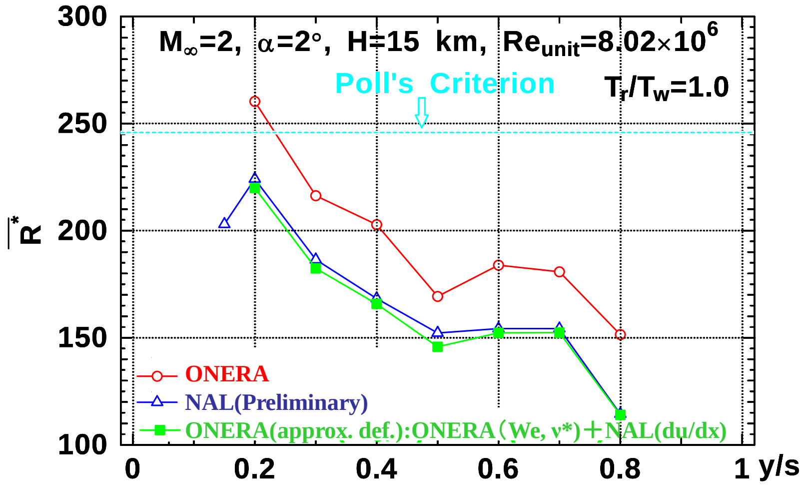

(d) Consideration of difference between ONERA and NAL
Figure 20. NAL's preliminary study by cylindrical approximation

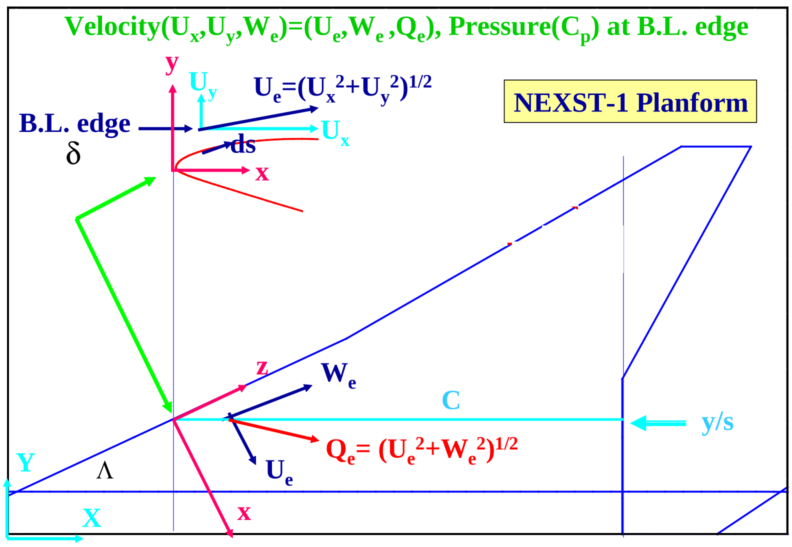

Figure 21. Notation of velocity components computed by NAL's NS code with laminar boundary layer condition

results on the NLF wing of the NEXST-1 airplane, here we briefly summarize transition measurement test results conducted by JAXA in the S2MA tunnel in order to validate JAXA's NLF wing design concept experimentally. The principal results are shown in Figure C-7 of Appendix C. JAXA measured transition locations by using hot-film sensors and infra-red (IR) camera techniques. A rearward movement of the transition location was observed at the design AOA, as clearly shown in the IR images in the figure. The extent of laminar region, however, was not as large as expected from JAXA's predicted results at the flight test condition, which was calculated at much larger Reynolds number. This is presumably because the experimental data was obtained at different freestream turbulence level conditions. Therefore, the NLF wing design concept was qualitatively but not quantitatively validated. Details of the test and its results are described in Ref. 10.

(1) Estimation of Cp distribution

JAXA calculated the pressure distribution on the NEXST-1 NLF wing at the above S2MA test condition using JAXA's NS code. The present NS analysis was conducted at all-turbulent condition as a first trial from the viewpoint of reducing both total number of grid points and convergence time

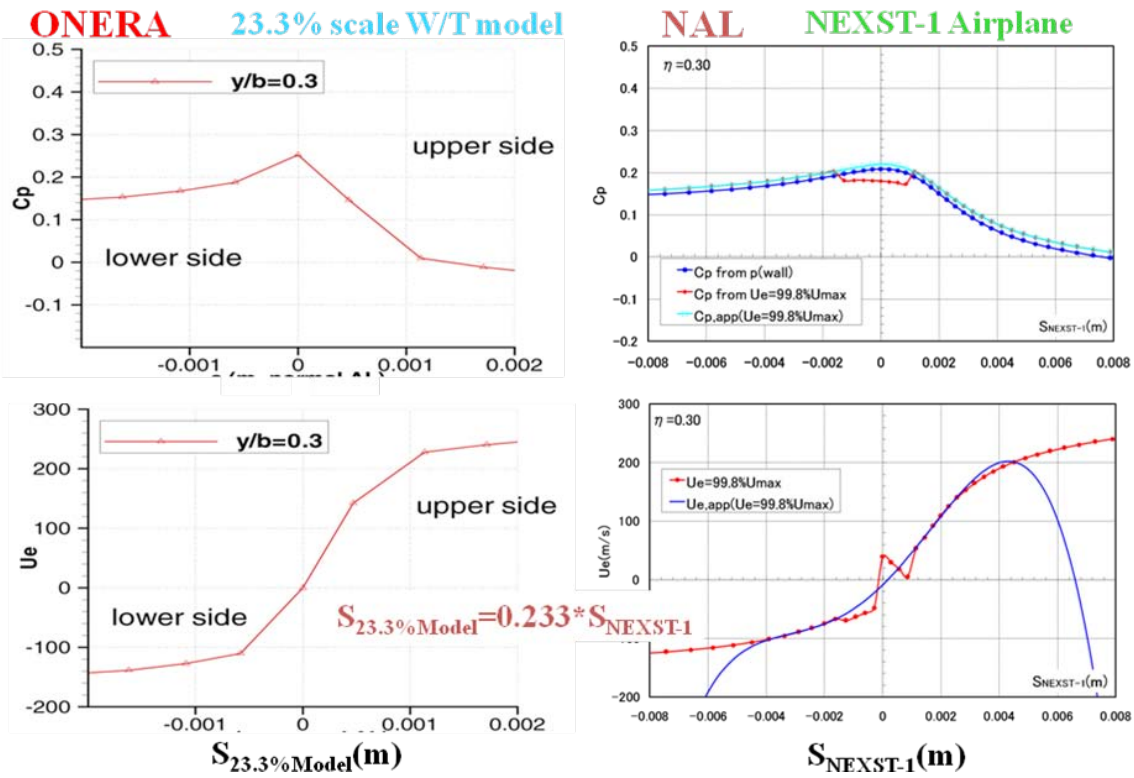

(a) y/s=0.3
Figure 22. New approach of NAL's study

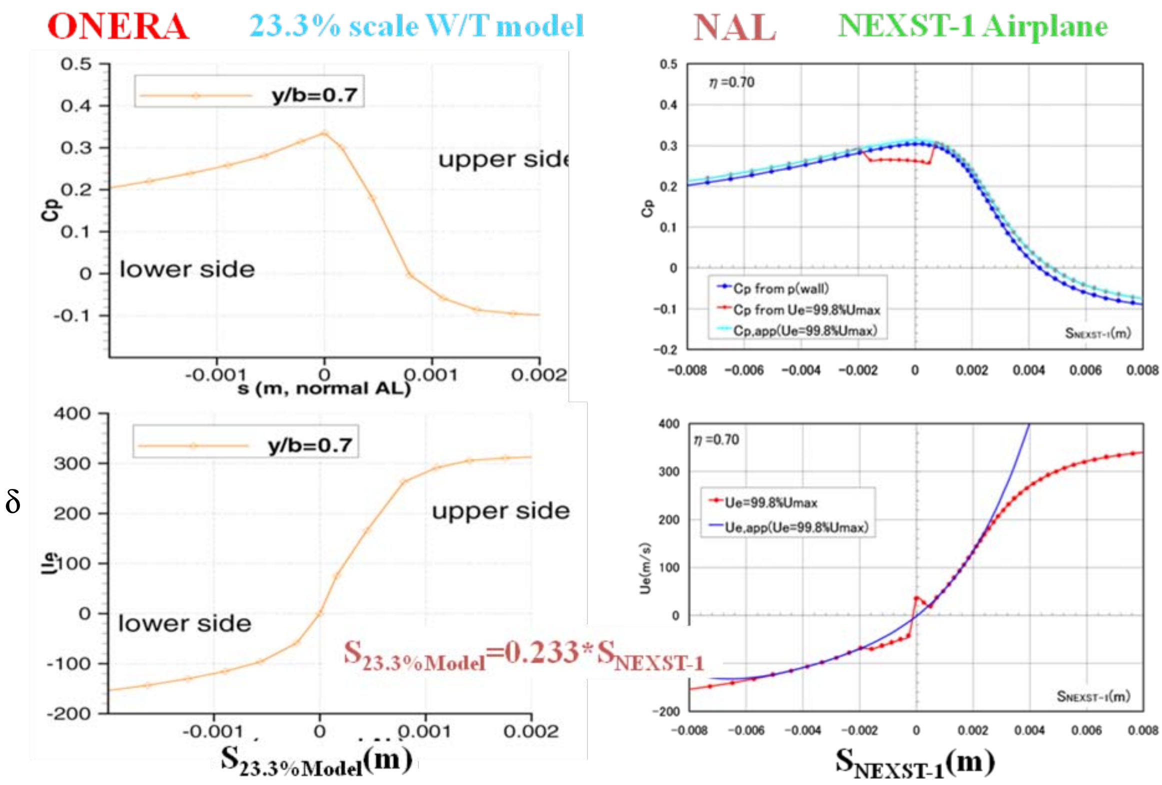

(b) y/s=0.7
FFigure 22. New approach of NAL's study

$$\overline{R^*} \equiv \frac{W_e \eta^*}{\nu^*} = \sqrt{\frac{W_e^{\,2}}{\nu^* \left(\dfrac{dU_e}{dx}\right)_{X=0}}}$$

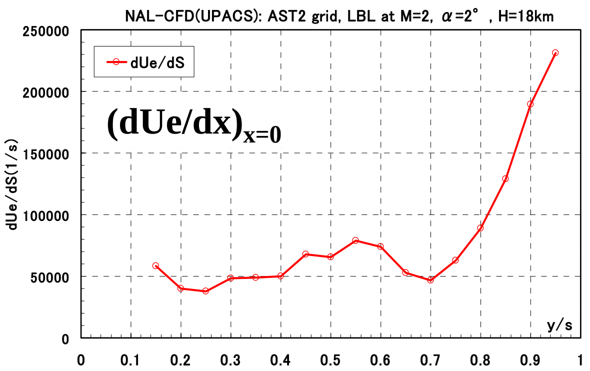

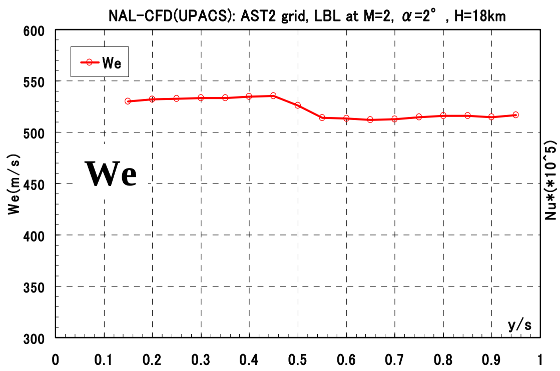

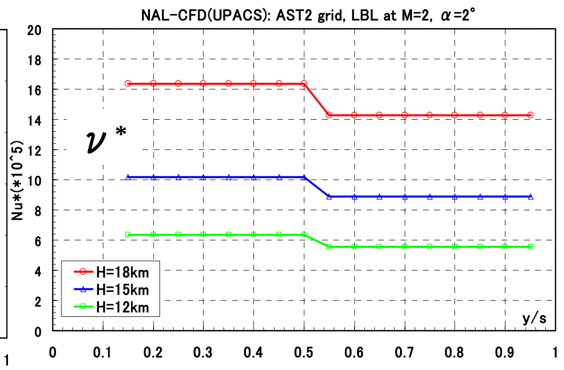

(c) Each quantity
Figure 22. New approach of NAL's study

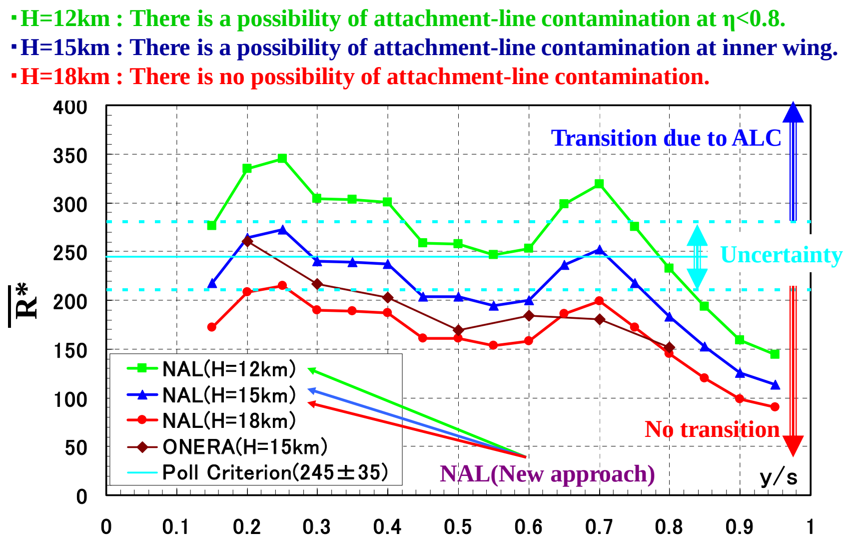

(d) Poll's index distribution at M=2, α =2°
Figure 22. New approach of NAL's study

since the pressure distribution was influenced little by boundary layer thickness.

(2) Laminar boundary layer computations

In order to perform the transition analysis based on laminar boundary layer instability, compressible laminar boundary layer profiles need to be estimated. For the boundary layer profile computation, ONERA used an in-house code called 3C3D and JAXA used a popular code developed by Kaups and Cebeci[31] for the estimation. Both computations by two laboratories were based on the same pressure distributions at several spanwise stations calculated using JAXA's NS code with turbulent condition. Of course, the reason of using turbulent condition is the same as the one as mentioned in the section 4.1.(2), that is, to suppress unexpected laminar separation in the flowfield around the NEXST-1 configuration calculated at all-laminar condition. As shown in Figures 23 and 24, ONERA and JAXA compared both their estimated boundary layer thickness and edge velocity direction distributions at the S2MA test condition and found very good agreements. A small difference in the velocity direction at the boundary layer edge in Figure 24 is probably due to different edge definitions used by ONERA and JAXA. In general, crossflow velocity at the boundary edge should be exactly zero. But the present approximation of estimating the edge yields a small non-zero crossflow velocity and it generates a small difference in the velocity direction.

(3) Stability analysis and comparison of the integral paths

While both e^N methods had the same envelope strategy[2)], each method is based upon a different formulation of the integral path for integrating amplification rate. The selection of the best integral path has been an open question for some time. ONERA chose a path along a polar arc indicated by “path A” in Figure 25 as a candidate because both 3C3D method and the Kaups and Cebeci

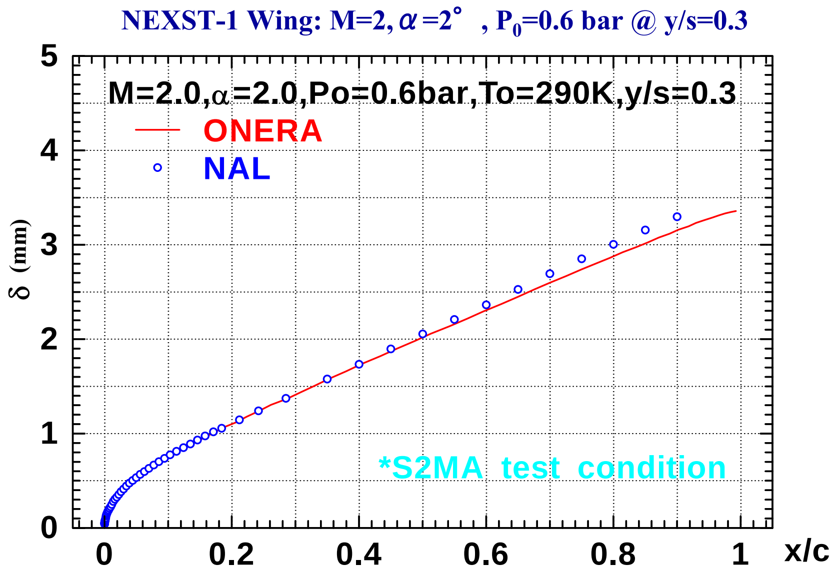

Figure 23. Estimation of boundary layer thickness

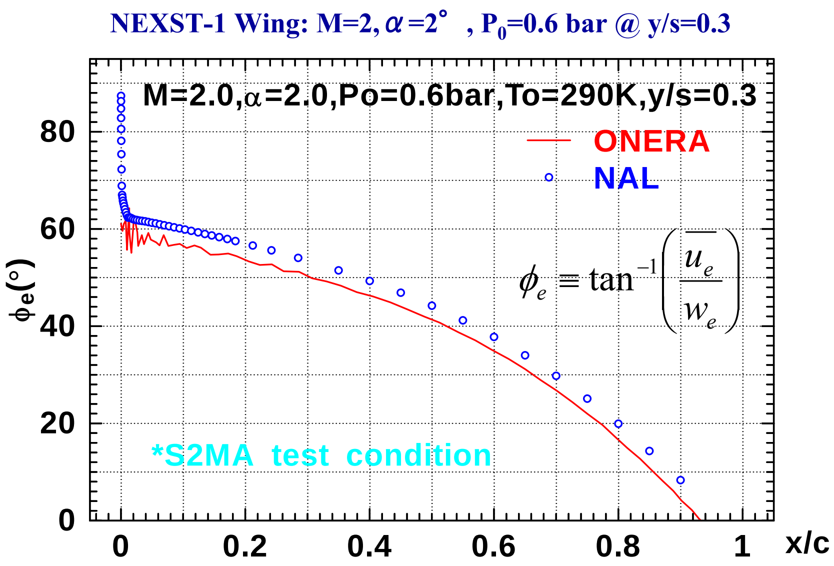

Figure 24. Velocity direction at edge of boundary layer

method were formulated in the polar coordinate (x_c, z_c) system. On the other hand, JAXA considered two candidates for the path in order to investigate an ideal integral path for practical applications. One was the same as ONERA's path. The other was a path along a local external streamline called "path B" as shown in Figure 25. The latter was selected because JAXA's stability code was formulated in the local streamline coordinate (x_s, z_s) system (see Appendix D)[9]. There had previously been no investigation on difference between these two integral paths. JAXA calculated using both paths in order to assess their reliability.

Path B has logical reasoning that path A does not have. Thus, we figured that the path B was more appropriate and adopted it for JAXA's analyses hereafter. Fidelity of the integral path B and its difference from path A will be investigated in the present section.

First of all, ONERA and JAXA made comparison both using the same integral path A. Figure 26(a) shows a comparison of amplification rate of the disturbance with a frequency of 10 kHz between ONERA and JAXA using the path A. Here we paid attention to the normalization of amplification rate. As a general rule, ONERA normalized the amplification rates by incompressible displacement thickness while JAXA (NAL) normalized them by compressible boundary layer thickness. In order to clarify the comparison, JAXA recalculated the results using the normalizations by incompressible displacement thicknesses. As shown in the figure, ONERA's and JAXA's amplification rates normalized by the incompressible displacement thickness were quite similar except in the rearward region.

Figures 26(b) shows a comparison of N-factor curve of the disturbance with the frequency of 10 kHz between ONERA and JAXA. As shown in the figure, there were four kinds of N evolution results calculated by JAXA: one using the path B and the other three using path A; with a view to clarify the comparison, one of the calculations using path A was divided by 0.86 and another was added an offset value of 0.5 (The value 0.86 and 0.5 is arbitrarily set in order to distinguish quantitative and qualitative differences). Although ONERA's N evolution is more similar to JAXA's one using the integral path A rather than one using the path B, there is a nonnegligible difference between ONERA and JAXA along the whole chord. As shown in the figure, the difference corresponds to either an offset of about 0.5 or a division by 0.86 except in the rearward region. The difference probably originated from the difference in the estimated amplification rate shown in Figure 26 (a). Any clear reason for the difference in the amplification rate, however, was not found at that time. Further study afterward revealed that the rearward difference is due to the fact that the

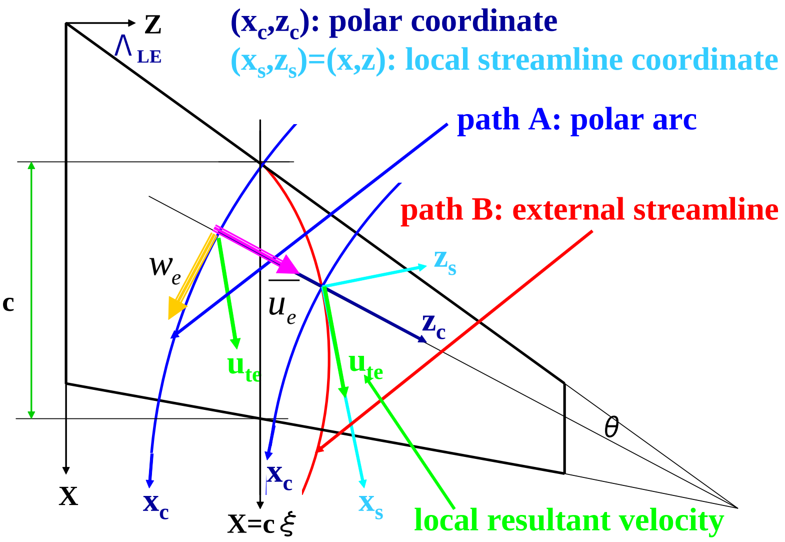

Figure 25. Typical candidates of integral path in stability analysis

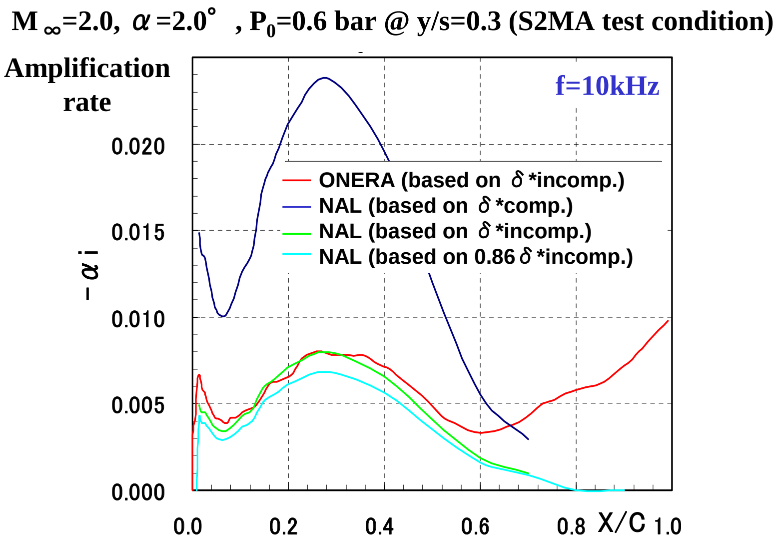

(a) Amplification rate with f=10kHz

Figure 26. Comparison of stability computation results on the NEXST-1 wing

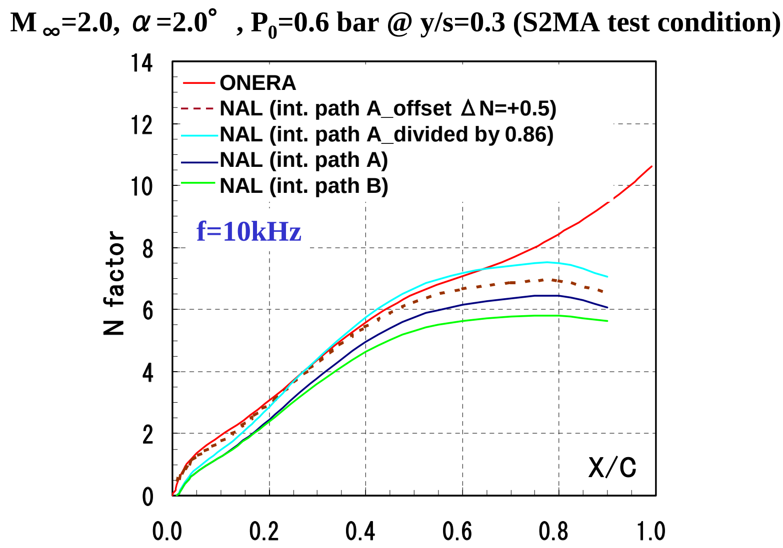

(b) N factor with f=10kHz

Figure 26. Comparison of stability computation results on the NEXST-1 wing

range of propagation direction angle Ψ in JAXA's computation, defined in Figure D-1, was limited to a positive side of Ψ ; this has been corrected in analyses in the sections 4.2.2 and 3.2.

Figures 27(a), 27(b) and 27(c) show comparisons of ONERA's and JAXA's calculated N characteristics at the S2MA test condition and a total pressure of 0.6 bar. Here ONERA calculated the N curves using the integral path A in Figure 27(a) and JAXA calculated them using the integral path A in Figure 27(b) and the path B in Figure 27(c). The figures show that N evolutions were quite similar except the rearward chordwise region.

However, JAXA's computation along the integral path A produced slightly lower N factors than that of ONERA. Moreover, JAXA's N factors, computed using the integral path B in Figure 27(c) were found to be about 0.3 less than those using the path A.

(4) Comparison with the transition measurements

When we compare the N evolutions with the S2MA test result [10] (see Appendix C), it was suggested that the N factor that correspond to the

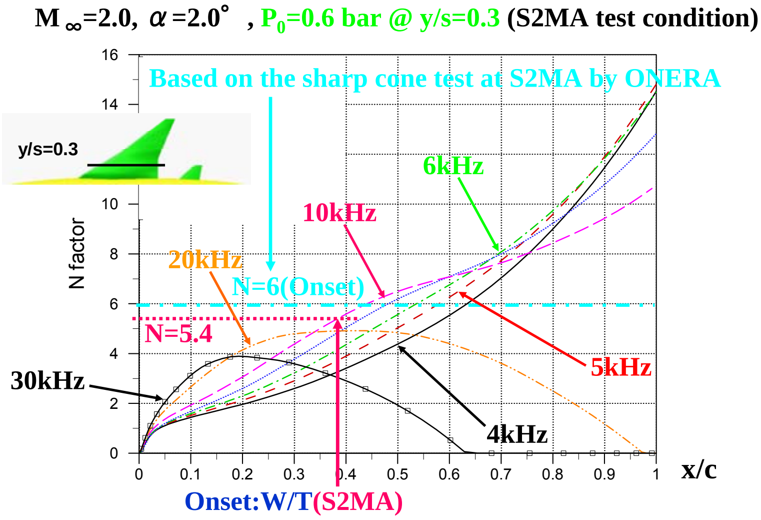

(a) ONERA's computations
Figure 27. Comparison of N-factors on the NEXST-1 wing

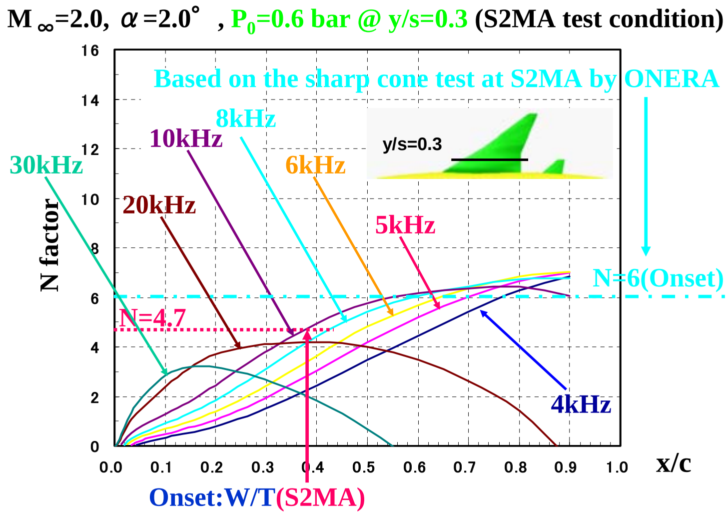

(b) NAL's computations with the integral path A
Figure 27. Comparison of N-factors on the NEXST-1 wing

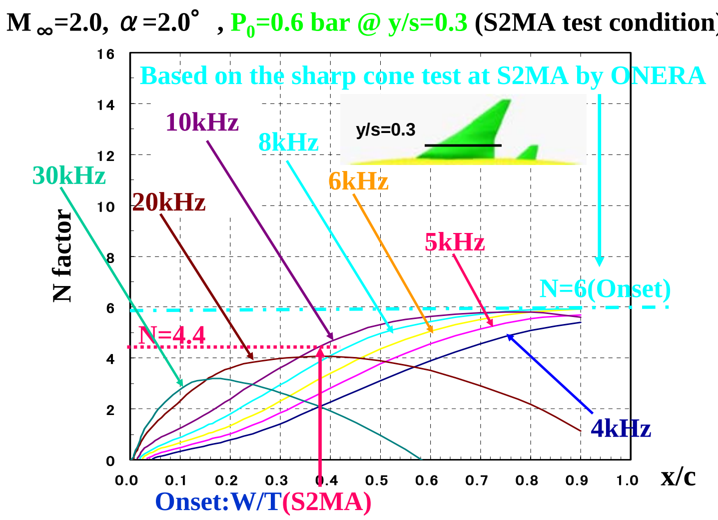

(c) NAL's computations with the integral path B
Figure 27. Comparison of N-factors on the NEXST-1 wing

transition onset was 5.4 in ONERA's analysis as shown in Figure 27(a), while in JAXA's analyses the N factor was 4.7 for the path A and 4.4 for the path B, as respectively shown in Figures 27(b) and 27(c). If we adopt the transition N criterion of N=6, based on the correlation for the 5-degree half-angle sharp cone, ONERA's prediction has better correlation with the S2MA test result than those of JAXA.

The N=6 criterion for the onset of transition was obtained in the S2MA sharp cone test conducted by ONERA as mentioned above. Since the criterion is for the sharp cone at zero AOA, it is clearly related to the transition dominated by T-S instability. The fact that N=6 criterion correlated well in both cases by ONERA's analyses on the sharp cone and the NEXST-1 wing may imply that T-S instability was also dominant on the NLF wing at the design point and that the C-F instability that is generally dominant on highly swept wings was suppressed by applying the present NLF wing design concept.

On the other hand, all the N factors estimated by JAXA were less than N=6. One of the main reasons for the difference may be the difference in the integral paths but a reason for the difference of the cases using the same path A between ONERA and JAXA remains unknown.

There are a few other observations that imply the T-S instability dominance. As shown in Figures 28(a) and 28(b), JAXA's estimated propagation directions of small disturbances were also very similar to those by ONERA. This means that the real parts of eigenvalues were very similar, which was in accordance with the high correlation between both laboratories in the 5-degree half-angle sharp cone case. The most amplified disturbance is 10kHz according to the Figures 27(a) and 27 (b). For the most amplified 10kHz waves, Ψ_{max} ranges from 60 to 70 degrees near the transition point of the 38% chordwise station (shown in Figures 27 and Table 2), which indicates that oblique T-S instability is dominant in the N evolution.

Furthermore, in the S2MA test, even a slight deviation in the AOA from the design AOA moved the transition location significantly upstream, confirming the NLF effect of the designed pressure distribution on the inner part of the wing[10]. These facts and the good correlation of the N-value between the NLF wing and the 5-degree half-angle sharp cone cases in the ONERA's analyses suggest that the transition on the NLF wing is dominated by streamwise instabilities. However, further measurement or analysis is needed for justification of the dominance of the streamwise instabilities, because the envelope method lacks certain physical information on the transition process; this is because streamwise and crossflow instabilities will exert additive effects in the method, and it is assumed that a crossflow wave can suddenly change to a streamwise wave within a short distance[2].

Similar comparisons at 70% semi-spanwise station and a relatively high total pressure of 1.4 bar are summarized in Table 2. Figures 29(a) ~ 29(d) show comparisons of N-factors at several semi-spanwise stations at P_0=0.6 and 1.4 bars; Figure 30 shows comparisons of N-contours.

Table 2. Comparison of ONERA's and NAL's N-factors on the NEXST-1 wing based on the S2MA test results

W/T			ONERA		NAL			
Cond.	HF Results		Path A		Path A		Path B	
P_0	y/s	$(x/c)_{Tr.}$	N_{onset}	f_{max}	N_{onset}	f_{max}	N_{onset}	f_{max}
0.6 bar	0.3	0.38	5.4	10kHz	4.7	10kHz	4.4	10kHz
	0.7	0.44	3.4	20kHz	3.1	20kHz	2.9	20kHz
1.4 bar	0.3	0.11	6.3	40kHz	5.2	30kHz	5.1	30kHz
	0.7	0.21	5.7	50kHz	4.5	50kHz	4.5	50kHz

M_∞=2.0, α=2.0°, P_0=0.6 bar @ y/s=0.3 (S2MA test condition)

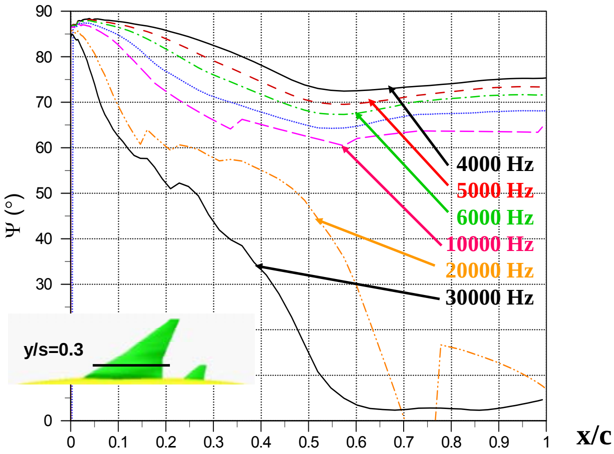

(a) ONERA's computations
Figure 28. Comparison of propagation direction angles on the NEXST-1 wing

M_∞=2.0, α=2.0°, P_0=0.6 bar @ y/s=0.3 (S2MA test condition)

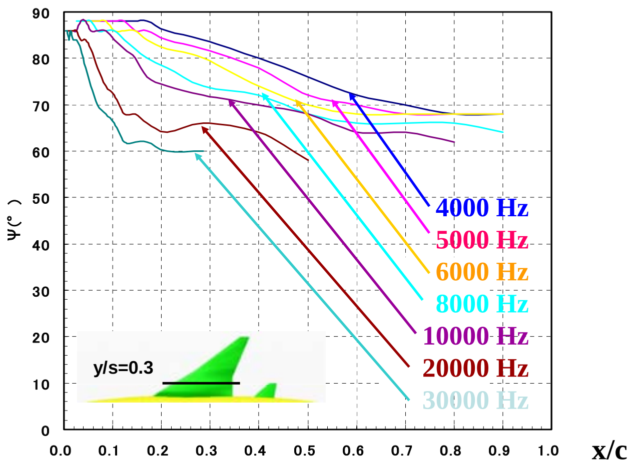

(b) NAL's computations
Figure 28. Comparison of propagation direction angles on the NEXST-1 wing

M_∞=2.0, α=2.0°, P_0=0.6 bar @ y/s=0.3 (S2MA test condition)

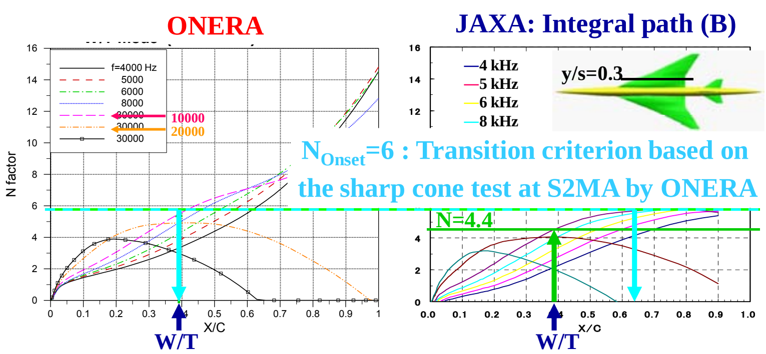

(a) P_0=0.6 bar @ y/s=0.3
Figure 29. Comparison of N-factors on the NEXST-1 wing

M_∞=2.0, α=2.0°, P_0=0.6 bar @ y/s=0.7 (S2MA test condition)

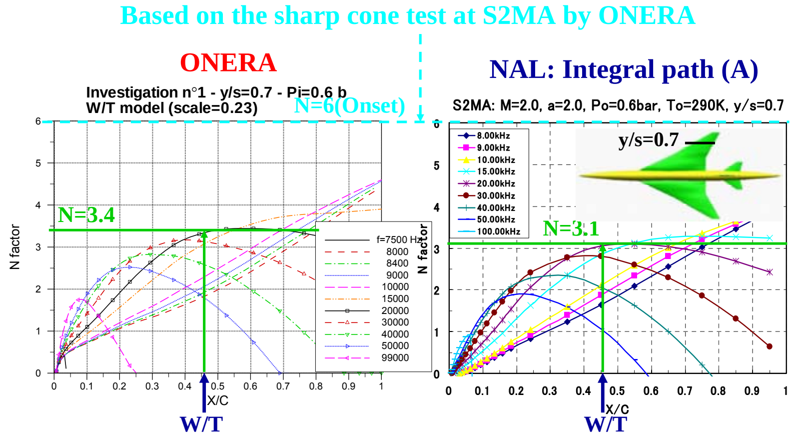

(b) P_0=0.6 bar @ y/s=0.7
Figure 29. Comparison of N-factors on the NEXST-1 wing

M_∞=2.0, α=2.0°, P_0=1.4 bar @ y/s=0.3 (S2MA test condition)

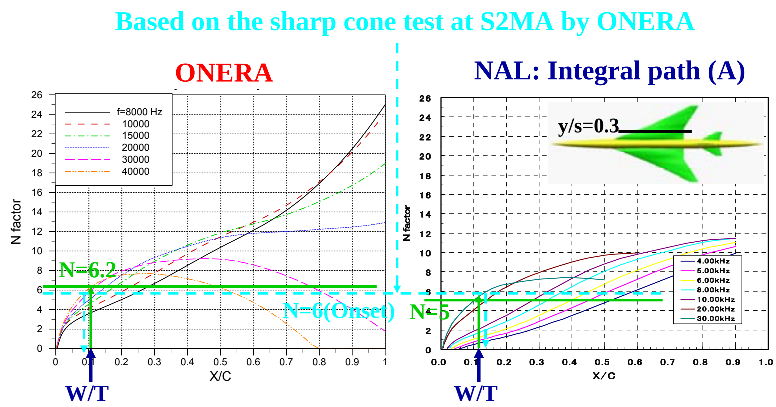

(c) P_0=1.4 bar @ y/s=0.3
Figure 29. Comparison of N-factors on the NEXST-1 wing

M_∞=2.0, α=2.0°, P_0=1.4 bar @ y/s=0.7 (S2MA test condition)

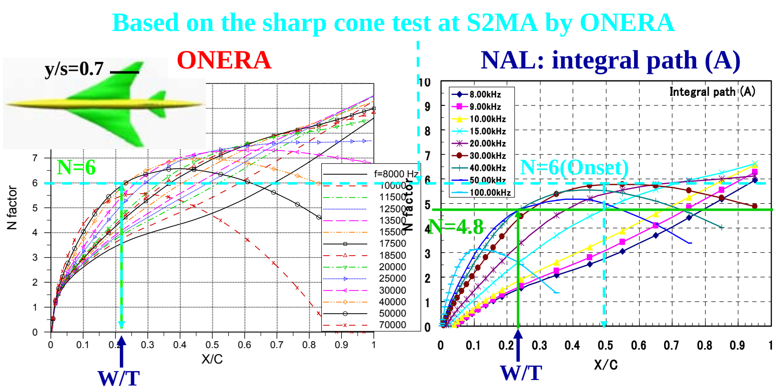

(d) P_0=1.4 bar @ y/s=0.7
Figure 29. Comparison of N-factors on the NEXST-1 wing

Table 2. Comparison of ONERA's and NAL's N-factors on the NEXST-1 wing based on the S2MA test results

W/T			ONERA		NAL			
Cond.	HF Results		Path A		Path A		Path B	
P_0	y/s	$(x/c)_{Tr.}$	N_{onset}	f_{max}	N_{onset}	f_{max}	N_{onset}	f_{max}
0.6 bar	0.3	0.38	5.4	10kHz	4.7	10kHz	4.4	10kHz
	0.7	0.44	3.4	20kHz	3.1	20kHz	2.9	20kHz
1.4 bar	0.3	0.11	6.3	40kHz	5.2	30kHz	5.1	30kHz
	0.7	0.21	5.7	50kHz	4.5	50kHz	4.5	50kHz

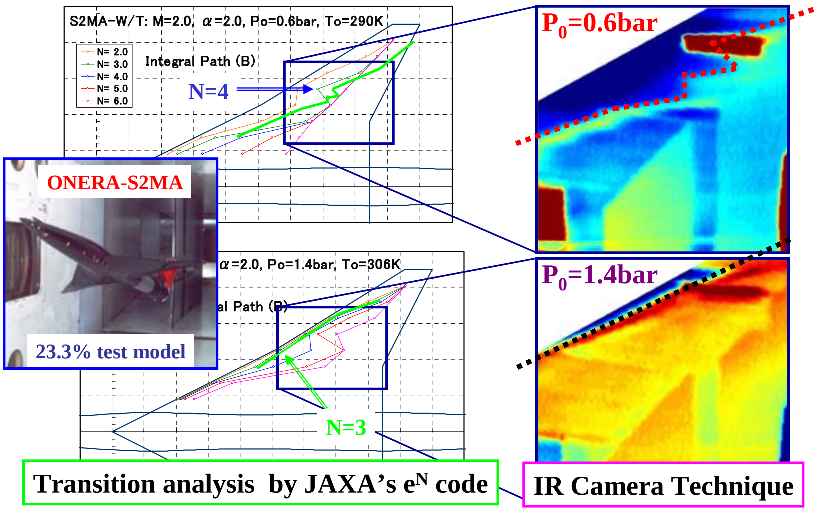

Figure 30. Comparison of N contours at P_0=0.6 and 1.4 bar

The Figure 29(b) shows that in the case of 70% semi-spanwise station at 0.6 bar both ONERA's and JAXA's N characteristics were also similar. However, both were much less than the N=6 criterion. It is supposed that this discrepancy is due to the difference between measured and calculated pressure distributions. However, any clear solution for diminishing this discrepancy has not been found yet. In the case of 1.4 bar, N evolutions calculated by both laboratories were similar. Here ONERA's predictions have a higher correlation with the N=6 criterion. As a conclusion, there was a good agreement between test results and ONERA's predictions under the assumption of applying the N=6 criterion for the 5-degree half-angle sharp cone to the NLF wing test case except only in the case of 70% semi-spanwise station at 0.6 bar.

(5) Summary

ONERA's and JAXA's stability analyses are in fairly good agreement and both had good correlation with the S2MA test results. ONERA's prediction using the estimated N value for the 5-degree half-angle sharp cone particularly had a good correlation with the NLF wing experiment results. We figured that the path B was more appropriate and JAXA adopted it hereafter because path B has logical reasoning that path A does not have. Finally, although JAXA's stability analysis method still has a room to be improved quantitatively, JAXA thinks JAXA's method is qualitatively effective for predicting transition characteristics for selective conditions.

4.2.2. Analysis at NEXST-1 flight test condition

4.2.2.1. Summary of flight test results

JAXA conducted the flight test of the NEXST-1 airplane in Woomera prohibited area, Australia on October 10th, 2005. The flight test was fully successful and a plenty of aerodynamic data including transition measurements was obtained[39-41]. The most important conclusion was that JAXA qualitatively validated the effect of the NLF wing design concept by confirming significant rearward movement of transition locations at the design condition in the flight test[45]. However, the amount of the movement of transition location was less than that in JAXA's predicted results. One of the candidates for the reason for this was the effect of surface roughness of the wing which was not small enough for certain areas of the wing that have relatively thin boundary layer i.e. higher sensitivity to surface roughness at the flight test Reynolds number condition. Principal flight test results are briefly summarized in Appendix A as a reference.

4.2.2.2. Preliminary analysis

In advance of the flight test, JAXA carried out a preliminary analysis at the flight test condition.

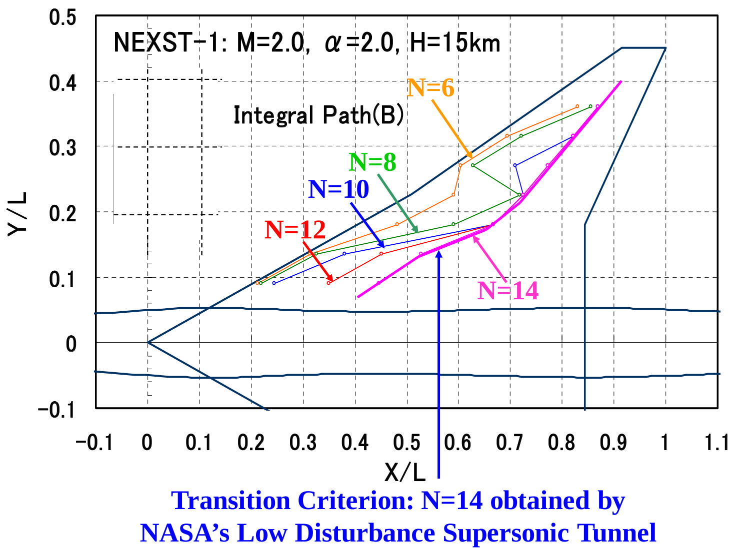

Figure 31. N contours on the NEXST-1 wing at flight condition

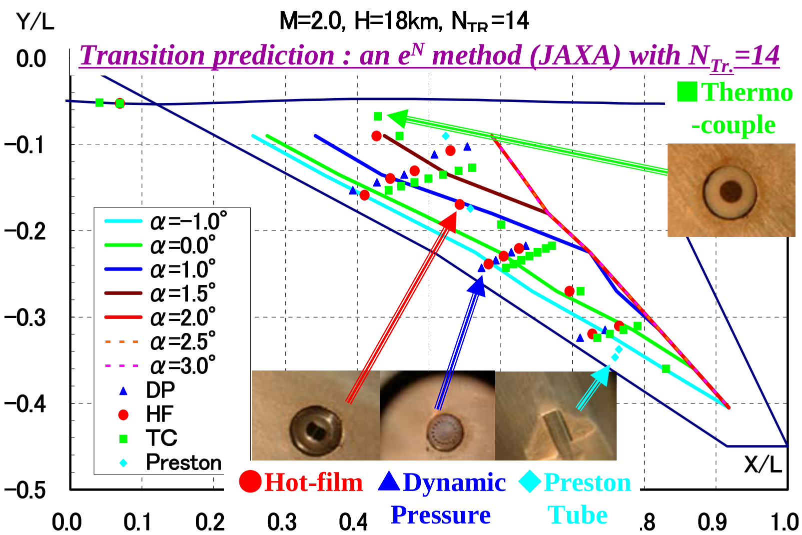

(a) H=18km case

Figure 32. Transition predictions on the NEXST-1 wing at flight condition

In other words, JAXA predicted transition location pattern at flight test condition using JAXA's e^N code that was improved by the present cooperative research project. A detailed analysis was carried out after the first failed flight test (conducted on July 14th, 2002), which will be described in the next section. Figure 31 shows predicted N contours on the NEXST-1 NLF wing at the design conditions of M=2.0, 2-deg AOA, and 15km altitude. Since the N criterion was necessary to predict transition location, JAXA applied the N=14 criterion[32), which was derived from the transition measurements on a F-16XL wind tunnel model at a low-disturbance supersonic wind tunnel of NASA at M=3.5 as described in Ref. 35. This criterion was applied because there was no other transition criteria for supersonic speed derived from a measurement in a low-disturbance environment at that point and flow disturbance greatly affects transition locations at supersonic speed.

Figures 32(a), 32(b), and 32(c) show predicted transition location patterns at different AOA and altitudes. These figures also include the location of four kinds of transition measurement sensors that are hot-film, dynamic pressure transducer, Preston tube and thermocouple. The estimated turbulent

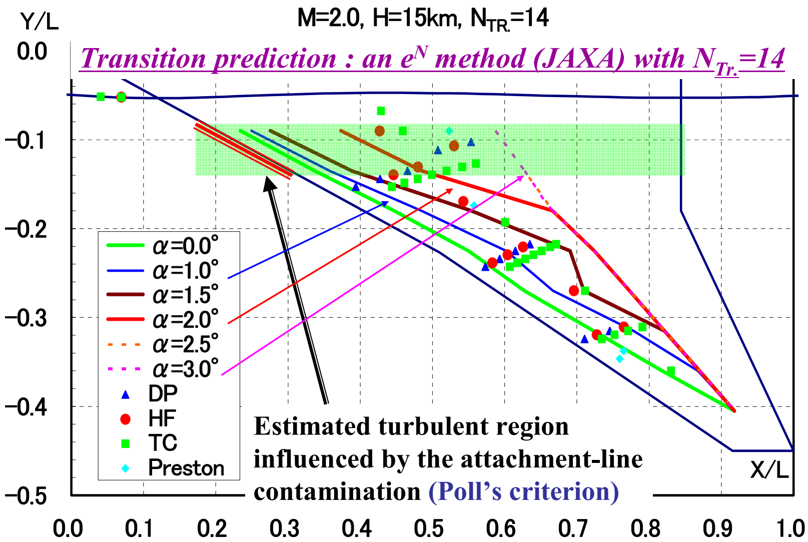

(b) H=15km case

Figure 32. Transition predictions on the wing at flight condition

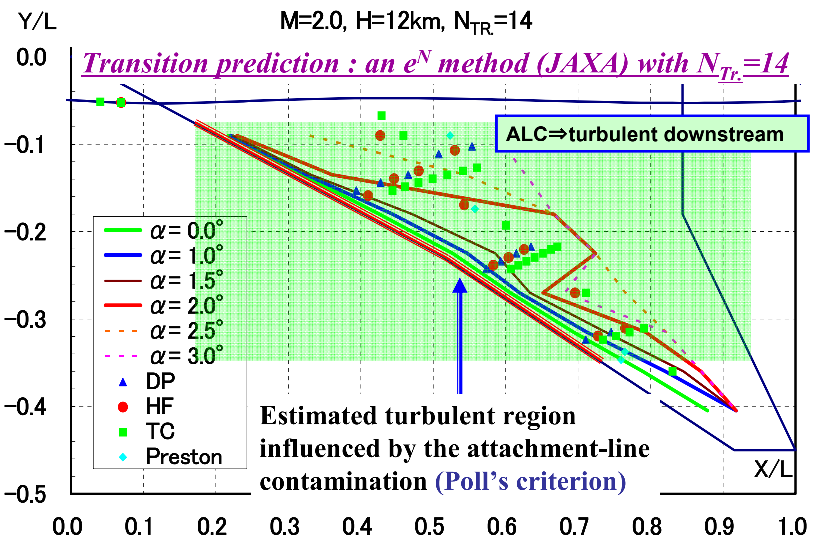

(c) H=12km case

Figure 32. Transition predictions on the wing at flight condition

regions from transition due to attachment-line contamination estimated by Poll's criterion are also shown in Figures 32(b) and 32(c). Since no transition due to the attachment-line contamination was predicted at 18km altitude, a large laminar region was estimated at the design AOA of 2.0 degrees as shown in Figure 32(a). On the other hand, the transition due to the attachment-line contamination along the whole span was predicted at 12km as shown in Figure 32(c).

4.2.2.3. Detailed analysis

This section describes the detailed transition analysis that was carried out in order to analyze the flight test data with a view to validate the NLF wing design concept.

(1) Estimation of the flowfield

(A) Pressure distributions

In order to acquire accurate laminar boundary layer characteristics, JAXA directly calculated them using the NS code at full-laminar condition without any approximations. Here JAXA did not use Kaups and Cebeci method that JAXA mostly used for the estimation of laminar boundary layer profiles in the present cooperative research project. This is because Kaups and Cebeci method is formulated in the polar coordiante system using a conical flow approximation; namely, no pressure gradient exists in radial direction. Although the approximation is considered to be valid for most of high aspect-ratio wings, its validity for low aspect-ratio wings such as SST configuration needs to be confirmed. One of trials by JAXA was described in Ref. 37 and it showed that the conical flow approximation was not effective for the NEXST-1 wing as shown in Figure D-25 of Appendix D.

The flowfield around the NEXST-1 wing at the flight test condition was solved by JAXA's NS code at full-laminar condition upstream x/c=0.8 (local x coordinate on each section) as shown in Figure 33. This is because the calculated laminar flow possibly separate downstream x/c=0.8 and the actual flow at flight is apparently not laminar and does not separate there.

Figure 33 shows a surface pressure contour calculated at the condition near the design point (M=2.02, 1.588-deg AOA, H=18km altitude) using JAXA's NS code. A distinctive feature of the figure is that pressure gradient is almost normal to the streamlines at inner wing region and is nearly parallel to the streamlines at outer wing region. Figure 34(a) shows a comparison between the calculated and measured chordwise pressure distributions. The chordwise pressure distribution generally agrees well except near leading edge (LE) at y/s=0.5 and in the rearward regions at y/s=0.3 and 0.5. Although the former difference is probably due to the influence of the kink located

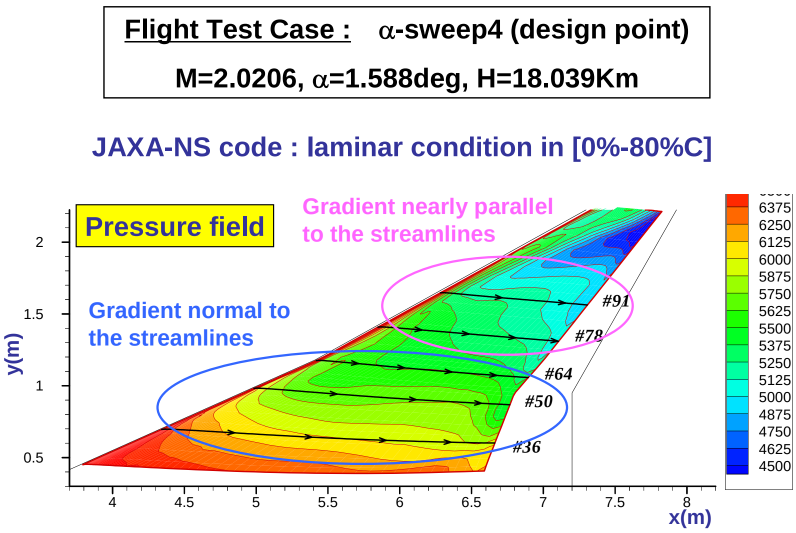

Figure 33. Cp contours by NS analysis with laminar condition

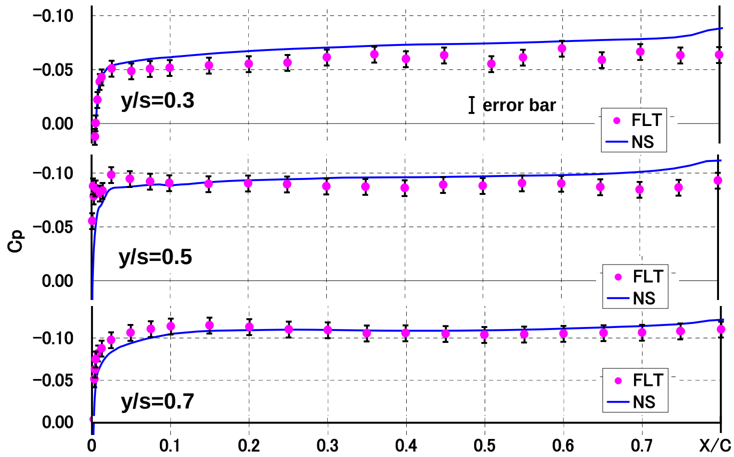

(a) Chordwise pressure distributions
Figure 34. Comparison of NS results with measurement results in flight test

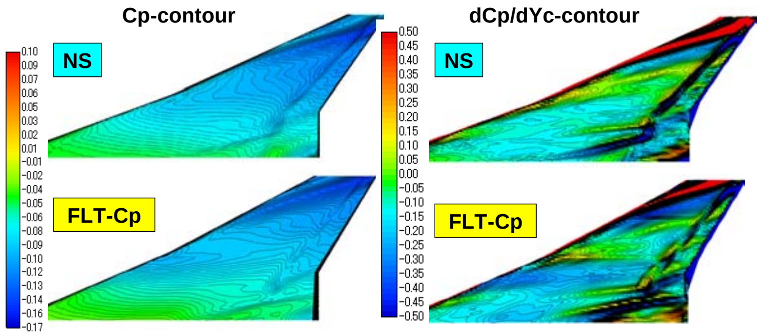

∗ FLT-Cp: surface interpolation of measured chordwise Cp distributions with CATIA smoothing technique

(b) Cp & spanwise pressure gradient contours
Figure 34. Comparison of NS results with measurement results in flight test

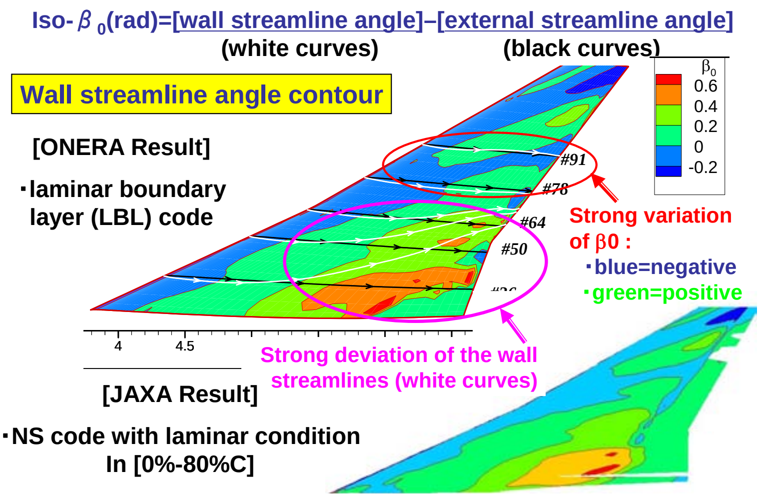

(a) Wall streamline angle contours
Figure 35. Laminar boundary layer results by NS analysis (JAXA) and boundary layer code (ONERA)

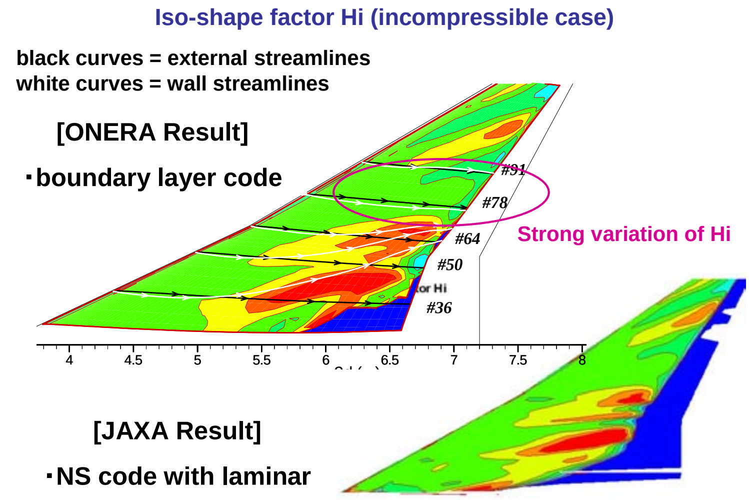

(b) Iso-shape factor contours
Figure 35. Laminar boundary layer results by NS analysis

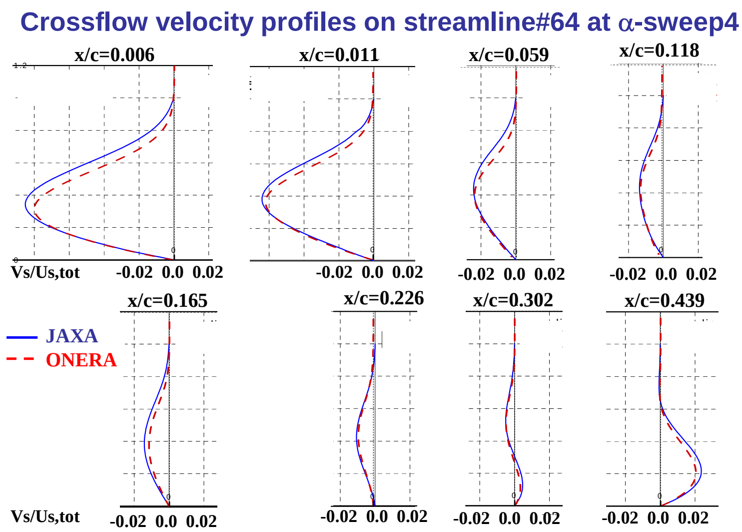

(c) Crossflow velocity profiles
Figure 35. Laminar boundary layer results by NS analysis

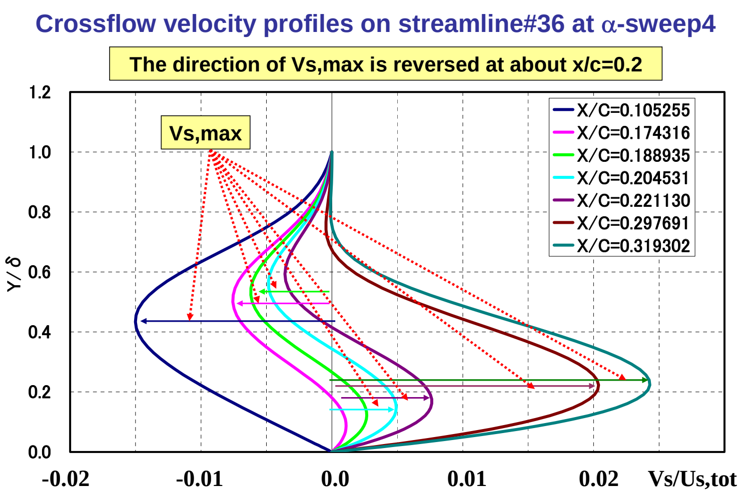

(d) Chordwise growth of crossflow velocity at streamline #36
Figure 35. Laminar boundary layer results by NS analysis

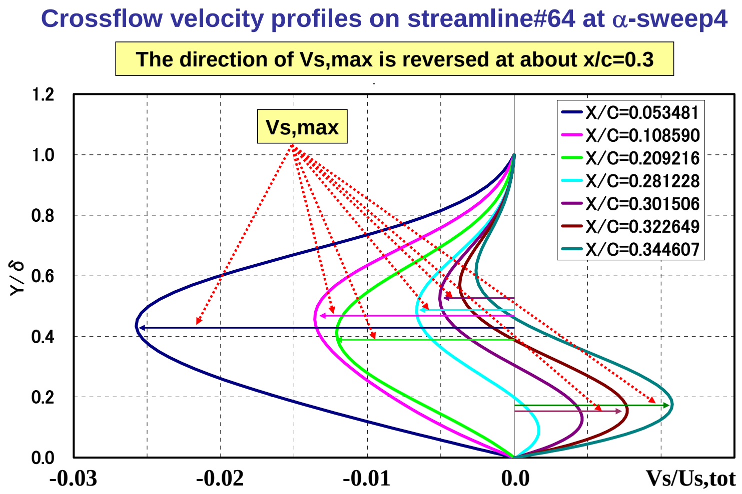

(e) Chordwise growth of crossflow velocity at streamline #64
Figure 35. Laminar boundary layer results by NS analysis

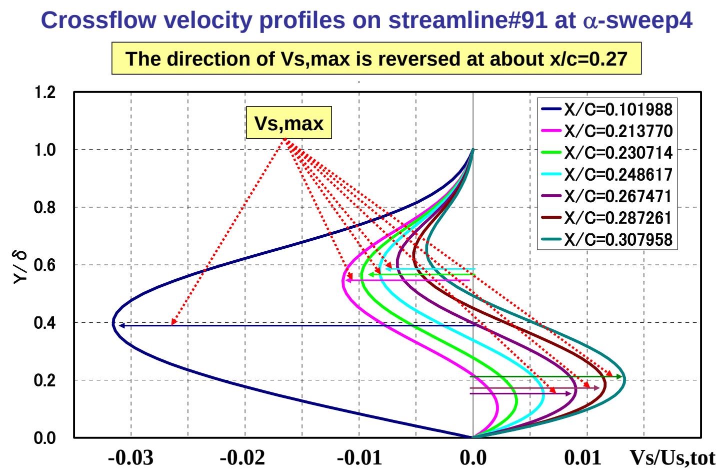

(f) Chordwise growth of crossflow velocity at streamline #91
Figure 35. Laminar boundary layer results by NS analysis

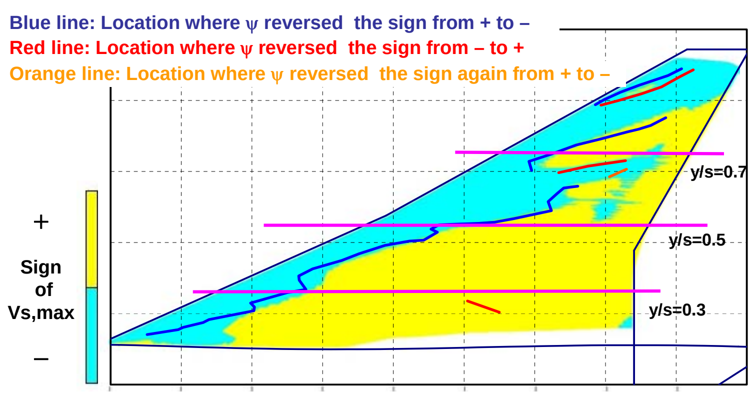

(g) Crossflow velocity information
Figure 35. Laminar boundary layer results by NS analysis

near LE at y/s=0.5, JAXA thinks the main reason of these differences is basically based on the effect of elastic deformation of the wing.

Figure 34(b) shows similar comparisons of nondimensional spanwise gradient and pressure contours. JAXA estimated the contours for the whole wing surface, from the measured chordwise pressure distributions at 10 spanwise stations, 5 stations each on the upper and lower surface of the wing, using a surface fitting function of CATIA that interpolates surface contours using a least square method. Here, dCp/dYc in Figure 34(b) means spanwise pressure gradient. There is a slight difference between the calculated and measured spanwise gradient contours. The difference may generate some differences in the crossflow distribution and may affect an agreement between the measured and calculated transition characteristics.

(B) Laminar boundary layer information

Figure 35(a) shows a comparison of wall-streamline angle contours calculated by ONERA and JAXA. Here the angles are plotted as β_0, which is a difference between the wall streamline and the external streamline angles. ONERA calculated them using the laminar boundary layer (LBL) code based on the calculated pressure distribution by JAXA and JAXA calculated them just using the NS code. Both contours by ONERA and JAXA look fairly similar. Typical wall streamlines and external streamlines are shown in white and black lines, respectively. The wall streamlines strongly deviate outward from the external ones in the mid- and inner regions. On the other hand, though a little deviation is observed in the outer region, the sign of β_0 frequently changes between negative and positive ones, which are respectively shown as blue and green surfaces, respectively. These trends are due to the pressure gradients; it was normal to the streamlines in the mid- and inner regions and was nearly parallel to the streamlines in the outer region as shown in the Figure 33.

Figures 35(b) shows similar comparison of iso-shape factor contours based on the incompressible definition of this parameter. Both contours by ONERA and JAXA look fairly similar.

Comparisons of crossflow velocity profiles in the mid-region calculated by ONERA and JAXA are shown in Figure 35(c). Both profiles have good agreement even in the mid-region, which is not easy to calculate with the presence of the kink. Chordwise changes of the crossflow velocity profiles in the inner, mid- and outer regions are shown in Figures 35(d), 35(e) and 35(f), respectively. The directions of maximum crossflow (C-F) velocities are reversed around x/c=0.2-0.3 in all of the figures. Figure 35(g) shows that the chordwise locations where the propagation angle Ψ changed its sign are in fairly good agreement with the ones where maximum crossflow velocity reversed its direction. This fact is probably important for understanding transition phenomenon dominated by C-F instability.

(2) Stability analysis and comparison with flight tests

Figure 36 shows comparisons of chordwise distributions of propagation direction angles of the disturbance at the frequency of 10kHz between ONERA and JAXA. The results calculated by the previous code of JAXA shown in green line agrees well with ONERA's code upstream x/c=0.15 but is quite different from that by ONERA downstream. The cause of this was investigated thoroughly and turned out to be due to the difference in the search area of Ψ as mentioned in the section 4.2.1.(3); while JAXA searched just for positive Ψ, ONERA searched for both positive and negative Ψ. JAXA's code was improved and the calculated results shown in blue line have much better agreement with that of ONERA. Figures 37(a)~37(c) show comparisons of the propagation directions for all the frequencies. ONERA and JAXA agree very well.

Figures 38(a)~38(c) show chordwise distributions of maximum crossflow velocity $V_{s,max}$ and amplification rate α_i along several streamlines, both of which were calculated by JAXA. The Figure 38(a) shows that the magnitudes of $V_{s,max}$ and α_i strongly correlate ($\alpha_i < 0$, amplified). The sign of V_s changes around x/c=0.2 i.e. V_s has zero magnitude there, which is quite close to the location of the minimum amplification rate. Figures 39(a)~39(c) summarize the effect of the correction

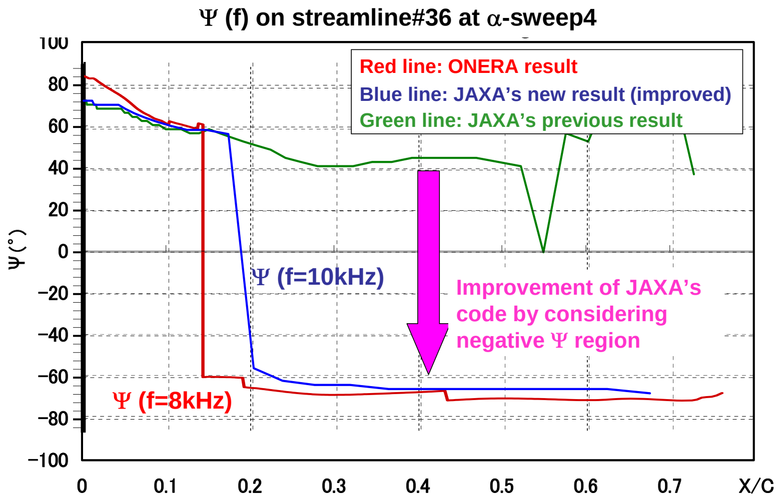

Figure 36. Improvement of JAXA's stability code

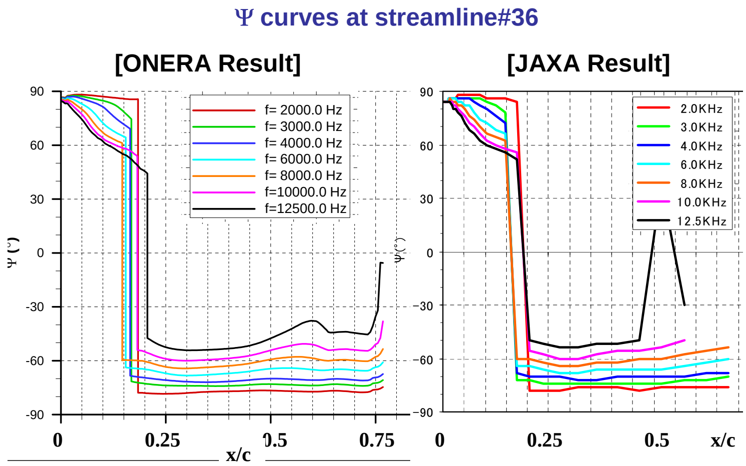

(a) Streamline #36
Figure 37. Comparison of propagation direction

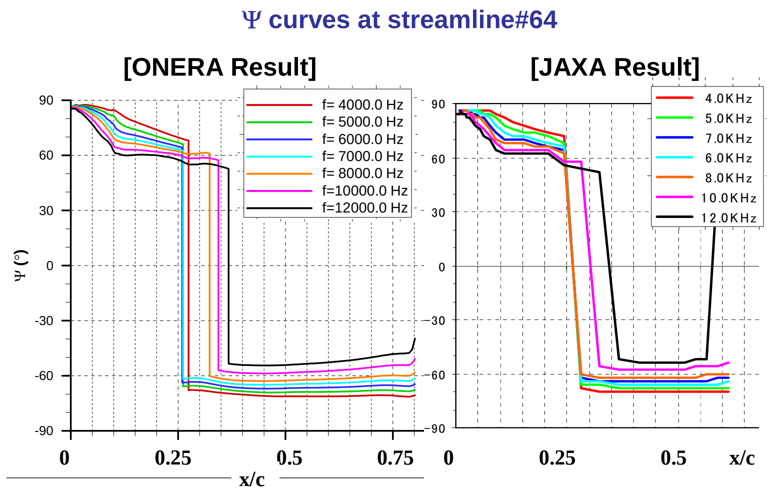

(b) Streamline #64
Figure 37. Comparison of propagation direction

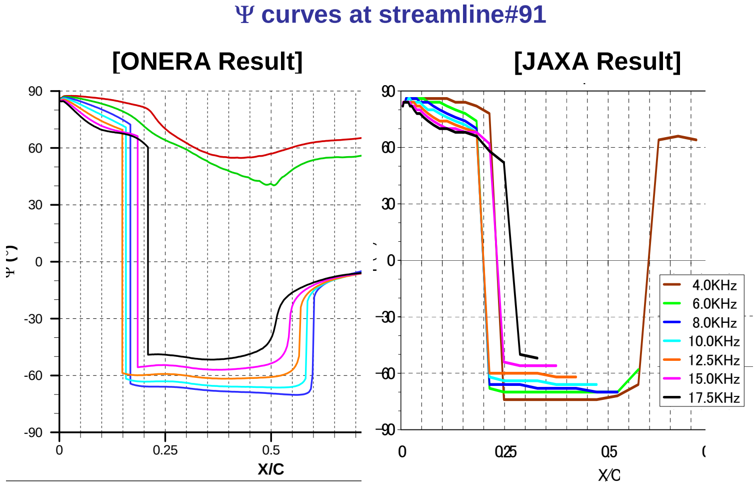

(c) Streamline #91

Figure 37. Comparison of propagation direction

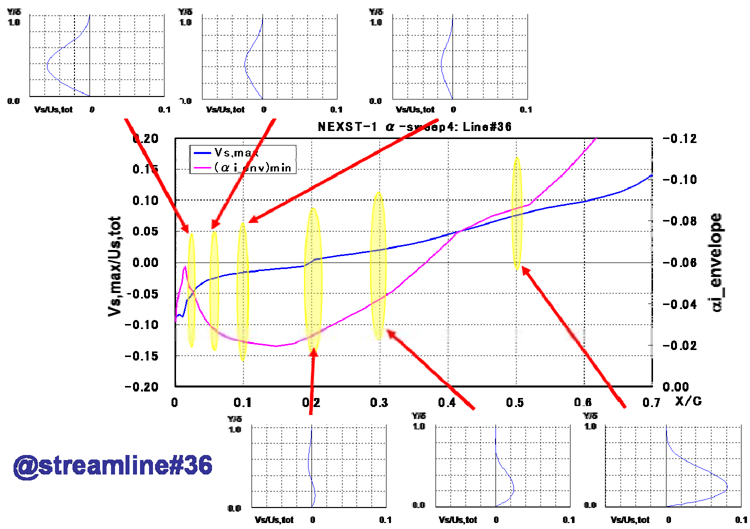

(a) Streamline #36

Figure 38. Relation of maximum crossflow velocity and α_i

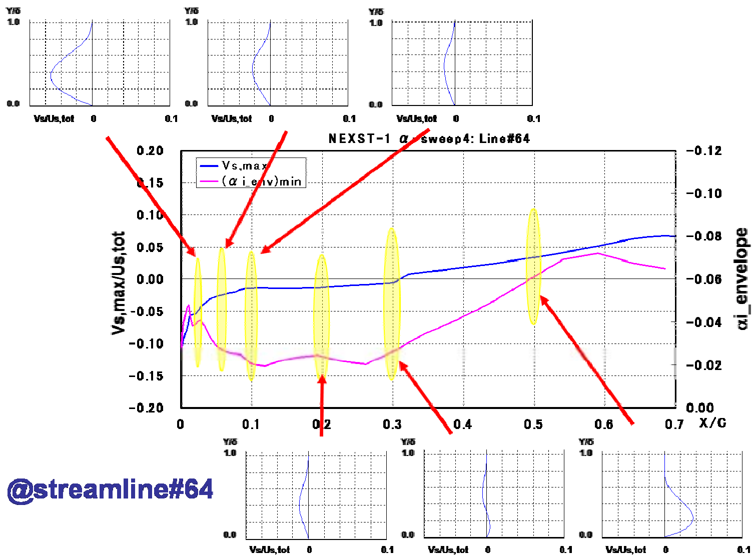

(b) Streamline #64

Figure 38. Relation of maximum crossflow velocity and α_i

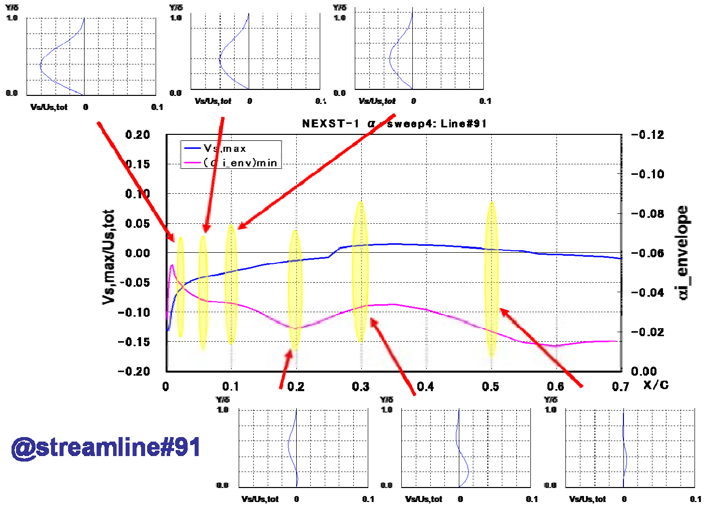

(c) Streamline #91
Figure 38. Relation of maximum crossflow velocity and αi

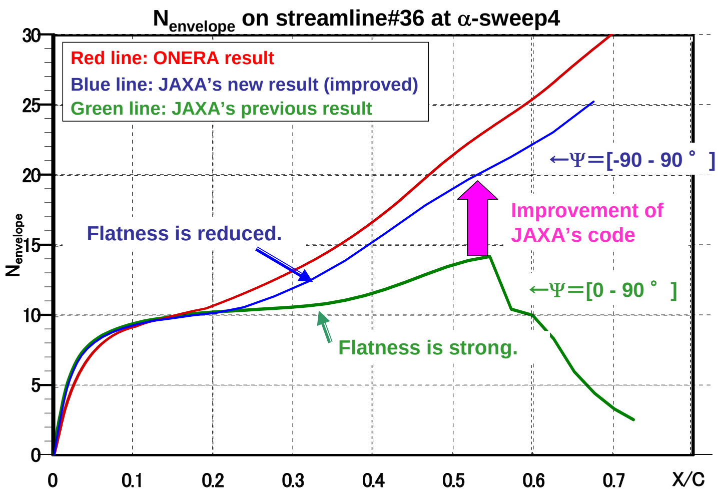

(a) Nenvelope on Streamline #36
Figure 39. Improvement effect of JAXA's stability code

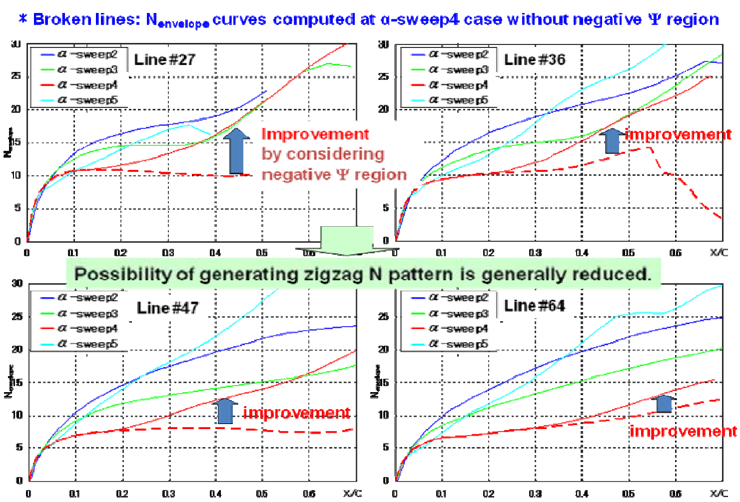

(b) Nenvelope on Streamline #27, 36, 47, 64
Figure 39. Improvement effect of JAXA's stability code

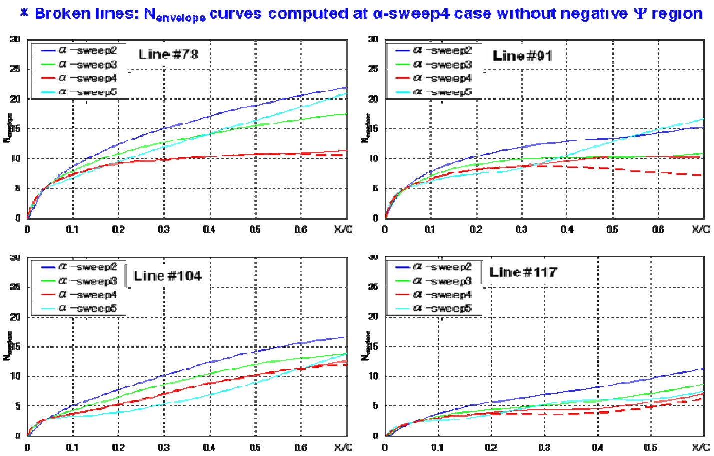

(c) Nenvelope on Streamline #78, 91, 104, 117

Figure 39. Improvement effect of JAXA's stability code

in the improved code of JAXA. While an N envelope curve calculated by JAXA's previous code was almost flat, that by the improved code monotonically increases in a similar manner as ONERA's curve as shown in the Figure 39(a). Since the estimated transition location is defined as the intersection point of the N envelope curve and a constant N line parallel to x-axis, the previous nearly flat N envelope tend to generate “zigzag” patterns in the transition location distribution as shown in Figure D-39 of Appendix D. Thus, the possibility of “zigzag” pattern is reduced by the improved N envelope. Figure 39(b) shows improved N envelopes in the inner wing at different AOA. All of them clearly show the effect of the improvement in JAXA's code. The Figure 39(c) shows that there is little difference between the N envelopes calculated by the previous and the improved code in the outer region; this is in accordance with the trend that the difference between the maximum positive and negative $V_{s,max}$ is small in the region as shown in the Figure 38(c).

Figures 40(a)~40(c) show comparisons of stability analysis results of the typical streamlines between ONERA and JAXA (Both using the envelope methods). The results by ONERA and JAXA are quite similar. The N values that give the best correlations with the measured results are plotted in the figure. The N values by ONERA and JAXA agree fairly well though the former is a little smaller than the latter.

Figures 40(a)~40 (c) also include measured transition location (X_{T_exp}) estimated from the transition detection data which are summarized in Table 3. Note that the reference chord length in ONERA's analysis is slightly different from that in JAXA's analysis. This difference was based on the following fact; ONERA's results were plotted along the external streamline, but JAXA's results were plotted along the line with y/s=constant at the same x-wise transition location as described in Table 3. Therefore, non-dimensional transition location is different in both N curves. According to the information of measured transition location, N criterion value that corresponds to the transition location was around 16 in the inner region, around 10 in the mid-span region, and about 8 to 9 in the outer region as shown in Figure 40(a)~(c). This means that there was no universal value for the N criterion on the NEXST-1 NLF wing at flight test condition. The reason of this is an open question.

However, one possible candidate of the reason for the much smaller N value in the outer region is a larger influence of surface roughness. The measurement of the surface roughness revealed that its magnitude was nearly constant for the whole wing. Since the boundary layer thickness is thinner in the outer region, the influence of the surface roughness is larger there. The important role of roughness in the outer wing region is confirmed by the fact that C-F instability is dominant in this part of the wing. This is because the receptivity of C-F instability towards surface roughness is much larger than that of T-S instability which is

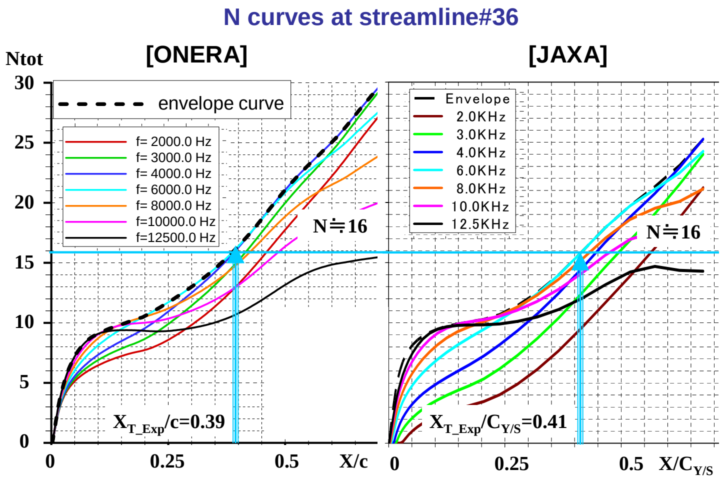

(a) Streamline #36

Figure 40. Comparison of stability results on NEXST-1 wing at flight test condition

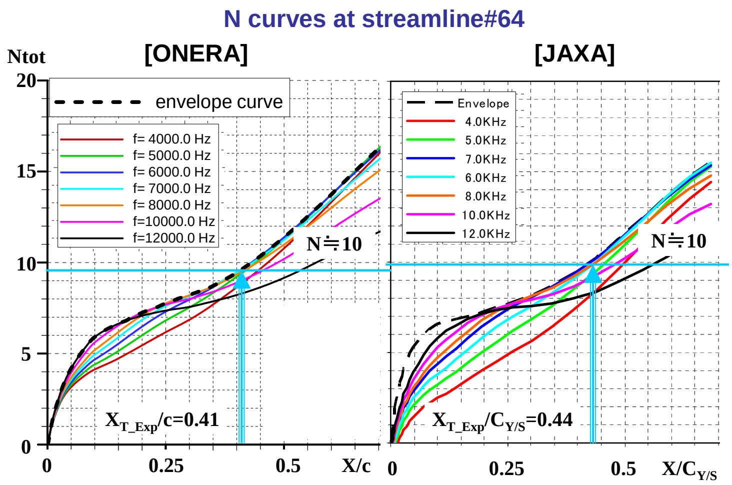

(b) Streamline #64

Figure 40. Comparison of stability results on NEXST-1 wing at flight test condition

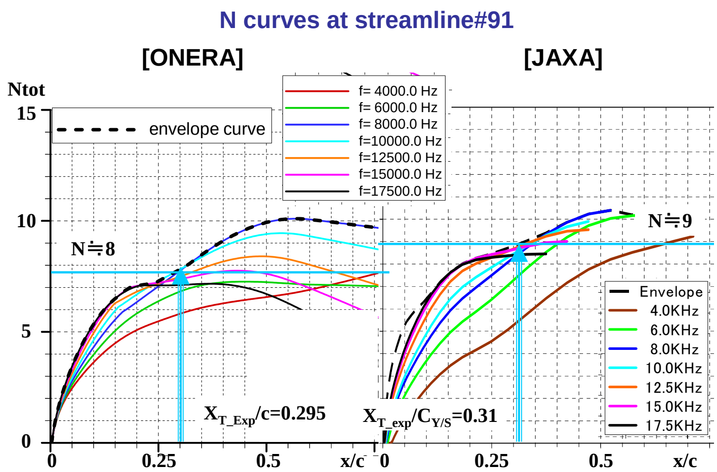

(c) Streamline #91

Figure 40. Comparison of stability results on NEXST-1 wing at flight test condition

Table 3. Measured transition location and corresponding N value

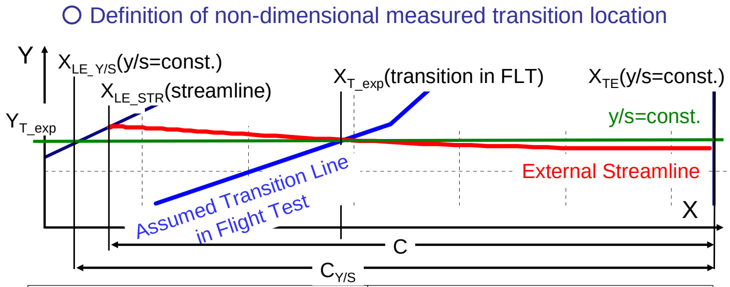

JAXA				ONERA			
Streamline	#36	#64	#91	Streamline	#36	#64 kink	#91
$X_{LE\_Y/S}$(m)	4.2108	5.2727	6.2255	X_{LE_STR} (m)	4.3419	5.4182	6.2825
$C_{Y/S}$(m)	2.9910	2.0259	1.3647	C(m)	2.8416	1.8242	1.256
$X'_{T\_exp}/C_{Y/S}$	0.414	0.441	0.313	X'_{T_exp}/C	0.39	0.41	0.295
X_{T_exp} (m)	5.450	6.166	6.653	X_{T_exp} (m)	5.450	6.166	6.653
Y_{T_exp} (m)	0.6383	1.1112	1.6164	Y_{T_exp} (m)			
Envelope strategy	N_{T_exp}=15.3 Ψ_{T_exp}= -66° F=6000 Hz	N_{T_exp}=9.3 Ψ_{T_exp}= -64° F=7400 Hz	N_{T_exp}=8.5 Ψ_{T_exp}=- 60° F=8200 Hz	Envelope strategy	N_{T_exp}=16 Ψ_{T_exp}= -67° F=6000 Hz	N_{T_exp}=9,6 Ψ_{T_exp}= -67° F=8000 Hz	N_{T_exp}=7.76 Ψ_{T_exp}=- 64° F=10000 Hz

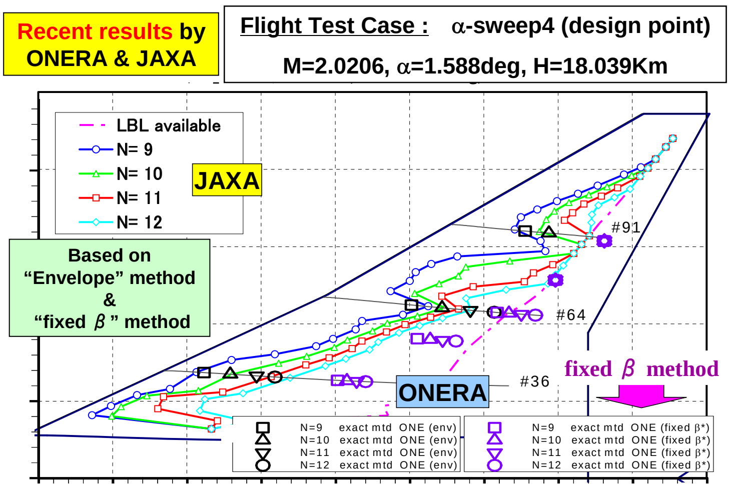

Figure 41. N contours computed with ONERA's and JAXA's e^N methods

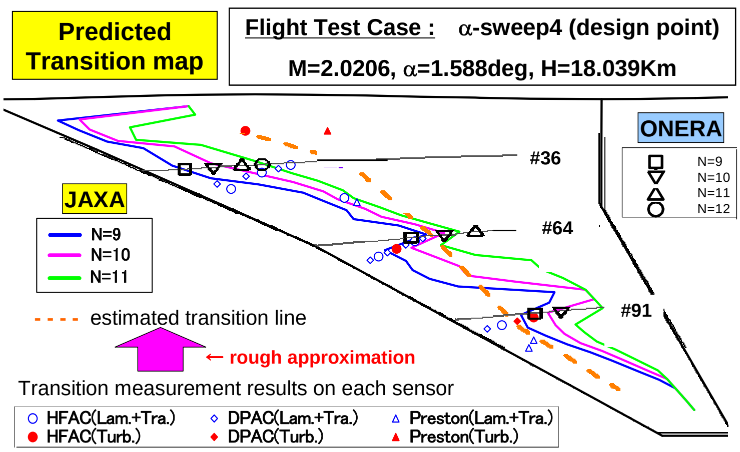

Figure 42. Comparison of predicted transition patterns by both ONERA and JAXA with measurement results

presumably dominant in the inner wing region.

Figure 41 shows the comparison of N contours between ONERA and JAXA. The contours calculated using ONERA's and JAXA's envelope methods agree very well. Here, the contours calculated by the fixed β method are also demonstrated in the figure as a reference. The fixed β method is roughly explained in Appendix D. Some results of the method are shown in Figures D-40(a)~(c) and positions corresponding to the same N value are much rearward than those by the envelope methods, which was to be expected from the comparison in the previous figures.

Figure 42 shows the comparison between the calculated and measured transition patterns. If we assume that transition due to laminar boundary layer instability can be predicted using N=11, there are good agreement between both calculated and measured results at inner wing region. Here the measured results are described by the blue open symbol at each transition detection point. These results are different from the estimated transition line which was roughly approximated. However, it is more reasonable to compare with just the measurement results at detection points because any evidence of laminar region was not obtained in the regions between any two detection points. In conclusion, the transition criterion of N=11 is a useful data for transition prediction.

However, there is a discrepancy between the calculated and measured results in the outer wing region. This might be based on the same origin as the difference that appeared in the comparison of wind tunnel test and transition analysis results at the S2MA test conditions. Presently, the main reasons are assumed to be the influence of surface roughness conditions and a slight difference between measured Cp and NS-based Cp distributions. Therefore, further investigation is required to understand the reason of this discrepancy. For example, as for the latter, laminar boundary layer (LBL) profile should be recalculated from the measured pressure distribution using JAXA's fully-3D LBL code and the boundary layer stability should be reanalyzed.

Finally, as for the transition due to the attachment-line contamination, the present flight test provides meaningful results. As described in Appendix B and as shown in Fig. B-22, transition measurement outputs of the most forward sensor position (15% chordwise location) at low altitude flight condition, namely high Reynolds number condition indicates laminar flow. It implies that there was no transition due to the attachment-line contamination that was predicted by Poll's method described in section 4.1 and this defied our prediction.

5. Concluding remarks

Through the present cooperative research, ONERA and JAXA individually developed the analytical methods for boundary layer transition prediction in supersonic flow. We, ONERA and JAXA, cross-verified their two similar methods and carried out in-depth comparison with the available experimental data measured by JAXA during the period. As a result, the joint research showed the validity of both methods i.e. possibility of transition location prediction. It also pointed out the problems in the methods and summarized research issues for further investigations. A summary of present analysis and results is described in Table 4.

The following insights and information were obtained from the joint research:

1) Verification of the compressible e^N method codes individually developed by ONERA and JAXA
   · Good agreements between the methods of ONERA and JAXA were confirmed;
   · For the following analytical cases: 5-degree half-angle sharp cone, NEXST-1 nose cone and NEXST-1 NLF wing.
   · In order to focus on a thorough comparison of stability computations, laminar boundary layer profiles calculated individually by the two laboratories were thoroughly compared and confirmed to have sufficient degree of agreement in advance.
2) Validation of the compressible e^N method codes
   · The validities of transition prediction methods using appropriate transition criteria were confirmed through comparisons between the measured transition location distributions and

Table 4. Summary of analysis cases and results

Case	α (deg)	ONERA				JAXA			
		Cp	LBL	Tr. Ana	Ntr. Criteria	Cp Ana.	LBL Ana.	Tr. Ana	Ntr. Criteria
Sharp Cone	0	analytic	analytic	eN (ONERA)	6 (@S2MA)	analytic	TUF	eN (JAXA)	
NEXST-1 Nose	0	Euler (JAXA)	3C3D	eN (ONERA)	4.4 (@S2MA) 5.8 (PSE@S2MA)	Euler	TUF	eN (JAXA)	4.5 (@S2MA)
NEXST-1 Nose	2	NS (JAXA)	3C3D	eN (ONERA)	N≒N(JAXA)+1	NS(LBL)	NS(LBL)	eN (JAXA)	8 (CF@FHI) 6 (TS@FHI)
NEXST-1 Wing attachment-line contamination	2	NS(TBL: JAXA)	3C3D	Poll method	no transiiton (H=15km)	NS(TBL)	cylindrical approx.	Poll method	no transiiton (H=15km)
						NS(LBL)	NS(LBL)		possibility at y/s=0.7 (H=15km)
NEXST-1 Wing at S2MA test	2	NS(TBL: JAXA)	3C3D	eN (ONERA)	5.4 (y/s=0.3@S2MA) 3.4 (y/s=0.7@S2MA)	NS(TBL)	Kaups & Cebeci	eN (JAXA)	4.4 (y/s=0.3@S2MA) 2.9 (y/s=0.7@S2MA)
NEXST-1 Wing at Flight test	1.58	NS(LBL: JAXA)	3C3D	eN (ONERA)	16 (y/s=0.3@FLT) 9.6 (y/s=0.5@FLT) 7.8 (y/s=0.7@FLT)	NS(LBL)	NS(LBL)	eN (JAXA)	15.3 (y/s=0.3@FLT) 9.3 (y/s=0.5@FLT) 8.5 (y/s=0.7@FLT)

***Comments**
*LBL: laminar boundary layer, TBL: turbulent boundary layer
*Tr. Ana.: Transition analysis or prediction
*Ntr. Criteria: N-value of transition criteria
*NS(TBL: JAXA): NS-based data with turbulent boundary layer condition provided by JAXA
*3C3D, TUF: names of laminar boundary layer codes of ONERA and JAXA
*PSE: Parabolized stability equation
*TS, CF: Tollmien-Schlichiting instability, crossflow instability

the calculated N-value distributions;

· For the following wind tunnel test cases: 5-degree half-angle sharp cone @ JAXA-TWT1 (via Preston tube technique), NEXST-1 nose cone @ FHI (via infrared (IR) thermography) and NEXST-1 NLF wing @S2MA (via IR and hot-film measurements).

· Future tasks: development of a setting method of N values for transition criteria and creation of its database.

3) Validation of JAXA's design concept of Natural Laminar Flow (NLF) wing

· Detailed analysis on boundary layer transition of NEXST-1 NLF wing using the compressible e^N method was carried out and its NLF effect of the wing on the design point was confirmed.

· The NLF effect of the wing was qualitatively confirmed through validation of the analytical methods by comparing with transition measurements in the S2MA wind tunnel.

4) Investigation of validity of transition criteria for attachment-line contamination

·Application limitation of Poll's criterion was confirmed. (The most forward sensor at 15% chordwise station confirmed laminar boundary layer at 15km altitude against the prediction of full-contamination of attachment line by Poll's criterion. However, a possibility of relaminarization cannot be excluded.)

5) Analysis of boundary layer transition on an axisymmetric body at nonzero angle of attack (AOA)

· An NS-based method of laminar boundary layer (LBL) calculation for complex 3-D flow around an axisymmetric body at nonzero AOA was developed.

· Validation and application limitation of the analytical methods were shown and further research issues were extracted through comparisons with FHI wind-tunnel test results for NEXST-1 nose cone.

The following issue and resolutions are pointed out in the present research; (the resolutions are shown after an arrow "→"):

i) Full analysis on the flight test results of NEXST-1 NLF wing is a task left incomplete (particularly analyses for cases with different AOA than the design AOA).
→ Laminar boundary layer (LBL) profile should be recalculated from the measured pressure distribution using JAXA's fully-3D LBL code and the boundary layer stability should be reanalyzed.

ii) Full analysis on the flight test results of NEXST-1 nose cone is a task left incomplete.
→ LBL profile should be recalculated from the measured pressure distribution using the fully 3-D LBL code and the stability

should be reanalyzed.

iii) In-depth comparison of S2MA wind-tunnel test results of the NLF wing is left incomplete (particularly effects of the difference in the measured and calculated pressure distributions).
→ Two sets of LBL profiles should be recalculated from the measured pressure distribution individually using the fully-3D LBL code and the N-S based LBL code and the stability should be reanalyzed.

iv) In-depth comparison of FHI wind-tunnel test results of the NEXST-1 nose cone is left incomplete.
→ LBL profile should be recalculated from the measured pressure distribution using the fully-3D LBL code and the stability should be reanalyzed.

v) Correlation analysis between the transition prediction and surface roughness of the NLF wing is incomplete.
→ Necessity and research project of parametric study on the correlation should be considered. Validation of a surface coating must be also studied.

vi) Creation of N-value database for transition criteria is incomplete.
→ Acquisition of literature transition data possibly under cooperation between the two laboratories should be sought for.

vii) Logical solution for integral path problem is unfound.
→ The latest research results for stability analysis method should be reconsidered.

Finally, spin-offs from the present cooperative research are summarized:

a) New insights and information on physical mechanisms behind boundary layer transition are obtained through discussions between ONERA and JAXA, including insights on correlation between maximum crossflow velocity and sign change of ψ .

b) Numerous validation example data for supersonic boundary layer transition is accumulated and JAXA's transition prediction code, LSTAB, is vastly improved.

c) ONERA and JAXA shared information on boundary layer transition research in both laboratories with each other.

References

1. Ueda, Y., and Yoshida, K.; "Numerical Study on Optimum Pressure Distribution for Supersonic Natural Laminar Flow Design" (in Japanese), Proc. of the 32nd Fluid Dynamics Conference, Japan Society for Aeronautical and Space Sciences, Tokyo, pp. 271-274, Octo. 2000
2. Arnal, D.; "Boundary layer transition: prediction based on linear theory" , AGARD FDP/VKI Special Course on Progress in Transition Modeling, AGARD Report 793, 3, 1993
3. Sakata, K.; "SST Research Project at NAL" , Proc. of 1st International CFD Workshop on Supersonic Transport Design, Tokyo, pp.1-4, Marc. 1998
4. Ogoshi, H.; "Aerodynamic Design of a Supersonic Airplane Wing – Application of the Natural Laminar Flow Concept to Airfoil" (in Japanese), Proc. of the 47th Nat. Cong. of Theoretical & Applied Mechanics, Janu. 1998
5. Matsushima, K., Iwamiya, T., Jeong, S. and Obayashi, S.; "Aerodynamic Wing Design for NAL's SST Using Iterative Inverse Approach" , Proc. of 1st International CFD Workshop on Supersonic Transport Design, Tokyo, pp.73-78, Marc.1998
6. Srokowski, A.J.; "Mass Flow Requirement for LFC Wing Design" , AIAA-77-1222, 1977
7. Yoshida, K.; "Overview of NAL's Program Including the Aerodynamic Design of the Scaled Supersonic Aircraft" , RTO Educational Notes 4, held at VKI, 15-1~16, 1998
8. Shimbo, Y., Yoshida, K., Iwamiya, T., Takaki, R. and Matsushima, K.; "Aerodynamic Design of the Scaled Supersonic Experimental Airplane" , Proc. of 1st International CFD Workshop on Supersonic Transport Design, Tokyo, pp.62-67, Marc.1998
9. Yoshida, K., Ishida, Y., Noguchi, M., Ogoshi, H. and Inagaki, K.; "Experimental and

Numerical Analysis of Laminar Flow Control at Mach 1.4", AIAA Paper 99-3655, 1999
10. Sugiura, H., Yoshida, K., Tokugawa, N., Takagi, S. and Nishizawa, A.; "Transition Measurements on the Natural Laminar Flow Wing at Mach 2", Journal of Aircraft, vol. 39, no. 6 (2002), pp. 996-1002
11. Fisher, D. F. and Dougherty, N. S. Jr.; "In-Flight Transition Measurement on a 10° Cone at Mach Numbers from 0.5 to 2.0", NASA TP-1971, 1982
12. Herring, H. J. and Mellor, G. L.; "Computer Program for Calculating Laminar and Turbulent Boundary layer Development in Compressible Flow", NASA CR-2068, 1972
13. Okuwa, T., Tokugawa, N, Takagi, S., Yoshida, K. and Ueda, Y.; "Prediction and validation of supersonic boundary layer transition on 10 degrees cone" (in Japanese), Proc. of The 29th NAL Workshop on "Investigation and Control of Boundary layer Transition", NAL-SP-56, 2002
14. Sawada, H.; "Status of Improving NAL 0.2 m Supersonic Wind Tunnel for Quiet Flow" (in Japanese), Journal of Wind Engineering, vol.78 (1999), pp. 69-72
15. Makino, Y.; "Near-field Inverse Design using Gradient-based Optimization with Continuous Adjoint Sensitivity Analysis," *CFD Journal*, vol. 12, no. 3, pp. 509-515, 2003.
16. Owen, F. K.; "Transition Experiments on a Flat Plate at Subsonic and Supersonic Speeds, AIAA Journal, vol. 8, no. 3 (1970), pp.518-523
17. Koshioka, Y. and Shiozawa, N.; "Freestream Turbulence Measurement Results in Fuji Heavy Industries Ltd. High-speed Wind Tunnel" (in Japanese), Proc. of 46th Wind Tunnel Conference, Tokyo, 1996
18. Beckwith, I. E.; "Development of a High Reynolds Number Quiet Tunnel for Transition Research", AIAA Journal, vol.13, No.3 (1975)
19. Sugiura, H., Tokugawa, N. and Ueda, Y; "Boundary layer transition on an axisymmetric body at incidence at Mach 1.2", AIAA Journal, vol. 44, no. 5 (2006), pp. 973-980
20. King, R. A.; "Three-Dimensional Boundary layer Transition on a Cone at Mach 3.5," Experiment in Fluids, vol. 13 (1992), pp. 305-314
21. Stetson, K. F.; "Mach 6 Experiments of Transition on a Cone at Angles of Attack," Journal of Spacecraft, vol. 19, no. 5 (1982), pp. 397-403
22. Krogmann, P.; "An Experimental Study of Boundary layer Transition on a Slender Cone at Mach 5," AGARD CP 224, 1977
23. Doggett, G. P., Chokani, N., and Wilkinson, S. P.; "Effect of Angle of Attack on Hypersonic Boundary layer Stability," *AIAA Journal*, Vol. 35, No. 3 (1997), pp. 464-470
24. Ladoon, D. W. and Schneider, S. P.; "Measurements of Controlled Wave Packets at Mach 4 on a Cone at Angle of Attack," AIAA paper 98-0436, 1998
25. Ivanov, A. R.; "The Effect of the Bluntness and the Half-Angles of a Cone on the Turbulent Transition of a Boundary layer at Free-Stream Mach 6" (in Russian), Uchenye Zapiski, Vol. 15, No. 3 (1984), pp.132-135
26. McDevitt, J. B. and Mellenthin, J. A.; "Upwash patterns on Ablating and Nonablating Cones at Hypersonic Speeds," NASA TN D-5346, 1969
27. Arnal, D., Kufner, E., Oye, I. and Iran, Ph.; "PROGRAMME TRP TRANSITION: computational results for transition prediction", Study Note 7, 1996
28. Reed, H. L., Kimmel, R., Schneider, S. and Arnal, D.; "Drag prediction and transition in hypersonic flow", AIAA paper 1997-1818, 1997
29. Poll, D.I.A.; "Boundary layer transition on the windward face of space shuttle during re-entry", AIAA paper 85-0899, 1985
30. Arnal, D.; "Boundary layer Transition: Prediction, Application to Drag Reduction", AGARD FDP/VKI Special course on Progress in Transition Modeling, AGARD Report 793, 5, 1993
31. Kaups, K. and Cebeci, T.; "Compressible Laminar Boundary layers with Suction on Swept and Tapered Wings", Journal of Aircraft, Vol.14, No.7 (1977), pp.661-667
32. Yoshida, K. and Makino, Y.; "Aerodynamic Design of Unmanned and Scaled Supersonic

Experimental Airplane in Japan", ECCOMAS 2004, Jyväskylä, July 2004
33. Jeong S., Matsushima K., Iwamiya T., Obayashi S. and Nakahashi K. ; "Inverse Design Method for Wings of Supersonic Transport", AIAA 98-0602, 1998
34. Yoshida, K., Makino Y., and Shimbo Y.; "An Experimental Study on Unmanned Scaled Supersonic Experimental Airplane", AIAA-2002-2842, 2002
35. Joslin, R.D.; "Aircraft Laminar Flow Control", Annual Review of Fluid Mechanics, Vol.30 (1998), pp.1-20
36. Rech, J. and Leyman, C. S.; "A Case Study By Aerospatiale and British Aerospace on The Concorde", AIAA Professional Study Series, 1981
37. Ueda, Y. Ishikawa, H. and Yoshida, K.; "Three Dimensional Boundary Layer Transition Analysis in Supersonic Flow Using A Navier-Stokes Code", ICAS 2004-2.8.2, 2004
38. Murakami, A. and Stanewsky E.; "Boundary layer Transition on Swept Cylinders at Hypersonic Speeds", AIAA Journal, Vol.34, No.4 (1996), pp.649-654.
39. Ohnuki, T., Hirako, K. and Sakata K.; "National Experimental Supersonic Transport Project", ICAS2006-1.4.1, 25th ICAS, Hamburg, Sept. 2006
40. Fujiwara, T., Hirako, K. and Ohnuki T.; "Flight Plan and Flight Test Results of Experimental SST Vehicle NEXST-1", ICAS2006-6.2.1, 25th ICAS, Hamburg, Sept. 2006
41. Machida, S., Yoshida, K. and Ohnuki, T.; "Supersonic Flight Testing of Unmanned Experimental Airplane for Next-generation SST", AIAA-2007-854, 2007
42. Kwak, D.-Y., Yoshida, K., Ishikawa, H. and Noguchi, M.; "Flight Test Measurements of Surface Pressure on Unmanned Scaled Supersonic Experimental Airplane", AIAA-2006-3483, 2006
43. Tokugawa N. and Yoshida K.; "Transition Detection on Supersonic Natural Laminar Wing in the Flight", AIAA-2006-3165, 2006
44. Tokugawa, N. Kwak, D.-Y. and Yoshida, K.; "Transition Measurement System of Experimental Supersonic Transport "NEXST-1", ICAS2006-6.2.1, 25th ICAS, Hamburg, Sept. 2006
45. Tokugawa, N. Kwak, D.-Y. Yoshida, K. and Ueda, Y.; "Transition Measurement of Natural Laminar Flow Wing on Supersonic Experimental Airplane (NEXST-1)", Journal of Aircraft, Vol. 45, no. 5 (2008), pp.1495-1504
46. Yoshida K.; "Aerodynamic Design of the NEXST-1 Airplane", (in Japanese), Concluding Report of Flight Test Data Analysis on the Supersonic Experimental Airplane (NEXST-1), JAXA-SP-08-008 (2008), pp.45-72

Appendixes

A. Summary of aerodynamic design of the NEXST-1 airplane

JAXA promoted the unmanned and scaled supersonic experimental airplane program called National EXperimental Supersonic Transport (NEXST) program from 1997 to 2006 with a view to develop new design technologies for next generation SST. Figure A-1 shows the structure of the NEXST program. At the beginning, JAXA planned two flight test vehicles, a non-powered vehicle called NEXST-1 and a jet-powered vehicle called NEXST-2. However, the first flight test of the NEXST-1 airplane failed on July 14th, 2002 and the NEXST-2 project was canceled afterwards. Therefore, just the aerodynamic design of the NEXST-1 airplane[32] is described in this Appendix.

In general, supersonic drag consists of pressure drag and friction drag. Pressure drag is divided into lift-dependent drag and wave drag due to volume. Figure A-2 shows aerodynamic design concepts to reduce the drag of NEXST-1 airplane at supersonic speed. The objectives of the flight test are to validate the effects of those design concepts at flight condition. The concepts consist of a warped wing with a cranked arrow planform to reduce lift-dependent drag, an area-ruled body to reduce wave drag due to volume, and a supersonic natural laminar flow (NLF) wing to reduce friction drag.

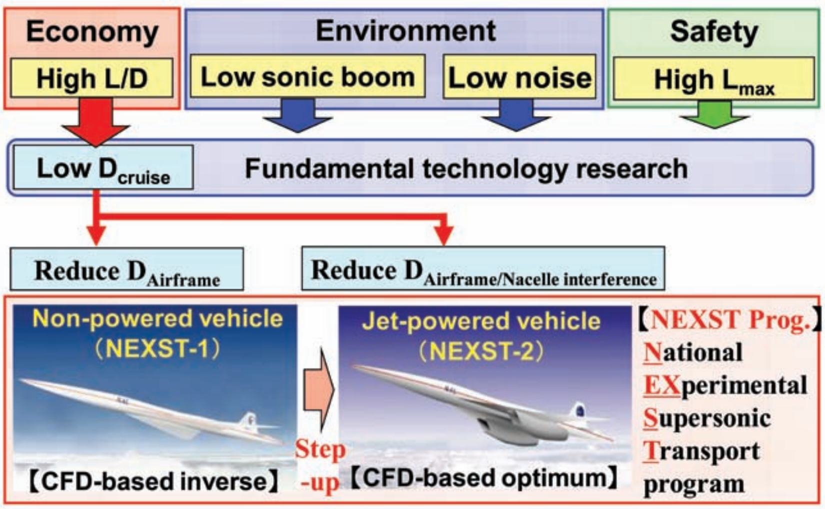

Figure A-1. Structure of JAXA's scaled supersonic experimental airplane program

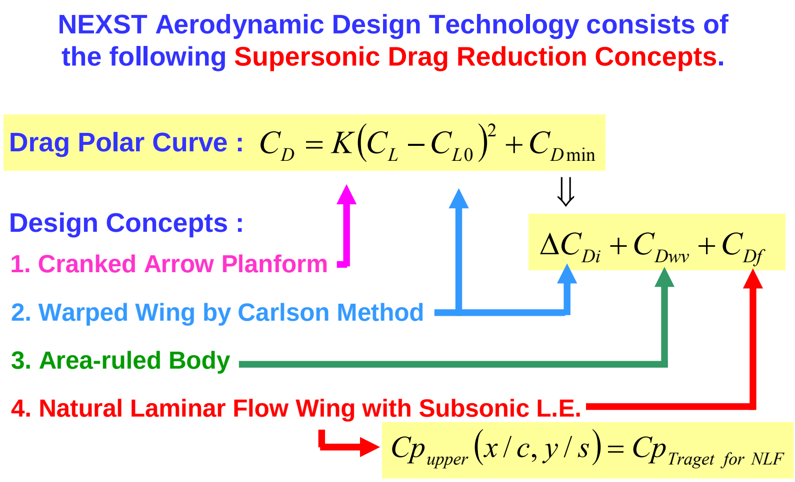

Figure A-2. NEXST-1 aerodynamic design concepts to reduce supersonic drag

In the NEXST program, JAXA developed a new CFD-based design method for a real size SST with 300 passengers and applied it to an 11%-scale experimental airplane as shown in Figure A-3. The figure also shows representative airframe parameters of Concorde, a real size next generation SST, and JAXA's NEXST-1 airplane.

Figure A-4 shows the final aerodynamic configuration of the NEXST-1 airplane designed using JAXA's original CFD-based inverse design method with the four drag reduction concepts described in Figure A-2.

There were two design phases in the aerodynamic design of the NEXST-1 airplane. In the first phase, in order to reduce the pressure drag of the NEXST-1, the initial configuration was designed by applying three design concepts based on supersonic linear theory, namely an arrow planform, a warped wing, and an area-ruled body. Figure A-5 shows principal results of planform and warp design studies. In these studies, Carlson's method[32] based on supersonic lifting surface theory was applied. JAXA selected 8 most effective arrow planforms from about 100 candidates and eventually designed an optimum warped wing with the most effective arrow planform as indicated by “H8-1st baseline”

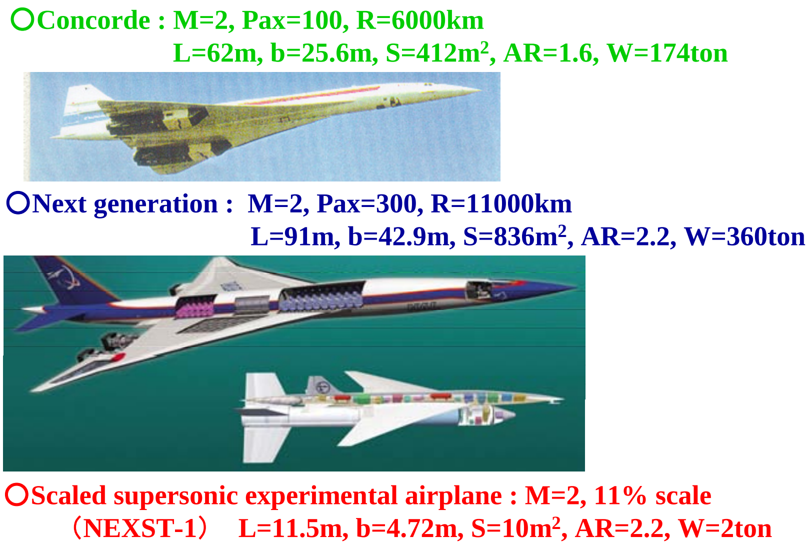

Figure A-3. Concorde and Next generation SST

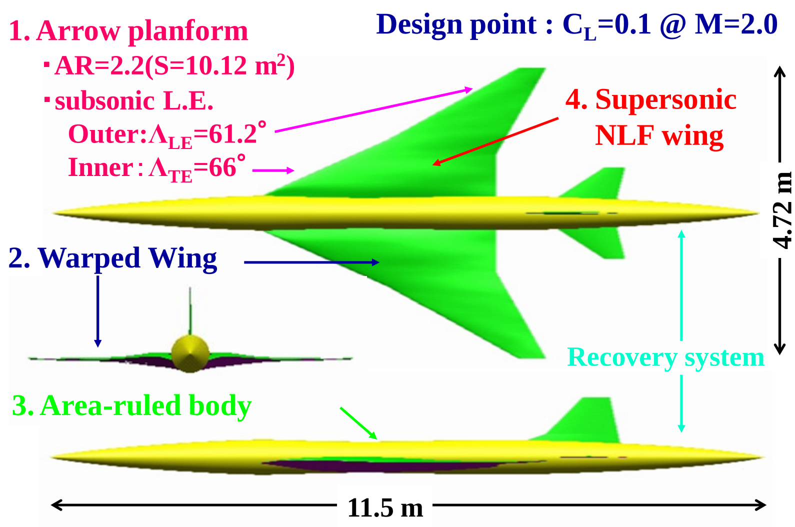

Figure A-4. Aerodynamic design configuration of the NEXST-1 airplane

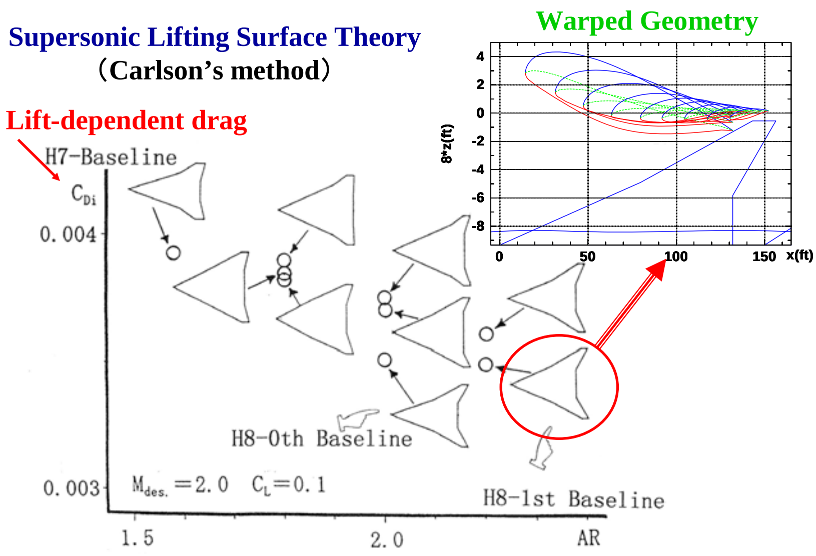

Figure A-5. Planform and Warp Design Results

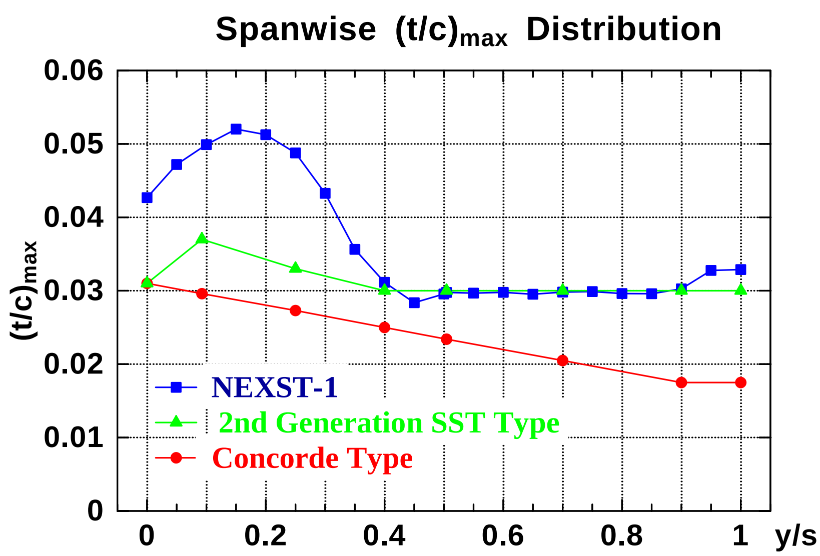

Figure A-6. Spanwise thickness ratio distribution

in Figure A-5.

Both chordwise and spanwise thickness distributions are generally required in warp design study. As for chordwise thickness distribution, JAXA used a family with similar thickness distribution as NACA 4-digit series. As for spanwise thickness distribution, JAXA used maximum thickness ratio distribution of a 2nd generation SST shown in Figure A-6. In the figure, the spanwise thickness ratio distribution of the final configuration is also demonstrated as a reference. The NLF wing design tended to be thicker in the inner region and thinner in the outer region. However, JAXA did not impose any constraint for thickness for the inner region but imposed a strong constraint to keep 3% thickness for the outer region.

Then, an area-ruled body design was applied to the "H8-1st baseline" after assuming a reference fuselage, horizontal and vertical tails. Figure A-7 shows supersonic cross sectional area distribution of each component of the NEXST-1 airplane. Here since the cross section of Sears-Haack body generates minimum wave drag due to volume, the

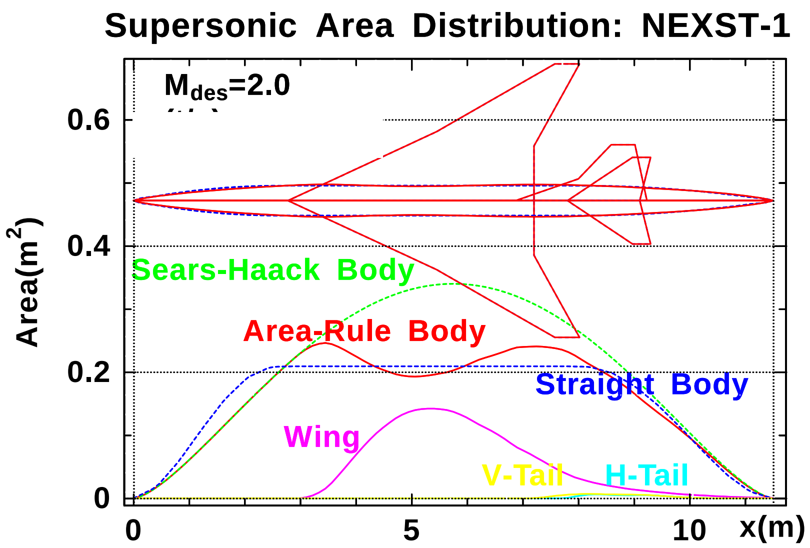

Figure A-7. Supersonic cross sectional area distribution of area-ruled body

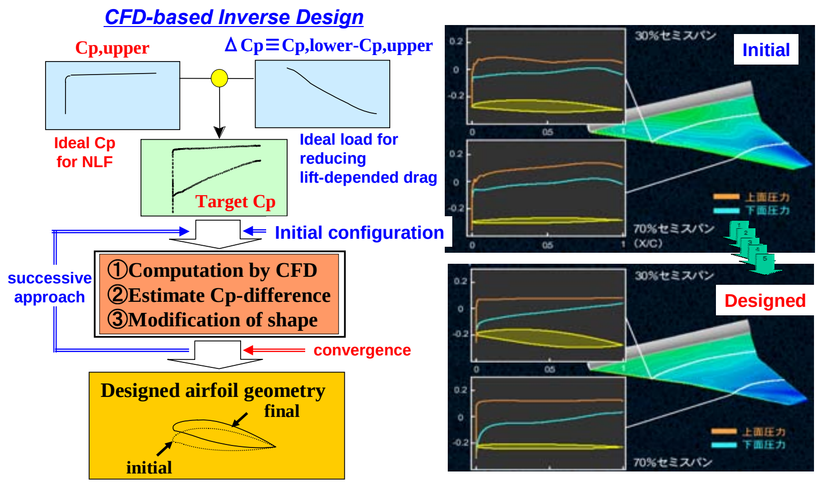

Figure A-8. CFD-based inverse design method

cross section of the area–ruled body was estimated based on the present Sears-Haack body.

In the second design phase, JAXA developed an original CFD-based inverse design method[33] incorporating JAXA's original NLF wing design concept[4] and applied the method to the aerodynamic design of NEXST-1 airplane. Figure A-8 shows flow a chart of the design procedure[32]. This method consists of two parts; first, an optimum pressure distribution with large laminar region over the wing is derived as a target and then, a configuration that has the optimum pressure distribution is designed using both CFD analysis and shape modification method based on supersonic lifting surface theory. To begin the application of this method, an initial configuration was required. JAXA used the above mentioned baseline configuration which was designed considering pressure drag reduction concepts.

Figure A-9 shows a comparison of the target pressure distributions with the estimated pressure distributions using CFD analysis on the final iterated configuration. As shown in the figure, both target and estimated pressure distributions were in fairly good agreement, which was the reason for determining the final iteration. This final

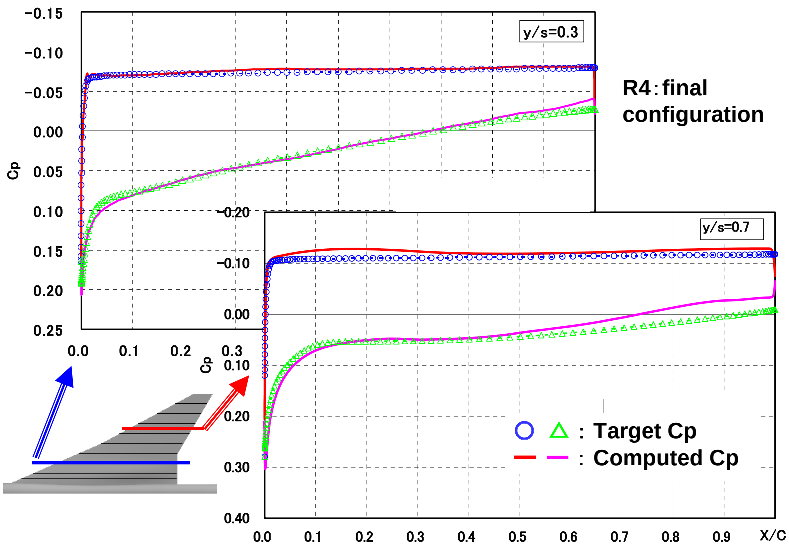

Figure A-9. Final result by the inverse design

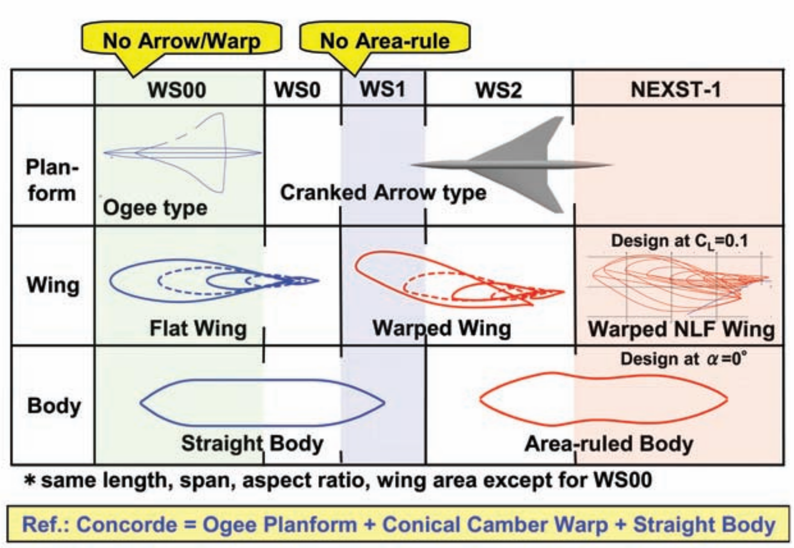

Figure A-10. Each configuration on each drag reduction concept

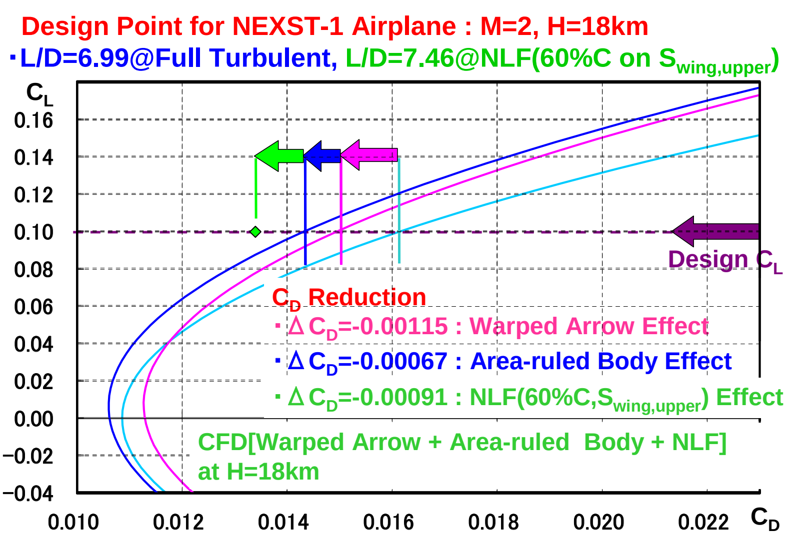

Figure A-11. Each design effect on each drag reduction concept configuration design is shown in the Figure A-4.

Figures A-10 and A-11 show each configuration design corresponding to a drag reduction concept and quantitative reduction effect on each configuration estimated using CFD analysis. By comparing with a reference configuration designed with a flat ogee planform and no area-ruled body, effects of the drag reduction concepts were estimated as follows; about 12 counts reduction due to the effect of Carlson's warped and cranked arrow wing, about 7 counts reduction due to the effect of the area-ruled body, and about 9 counts reduction due to the effect of the NLF wing.

Figures A-12 and 13 show principal results of experimental validation[10] for the pressure distribution to delay transition and for rearward movement of transition at design AOA respectively. There were good agreement between the CFD-estimated Cp and measured Cp distributions, and JAXA qualitatively confirmed remarkable rearward movement of transition by detecting surface temperature using IR camera. These results suggested the validity of the final configuration design.

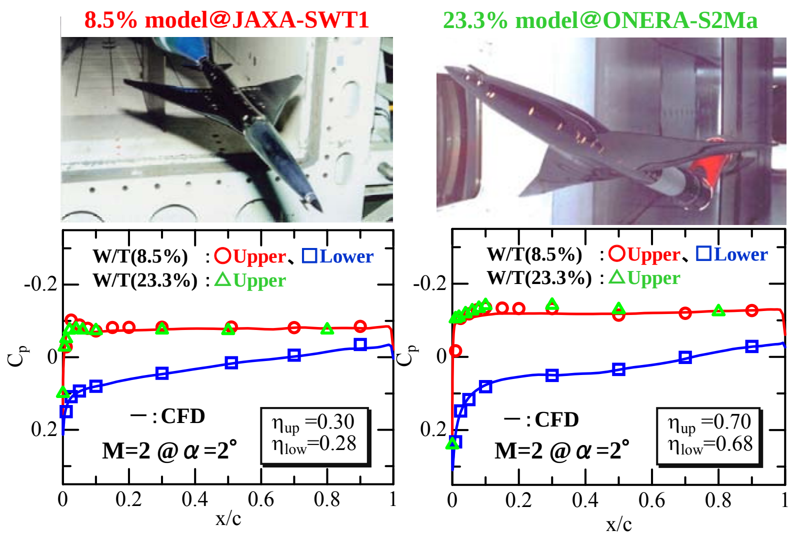

Figure A-12. Experimental validation for pressure distribution

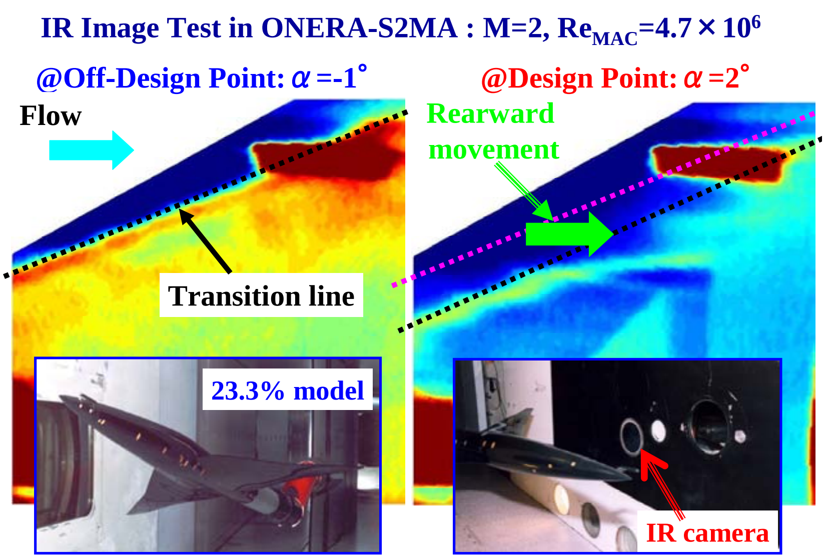

Figure A-13. Experimental validation for transition characteristics

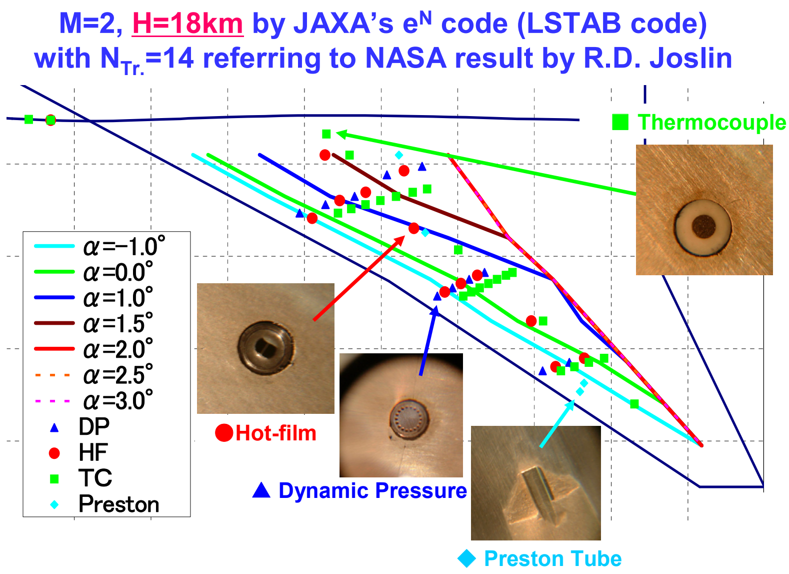

Figure A-14. Transition prediction on the NEXST-1 wing at flight test condition I

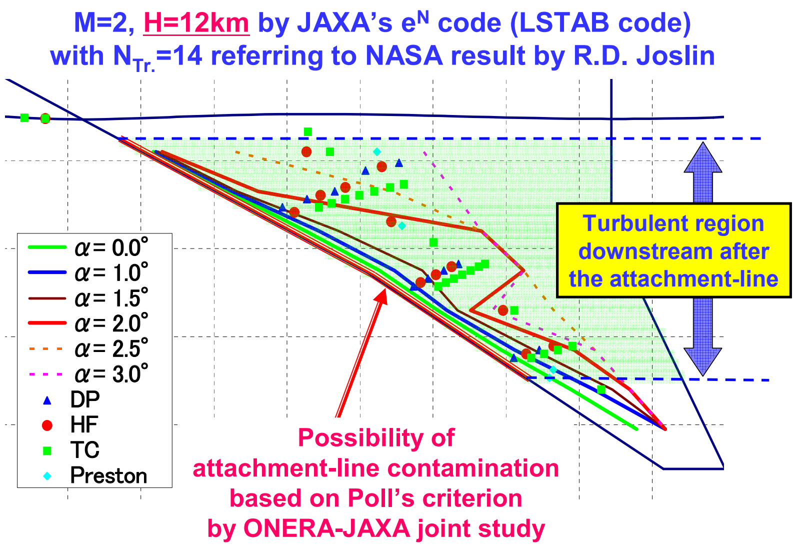

Figure A-15. Transition prediction on the NEXST-1 wing at flight test condition II

Figures A-14 and 15 show predicted transition locations using JAXA's e^N method (see Appendix D) with the N=14 transition criterion[35] and Poll's method[29, 38], which are described in the present report in detail.

Figures A-16, 17 and 18 show an outline of the aerodynamic measurement system of the NEXST-1 airplane[42-45]. Especially, Figures 16 and 17 show transition measurement system. JAXA applied four kinds of transition detection methods, namely hot-film (HF) sensors, dynamic pressure (DP) sensors, Preston tubes and thermocouples as shown in Figure A-16.

Figure A-19 shows an outline of aeroelastic design procedure for the real NEXST-1 airplane. JAXA used NASTRAN to estimate elastic deformation due to inertia and aerodynamic loads. For convenience, the aerodynamic shape of the NEXST-1 airplane was called AS, and real elastic deformed shape was called ES. Figure A-20 shows a comparison of the AS and the ES including several additional parts such as a camera, air data sensor (ADS), total temperature (TAT) sensor, and so on. Figure A-21 shows a photograph

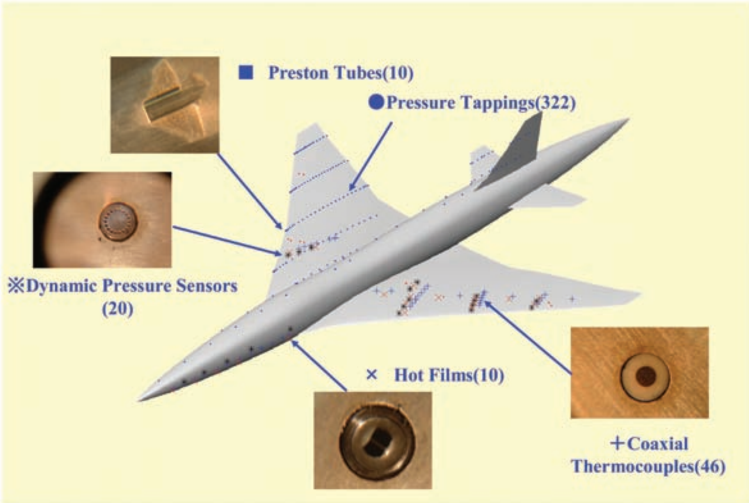

Figure A-16. Aerodynamic measurement system of the NEXST-1 airplane

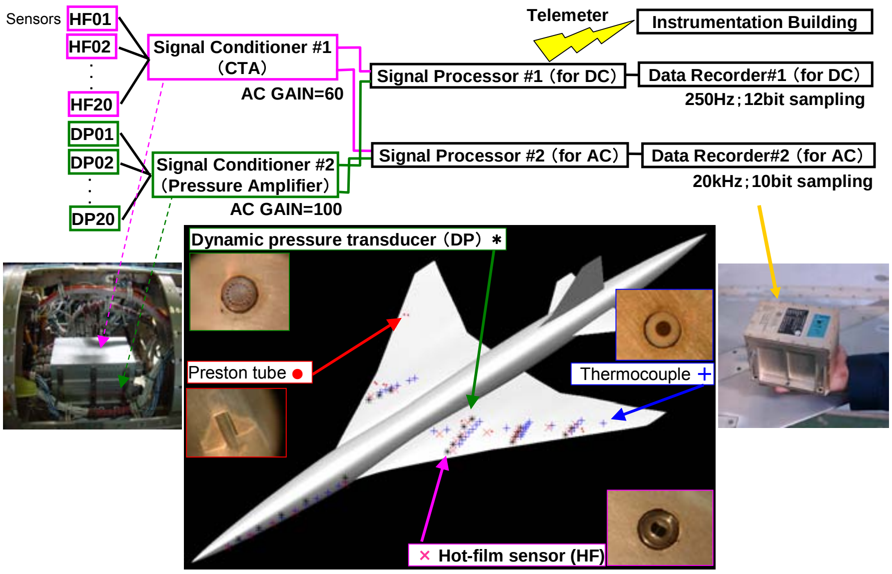

Figure A-17. Transition measurement system of the NEXST-1 airplane

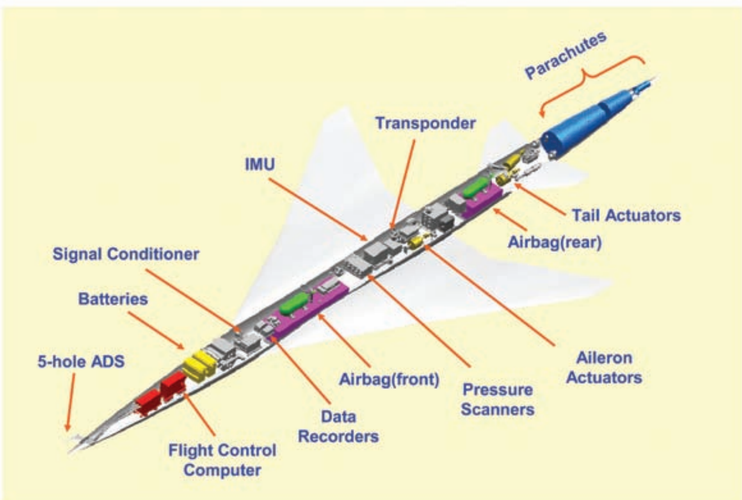

Figure A-18. Aerodynamic measurement and flight control systems of the NEXST-1 airplane

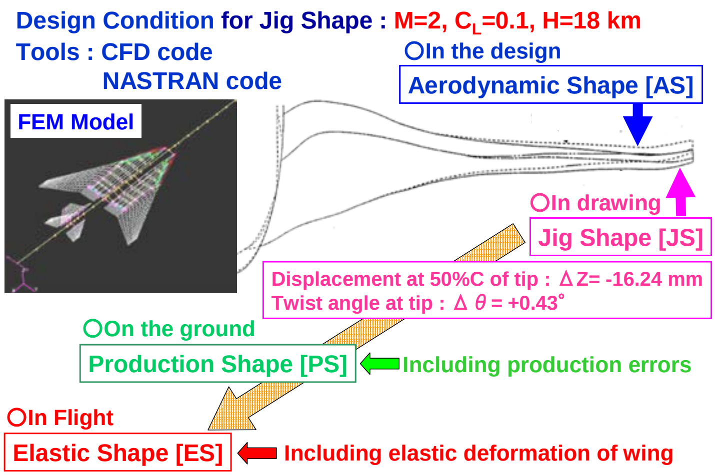

Figure A-19. Aircraft design structure with elastic deformation

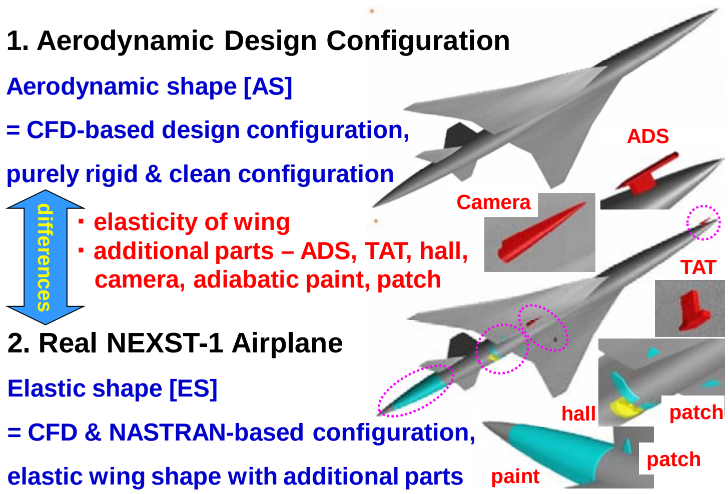

Figure A-20. Aerodynamic design and real design of the NEXST-1 airplane

Figure A-21. Real NEXST-1 airplane configuration

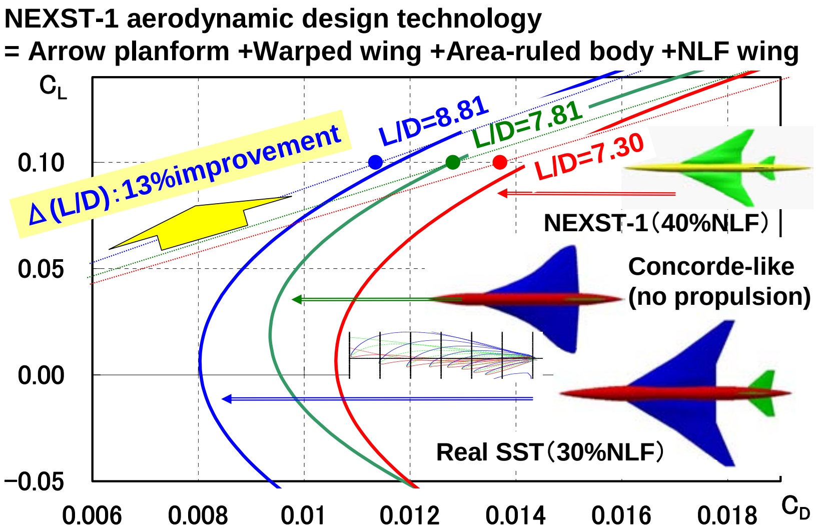

Figure A-22. Design effect of NEXST-1 aerodynamic design technology on a real SST design

of the JAXA's real NEXST-1 airplane.

After the detailed analysis of the flight test data, about 40% laminarization over the wing was roughly confirmed at design point. This validation leads to estimation of quantitative effect of the NEXST-1 aerodynamic design technology when it is applied to a real size SST design. Finally JAXA estimated about 13% improvement of lift-to-drag ratio (L/D) at design lift condition[46)], compared with the lift-to-drag ratio of a Concorde-like configuration without any propulsion system, as shown in Figure A-22. Note that the Concorde-like configuration was not real and was a JAXA's original configuration designed using JAXA's design method under several assumptions[36)].

B. Summary of principal flight test results[40-46)]

Figure B-1 shows the flight test plan[39)] of the NEXST-1 airplane conducted on October 10th, 2005. Figures B-2, B-3 and B-4 show several photographs at its preparation and launch phases. Figure B-5 shows the flight trajectory[40)] and Figure B-6 shows several photographs of the NEXST-1 airplane in flight.

Figure B-7 shows two aerodynamic measurement test phases which are AOA-sweep test phase around 18 km altitude and Reynolds number-sweep (Re-sweep) test phase from 13 to 12 km altitude[41)]. In the AOA-sweep test phase, six AOAs were planned to obtain drag polar characteristics of the NEXST-1 airplane, In the Re-sweep test phase, the airplane was maintained to have design lift coefficient condition, namely 0.1.

Figure B-8, B-9, B-10, B-11 and B-12 show time history of principal flight condition data, namely Mach number, altitude, Reynolds number, AOA, and normal acceleration. Figure B-12 particularly demonstrates relation between forces and measured acceleration data.

Figure B-13 shows a comparison of measured lift data with CFD analysis results on lift characteristics under AOA change. From this figure, good agreement

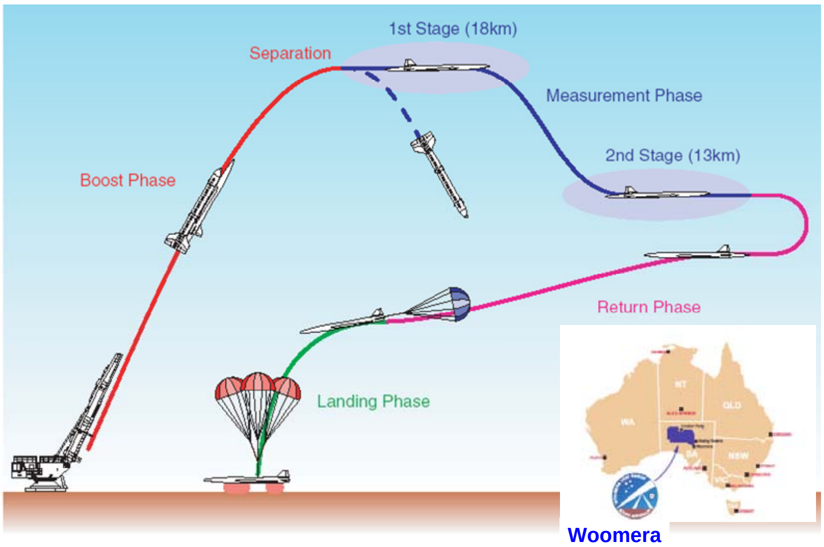

Figure B-1. Flight test plan of the NEXST-1 airplane

Figure B-2. Preparation for flight test of the NEXST-1 airplane

Figure B-3. Lift-off at launch (part I)

Figure B-4. Lift-off at launch (part II)

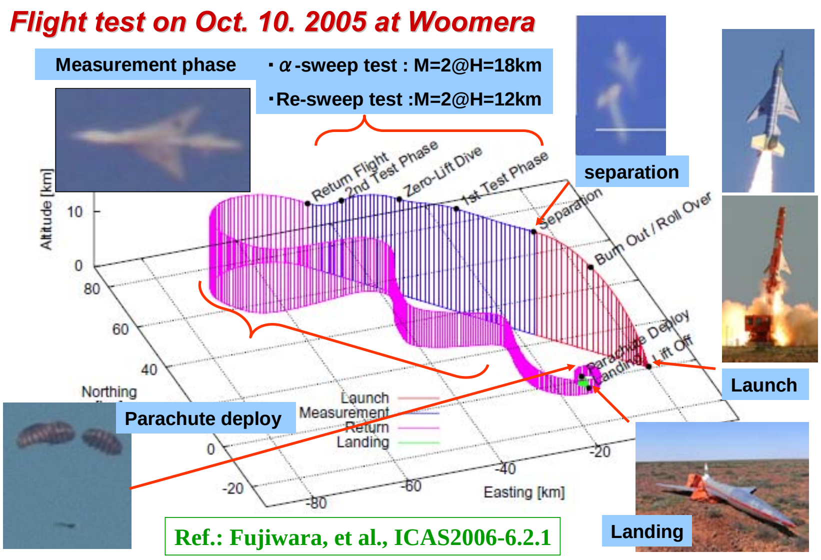

Figure B-5. Flight trajectory of the NEXST-1 airplane

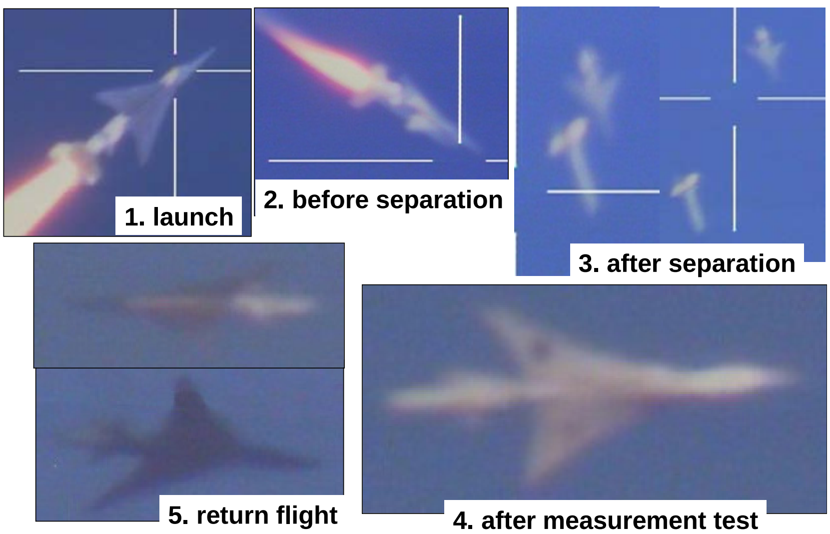

Figure B-6. Each flight status

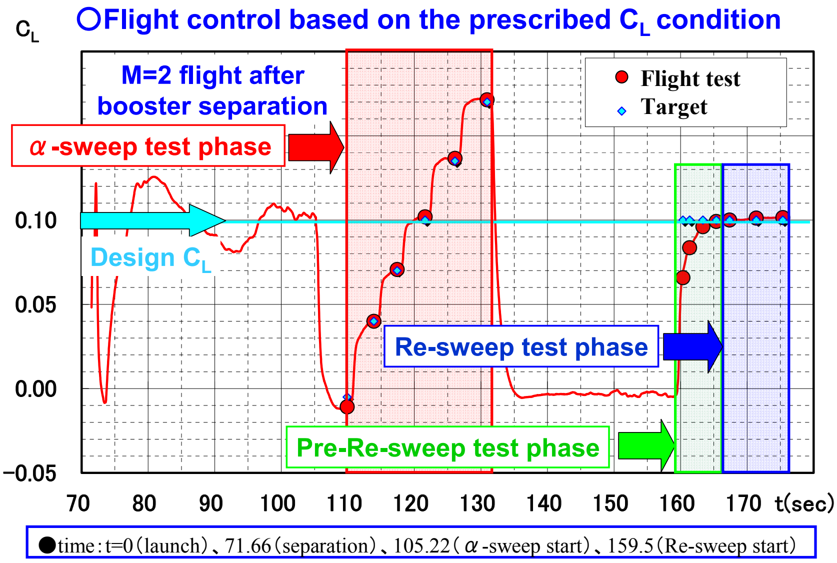

Figure B-7. Aerodynamic measurement test phases

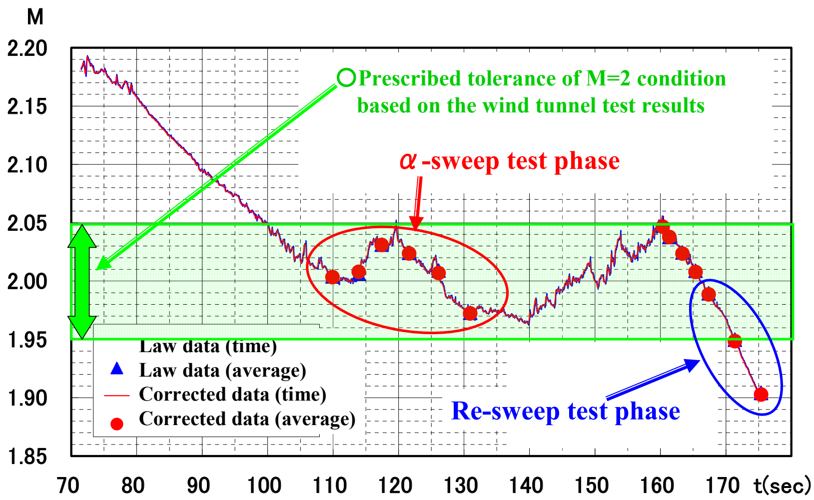

Figure B-8. Flight data I – Mach number

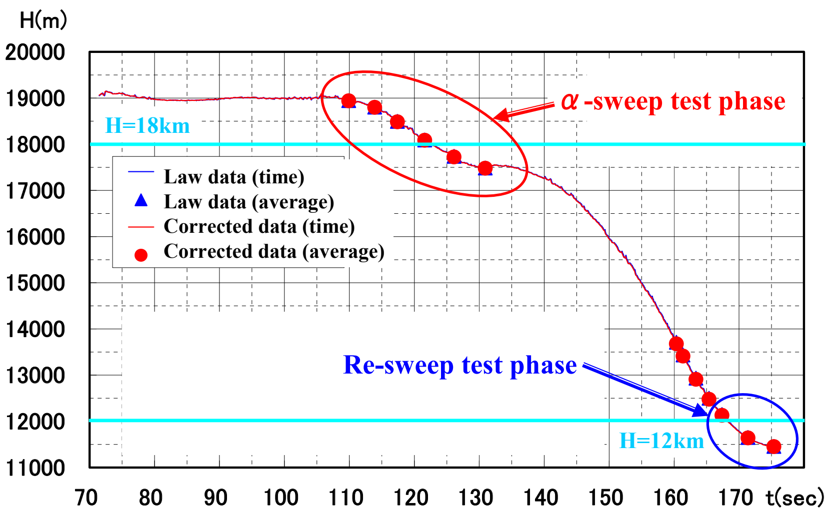

Figure B-9. Flight data II – altitude

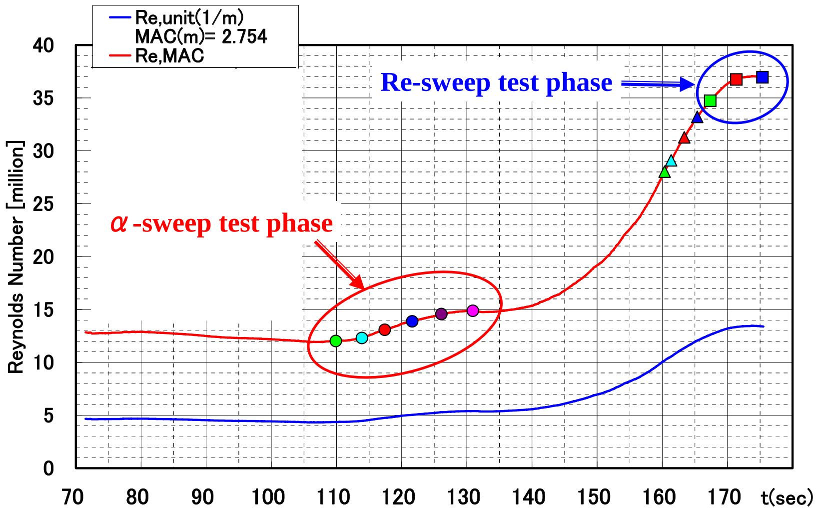

Figure B-10. Flight data III – Reynolds number

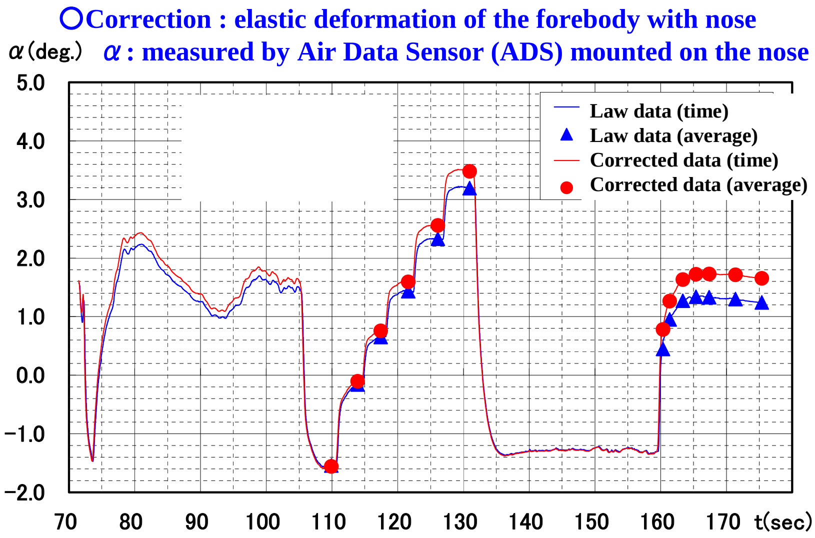

Figure B-11. Flight data IV – angle of attack

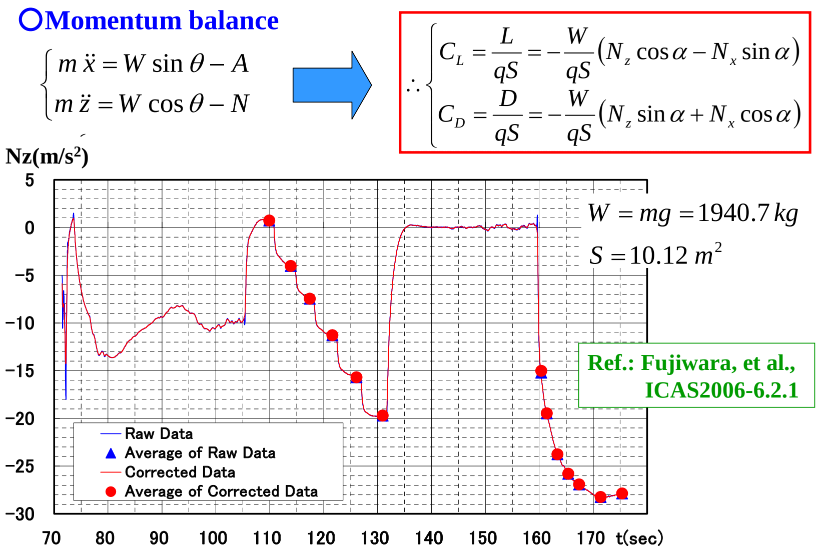

Figure B-12. Data analysis method for force characteristics

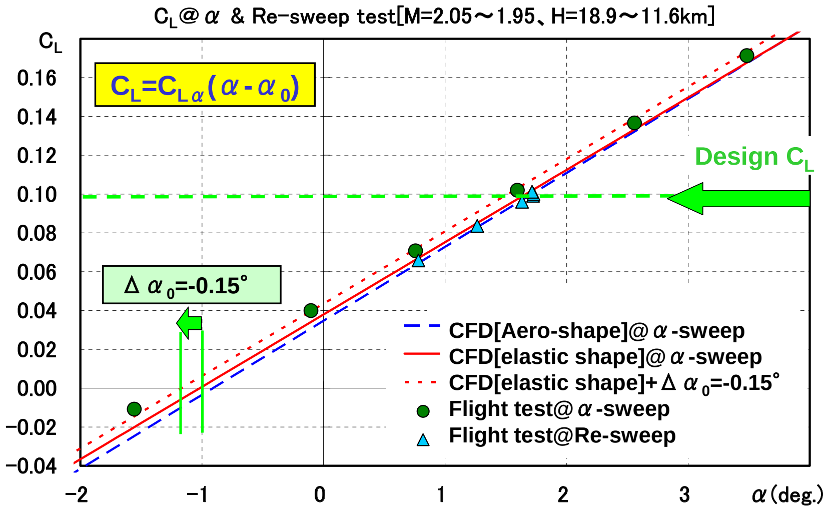

Figure B-13. Flight data analysis I - lift characteristics

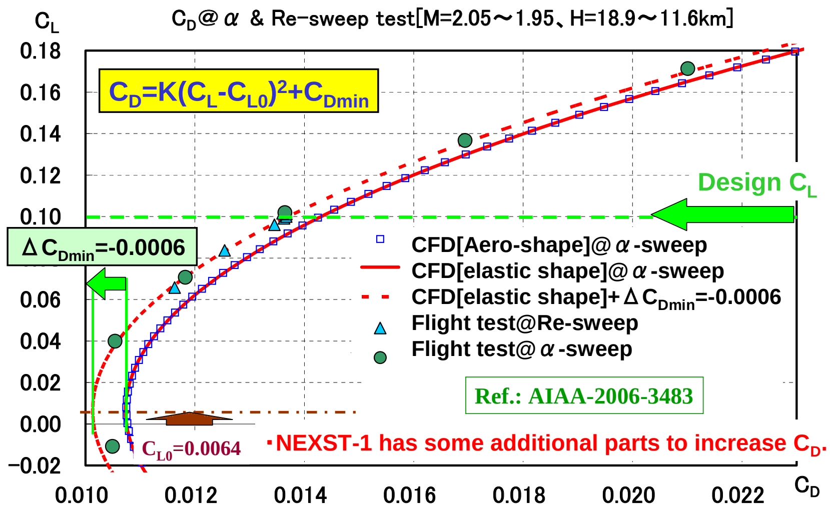

Figure B-14. Flight data analysis II - drag characteristics

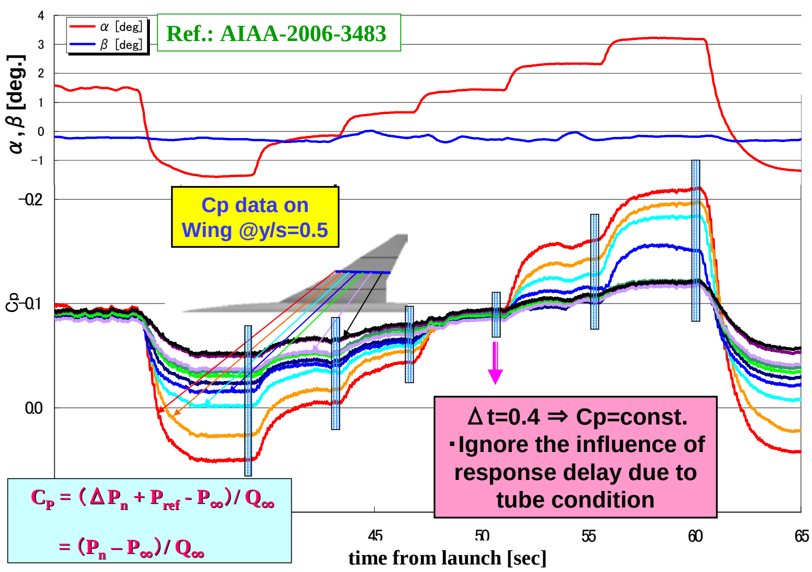

Figure B-15. Flight data analysis III – measured pressure

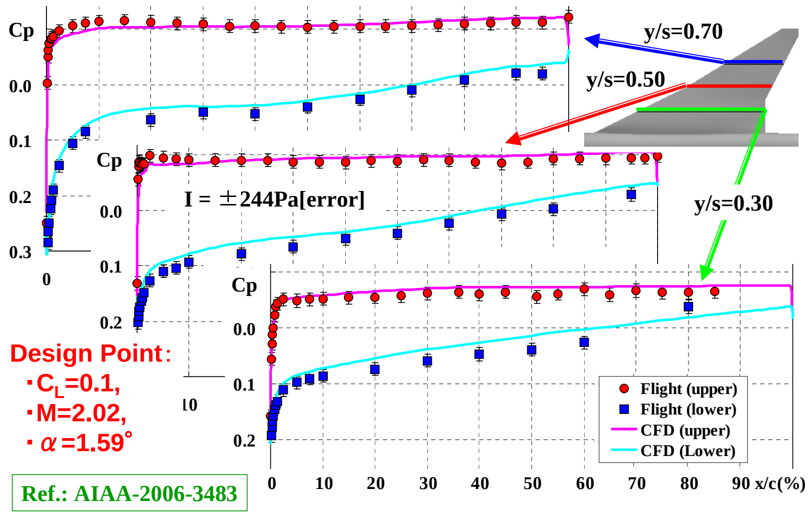

Figure B-16. Flight data analysis IV – Cp characteristics on wing

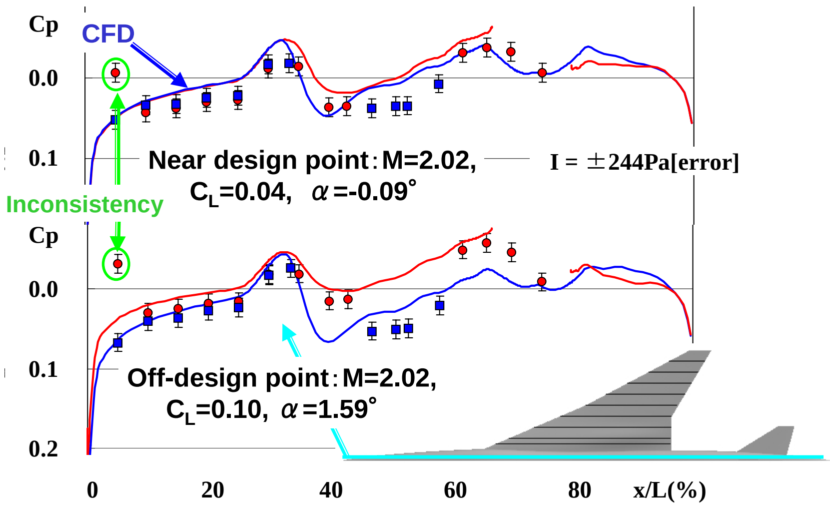

Figure B-17. Flight data analysis V – Cp characteristics on body

in lift slope, $C_{L\alpha}$ was obtained considering elastic deformation of the wing[42]. However, zero lift angle α_0 was slightly different from CFD analysis. Its main cause has not been investigated yet.

Figure B-14 shows a comparison of measured drag data with CFD analysis results on drag characteristics under AOA change. From this figure, good agreement in K and C_{L0} was obtained except C_{Dmin}. In general, real C_{Dmin} of the NEXST-1 airplane is influenced by certain increases due to additional parts such as ADS, TAT, a camera and so on, and due to elastic deformation effect. On the other hand, since the present CFD analysis has an error in the turbulence model applied in the estimation of friction drag, the disagreement of C_{Dmin} suggests no validation of the effect on the area-ruled body[42].

Figure B-15 shows a time history of several pressures on the upper surface. JAXA's pre-investigation for the influence of delayed response due to tube condition indicated that the time interval of Δt=0.4 sec. for measurement at constant AOA was enough to ignore the response delay; this led to realize constant Cp conditions[42].

Figure B-16 shows a comparison between measured and computed pressure coefficient distributions on the wing at the design point condition in flight test. Good agreement in the upper Cp distributions was confirmed[42] within the

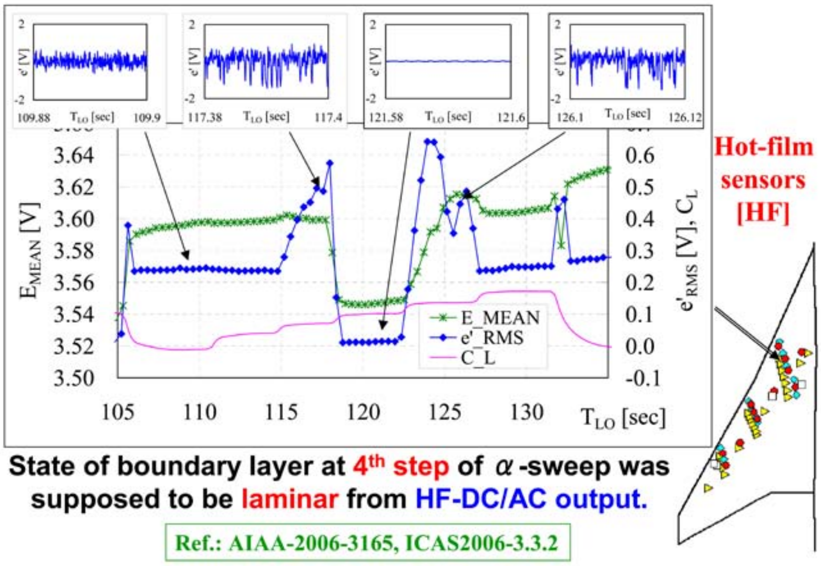

Figure B-18. Flight data analysis VI – transition data : HF

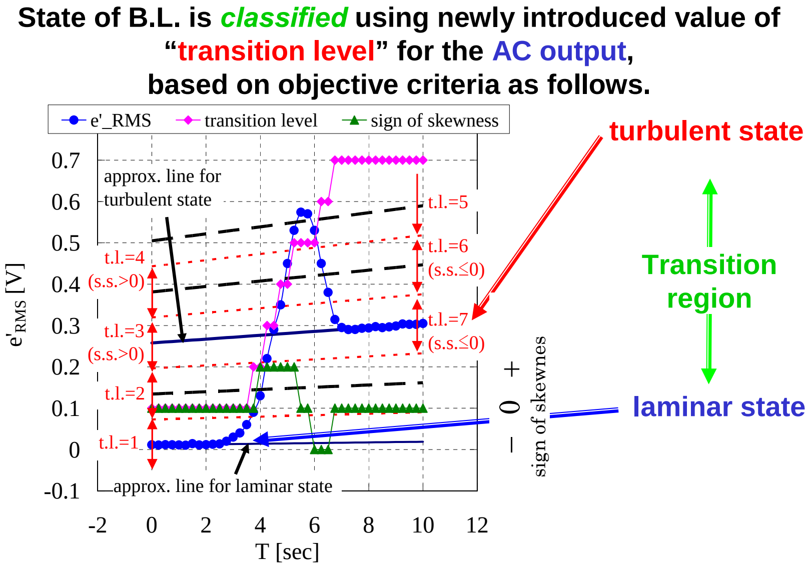

Figure B-19. Data analysis method with new transition level

measurement error bar of 244 Pa. However, a slight difference in the lower Cp distributions between the flight test and CFD was recognized. The main reason has not been cleared yet.

Figure B-17 shows a comparison between measured and computed pressure coefficient distributions on the center section of the fuselage at near the design and off-design point conditions in flight test. First of all, a qualitatively fairy good agreement in the Cp distributions was confirmed. However, a remarkable difference between the flight test and CFD results was quantitatively clear. JAXA thinks that the principle reason of the difference originates in the non-smoothness of curvature of each panel that formed the fuselage contour.

Figure B-18 shows a typical measurement result using transition detection sensors[43-45]. The figure shows time history of DC and AC components of a hot-film signal located on the surface of the inner wing. The symbols of E_MEAN and e'_RMS are corresponding to the DC and AC components

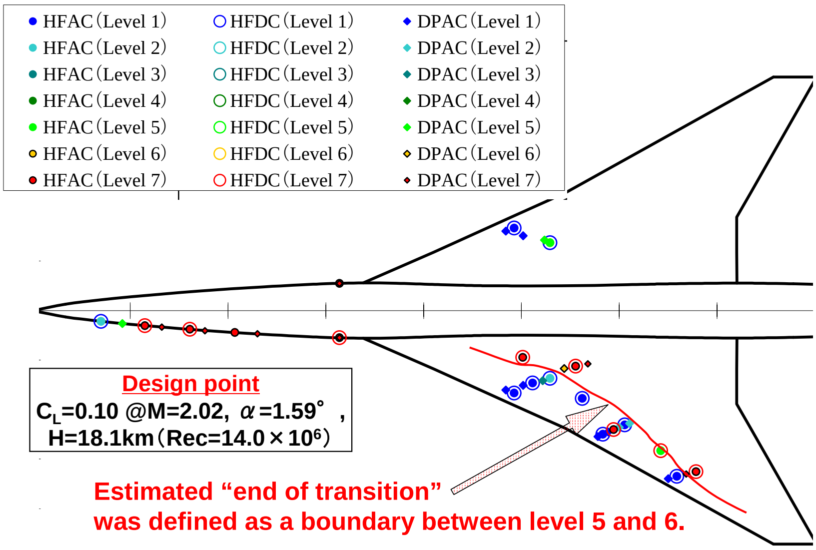

Figure B-20. Measured transition location

respectively. In general, higher DC level indicates that the boundary layer is turbulent. On the other hand, AC level is lower at laminar, maximum at transition, and relatively higher than laminar level at turbulent. Laminar boundary layer was clearly demonstrated by both DC and AC levels during the time interval from 118 to 122 [sec]. which corresponded to the design lift condition, namely the condition of 4th step of AOA-sweep.

Figure B-19 shows a new trial to analyze the measurement transition data more precisely[43]. The state of boundary layer was classified using newly introduced value of transition level for the AC output. Transition level 1 and 7 correspond to full laminar and turbulent state respectively. And the transition process is divided into the level 2 to 6 as demonstrated in the figure.

Figure B-20 shows a surface pattern for the transition level of each transition detection sensor at the design point. These detection sensors were placed in the region from 15% to 45% chordwise locations at three spanwise stations. In comparison with transition analysis result, an estimated "end of transition" line was defined as an assumed boundary between levels 5 and 6 as shown in the figure. This line indicates the boundary between non-turbulent and turbulent regions.

Figure B-21 shows summary of comparison of transition analysis results with measured transition data, namely turbulent or non-turbulent at AOA-sweep test phase. The rearward movement of the boundary between turbulent and non-turbulent was confirmed at the design AOA condition as shown in the figure. However, there were inconsistencies between detections using HF and DP in the mid-wing region. Its main reason has not been cleared yet.

Figure B-22 shows also summary of comparison of analysis results with measured data at Re-sweep test phase. Unfortunately remarkable rearward movement of the boundary layer transition was not observed against our expectation. Of course, the measured results of all the sensors located at the most forward positions indicate laminar condition at design C_L condition. This implies that there was no transition due to the attachment-line contamination. However, the reason for the absence of significant rearward movement is still an open question. But JAXA speculated that influence of surface roughness is one of the main causes, because measured roughness data indicated about 2 micron meter for the Ra metric and it is much larger than the JAXA's target level of 0.3 micron meter. In this phase, there was also inconsistency between detections using HF and DP in the mid-

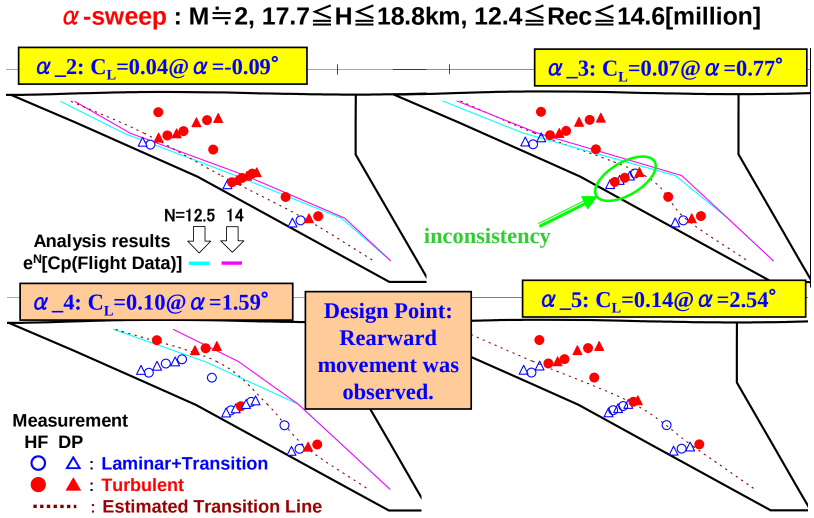

Figure B-21. Principal results on transition measurements at α-sweep test phase

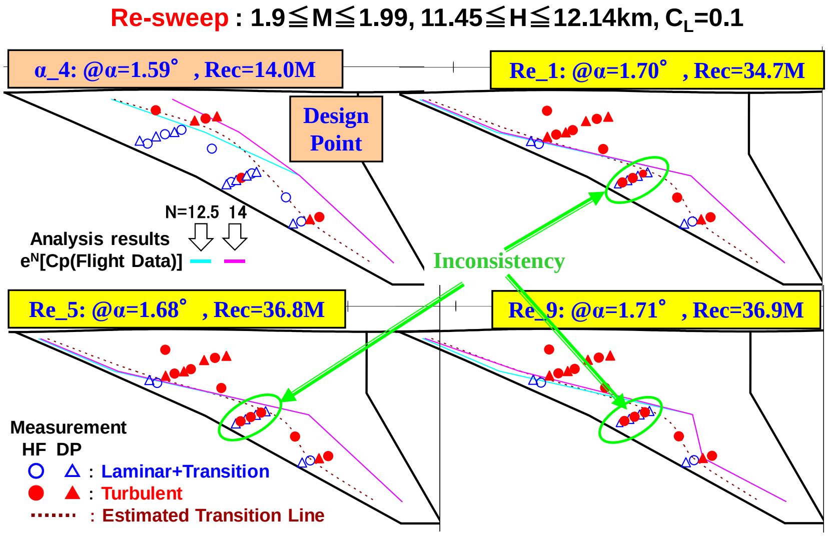

Figure B-22. Principal results on transition measurements at Re-sweep test phase

wing region. But its main reason has not been cleared yet.

C. Summary of JAXA's transition experiments

C-1. Transition measurement test on the NEXST-1 nose cone at zero AOA and ONERA-S2MA test condition

JAXA conducted transition measurement test on the NEXST-1 nose cone at the conditions of M=2 and zero AOA in ONERA's S2MA wind tunnel using a 23.3% wing-body model. Four HF sensors were located on the side surface of the nose part of the model with staggered arrangement to reduce the influence of the wake of HF sensor.

To estimate transition location, sweep of the total pressure, P_0 was carried out in the transition test. Figure C-1 shows the AC outputs of four HF signals during the P_0 change. In general, the AC output has typical trend as indicated in a function form of 4th order polynomial type. So, JAXA approximated measured data with the 4th order polynomial function using least square method as shown in the figure.

Then, the locations corresponding to “onset of transition” and “peak” during the P_0 change were estimated and plotted as shown in Figure C-2. Finally, JAXA estimated transition location at P_0=1.0 bar condition, as demonstrated in the figure.

C-2. Transition measurement test on the NEXST-1 nose cone at nonzero AOA and FHI-W/T test condition

JAXA conducted a transition measurement test on the NEXST-1 nose cone at the conditions of M=2 and nonzero AOA in the high speed wind tunnel of Fuji Heavy Industries (FHI) using an about 10% scale nose model of the NEXST-1 airplane. Transition characteristics were detected using IR technique.

Figure C-3 shows the definition of transition

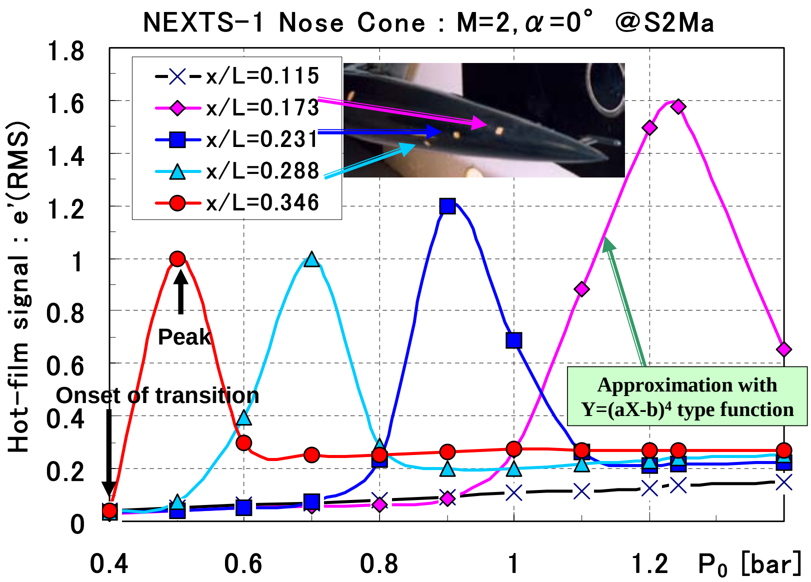

Figure C-1. Interpolated HF signals on the NEXST-1 nose cone

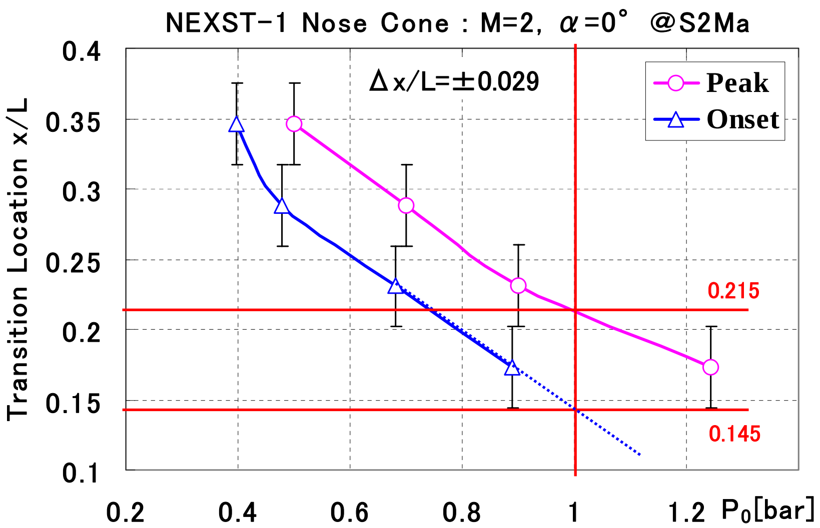

Figure C-2. Estimated transition location on the NEXST-1 nose cone at S2MA test condition

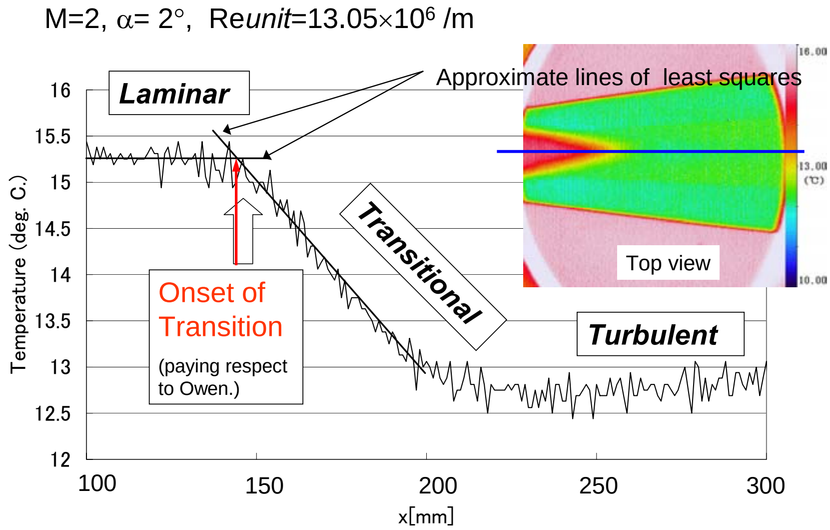

Figure C-3. Definition of transition location due to IR image technique at FHI W/T test conditions

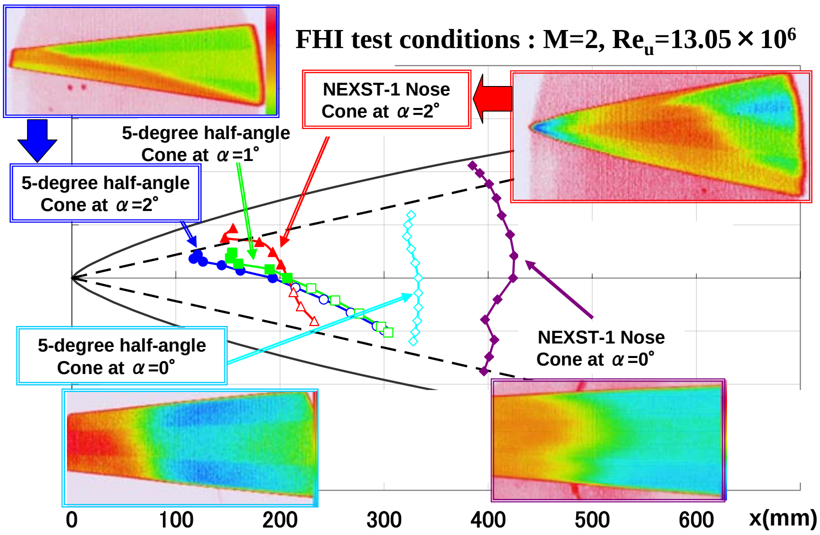

Figure C-4. Transition experiments by JAXA on the 5-degree half-angle sharp cone & NEXST-1 nose cone – (a) side view

location for the IR image technique at FHI W/T test conditions. Surface temperature was detected using an adiabatic model and IR camera in the wind tunnel test.

Figures C-4 and C-5 show a summary of transition locations at several AOAs, compared with the test results of the 5-degree half-angle sharp cone. Measured transition locations are shown for side view in Figure C-4. Measured transition locations in the top and bottom views were shown in Figure C-5. At zero AOA condition, it was confirmed that transition of the NEXST-1 nose cone was delayed compared to that of the 5-degree half-angle sharp cone because of a favorable streamwise acceleration on the NEXST-1 nose cone. At nonzero AOA condition, for example at AOA=2 degrees condition, transition locations in the windward regions of both models were almost similar, but transition location of the NEXT-1 nose cone was relatively rearward in the leeward region than that of the 5-degree half-angle sharp cone.

Figure C-6 shows another summary of transition measurement results from a circumferential viewpoint. In the comparison of measurement results at 2-degree

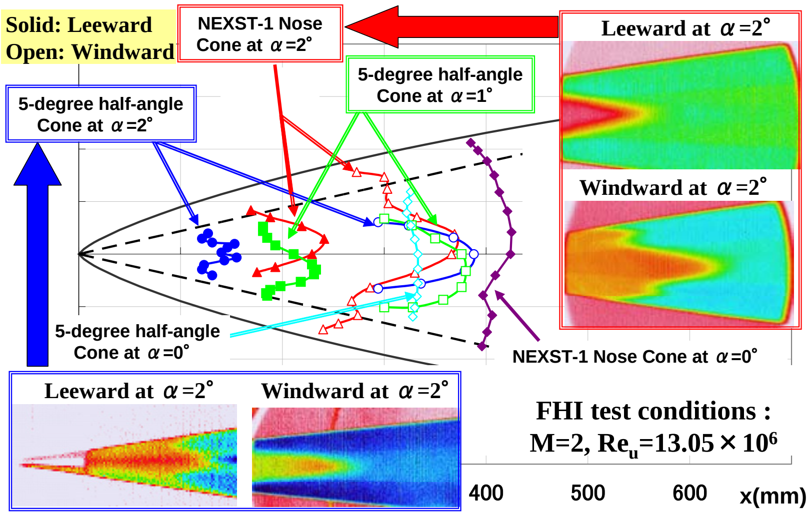

Figure C-5. Transition experiments by JAXA on the 5-degree half-angle sharp cone & NEXST-1 nose cone – (b) top & bottom views

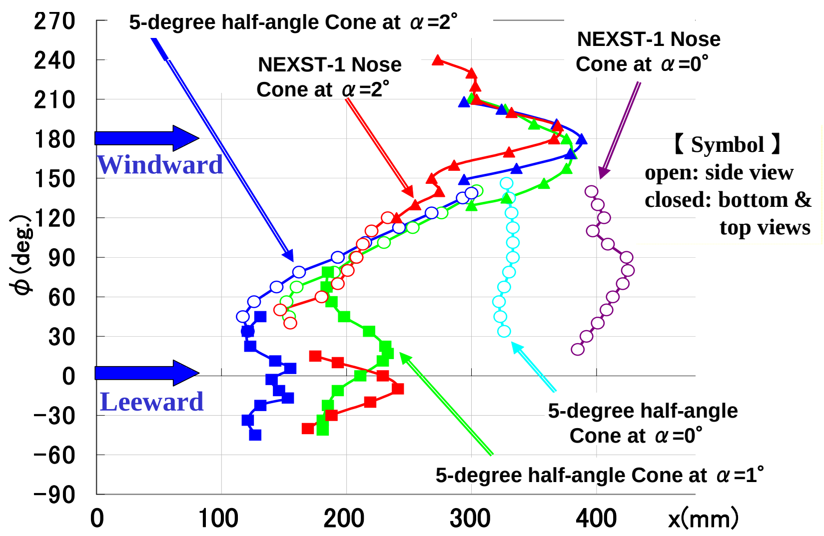

Figure C-6. Transition experiments by JAXA on the 5-degree half-angle sharp cone & NEXST-1 nose cone – (c) circumferential view

AOA, a remarkable difference of transition locations between the NEXST-1 nose cone and the 5-degree half-angle sharp cone was found in the region of -45< ϕ <45.

C-3. Transition measurement test on the NEXST-1 NLF wing at ONERA-S2MA test condition[10)]

JAXA conducted transition measurement on the NEXST-1 wing to validate JAXA's supersonic natural laminar flow (NLF) wing design concept. For the present objective of the test, lower freestream turbulence level of the tunnel was required. JAXA decided to use the ONERA-S2MA of a circuit type supersonic wind tunnel because it was considered that freestream turbulence level of such circuit type tunnels were lower than that of any blowdown type tunnels. Since the ONERA-S2MA has a large test section, JAXA was able to use a relatively large test model. This enabled to conduct a higher Reynolds number test. JAXA made a 23.3% scale wing-body model with several transition detection sensors such as multi-HF sensors. Since the surface of this model was

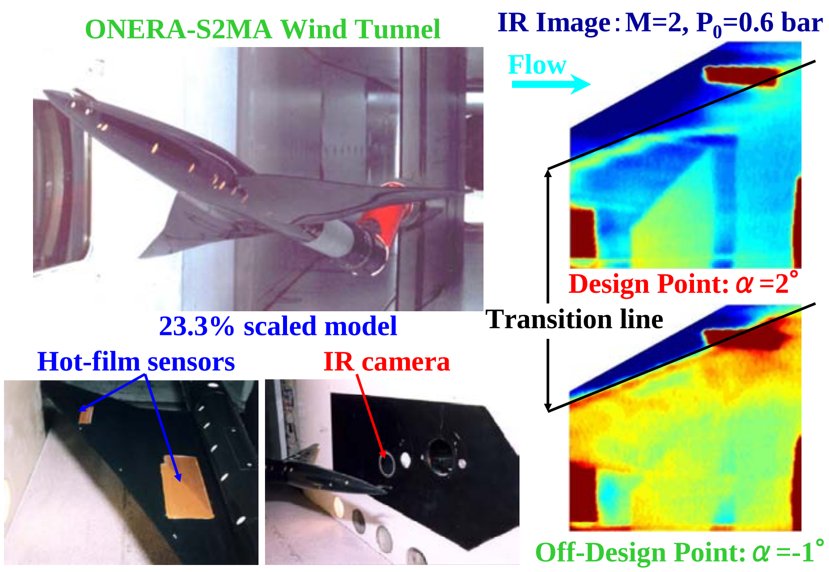

Figure C-7. Transition measurement test of the NEXST-1 NLF wing : IR image test result

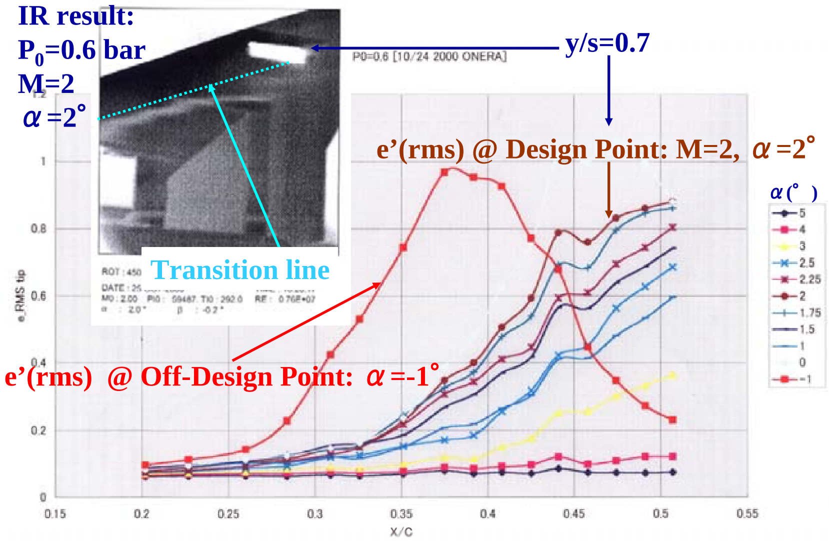

Figure C-8. Transition measurement test of the NEXST-1 NLF wing : HF detection test result

made from adiabatic material, surface temperature measurement was easily detected using IR camera.

Figure C-7 shows the test set-up and principal result of IR camera technique. At the design AOA condition, remarkable rearward movement of transition was qualitatively confirmed, but the amount of the movement was not always similar to JAXA's prediction. The main reason was presumed to originate in the freestream turbulence of the S2MA. But this test result was enough to perform the test objective. In addition, a comparison of measured pressure distribution with CFD results is summarized in Figure A-12. At the design AOA condition, a good agreement between measured and computed pressure distributions was confirmed.

Figure C-8 shows a summary of HF measurement data in the outer wing of the model. These data also indicate that JAXA's NLF design concept is valid at the design AOA condition.

Figure C-9 shows measured transition location characteristics at both inner and outer wing regions for variable AOA for different P_0 conditions. At the inner wing region, the case at AOA=2 degrees

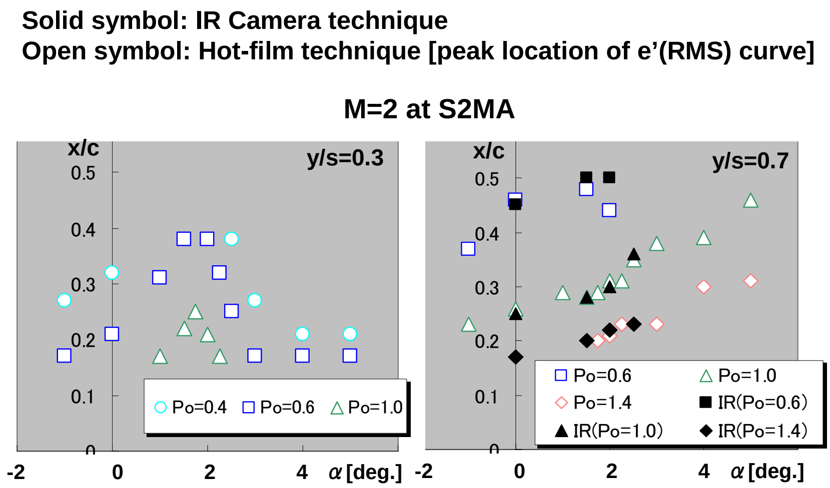

Figure C-9. Transition measurement test of the NEXST-1 NLF wing : Summary of measured transition locations

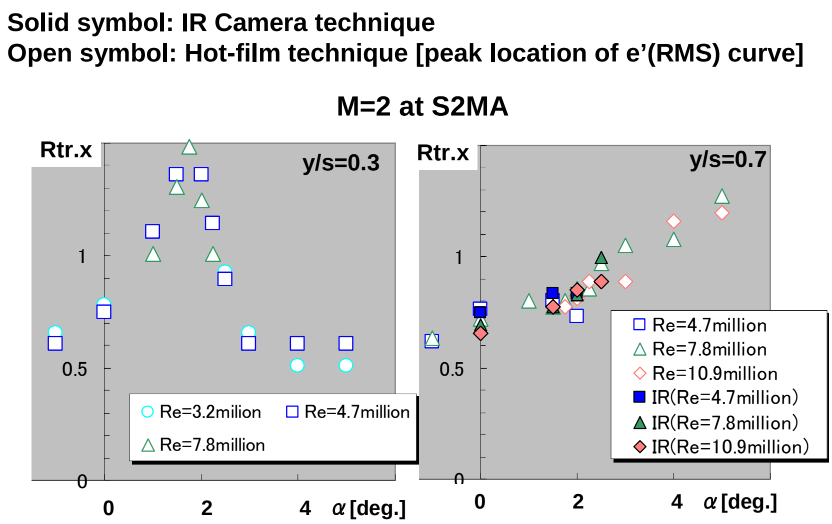

Figure C-10. Transition measurement test of the NEXST-1 NLF wing : Summary of transition Reynolds numbers

corresponds to the most rearward transition location. But at the outer wing region, a higher AOA rendered more rearward transition movement. The reason has not been cleared yet.

Figure C-10 shows transition Reynolds number characteristics in both inner and outer wing regions with variable AOA. Good correlation among several P_0 conditions was obtained. JAXA has considered from the present result that the effects of freestream turbulence and surface roughness on transition location were almost constant in the test P_0 range.

D. Summary of JAXA's transition analysis results

D-1. Formulation and several relations of JAXA's e^N code

In general, transition prediction system based on a current e^N method consists of four parts; the first part is to compute laminar boundary layer characteristics using a boundary layer code, the second part is to compute stability characteristics of laminar boundary layer such as amplification rates at several frequencies, the third part is to integrate the most suitable amplification rate with a model

(1) Small Disturbance

$$\{u',v',w',p',T',\rho',\mu'\} \equiv q'(x,y,z,t)$$

Plane Wave Approx. $= \tilde{q}(y)\, e^{i(\alpha x+\beta z-\omega t)}$

$(\alpha=\alpha_r+i\alpha_i)$

$(\beta=\beta_r+i\beta_i)$

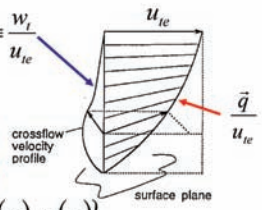

(2) Laminar Boundary Layer

$$\{U,V,W,P,T,\rho,\mu\} = \{U(y),\underset{\uparrow}{0},W(y),\underset{\uparrow}{1},T(y),\rho(y),\mu(y)\}$$

Parallel Flow Approx. *Boundary Layer Approx.*

(3) Basic Equations *Streamline Coordinate* ⇒ $W(\delta)=0$

$$\frac{d\varphi_i}{dy} = \sum_{j=1}^{8} a_{ij}\varphi_j \quad , \quad i=1\sim 8$$

Eigenvalue Eq. ⇒ *Amp. rates* (α_i, β_i)

(4) Transition Criterion *N-factor* ⇒ $N = \int(-\alpha_i\, dx_s - \beta_i\, dy_s)$

Envelope Method $\alpha_i = \underset{\psi}{Max}\left[\,|\alpha_i(\psi)|\,\right]$ *where* $\alpha_i = \alpha_i^{*}\delta \quad , \quad \psi \equiv \tan^{-1}\left(\frac{\beta_r}{\alpha_r}\right)$

Figure D-1. Formulation of JAXA's stability Code

$\vec{q}(z_c) = w(z_c)\vec{i} + \bar{u}(z_c)\vec{j}$ **: velocity vector within L.B.L.**

$\vec{q}(\delta) \equiv \vec{q}_e = w_e\vec{i} + \bar{u}_e\vec{j}$ **: velocity vector at L.B.L. edge**

$(\vec{i},\vec{j})$: unit vector at (x_c, y_c) coordinate system

$u_t = \vec{q}\cdot\vec{e} = \frac{\bar{u}+\beta w}{\sqrt{1+\beta^2}}$ *where* $\beta \equiv \frac{w_e}{\bar{u}_e}$ **: streamwise velocity component**

$w_t = \vec{q}\cdot\vec{t} = \frac{-w+\beta\bar{u}}{\sqrt{1+\beta^2}}$ **: crossflow-wise velocity component**

$\vec{e} \equiv \frac{\vec{q}_e}{|\vec{q}_e|} = \frac{\beta\vec{i}+\vec{j}}{\sqrt{1+\beta^2}} \quad , \quad \vec{t} \equiv \vec{k}\times\vec{e} = \frac{-\vec{i}+\beta\vec{j}}{\sqrt{1+\beta^2}}$: unit vector at streamline coordinate

$\frac{u_t}{u_{te}} = \frac{1}{1+\beta^2}\left(\frac{\bar{u}}{\bar{u}_e}+\beta\frac{w}{\bar{u}_e}\right) = \frac{f'+\beta^2 g'}{1+\beta^2}$ **: normalized streamwise velocity**

$\frac{w_t}{u_{te}} = \frac{1}{1+\beta^2}\left(-\frac{w}{\bar{u}_e}+\beta\frac{\bar{u}}{\bar{u}_e}\right) = \frac{\beta(f'-g')}{1+\beta^2}$ **: normalized crossflow-wise velocity**

where $u_{te} = \frac{\bar{u}_e+\beta w_e}{\sqrt{1+\beta^2}} = \bar{u}_e\sqrt{1+\beta^2} \quad , \quad f' \equiv \frac{\bar{u}}{\bar{u}_e} \quad , \quad g' \equiv \frac{w}{w_e}$

Figure D-2. Definition of boundary layer profiles

of an integral path and an auxiliary condition such as envelope method, the last part is to specify a transition criterion for the N value corresponding to transition.

First of all, the formulation of JAXA's stability computation code is summarized in Figure D-1. This formulation was derived with linear and parallel flow approximations[9]. A shooting method was used as one of method of solutions. Then to determine unknown variables, so-called envelope method was applied. Finally, as an integral path, JAXA selected an external streamline after detailed investigation of integral path problem for S2MA test results.

Figure D-2 shows the definition of laminar boundary layer profiles. In computing the profiles, normalization must be carefully conducted because precision of the profiles dominantly affect the precision of computing eigenvalues of stability equation.

Figure D-3 shows formulation of Kaups and Cebeci method[31] for computing laminar boundary layer. This method is very popular as one of practical codes. Therefore, JAXA selected this code to compute laminar boundary layer in the transition

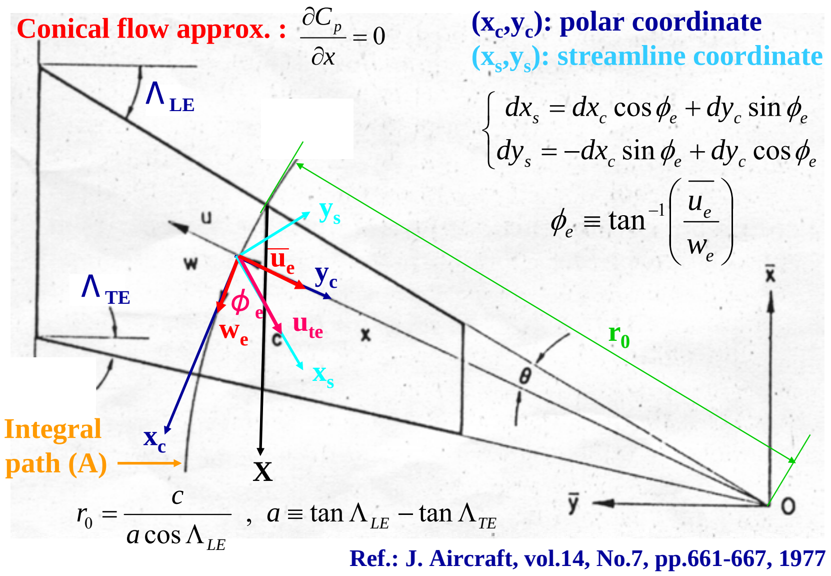

Figure D-3. Formulation of Kaups & Cebeci method

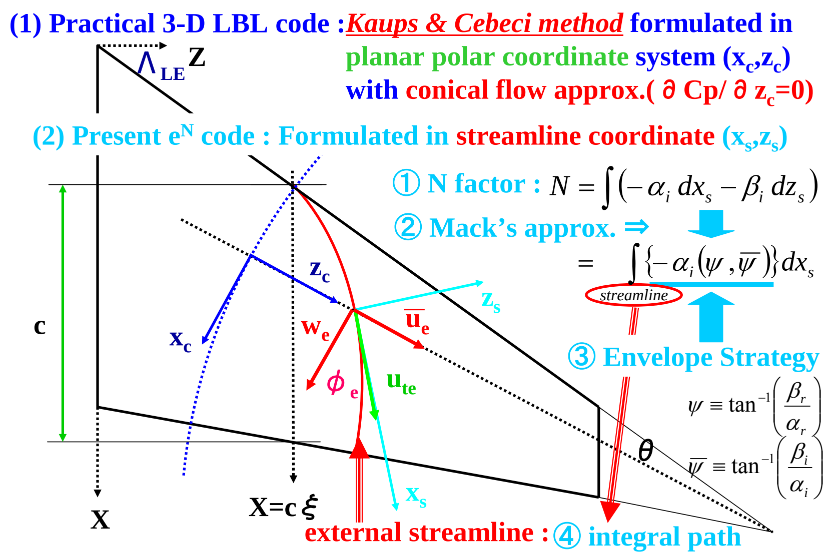

Figure D-4. Formulation of JAXA's e^N method

analysis for wings. This code was formulated in polar coordinate system and so-called conical flow approximation which consists of zero pressure gradient in the radial direction was applied in its formulation.

JAXA's stability method is formulated in streamline coordinate system and based on both envelope strategy and Mack's approximation as shown in Figure D-4. Here, envelope strategy and Mack's approximation are also explained in Figure D-5 or D-6, including the formulation of the Kaups and Cebeci method for laminar boundary layer computation.

Figure D-5 shows a candidate of integral path in JAXA's e^N method. The first candidate is a circular arc. In this model, the integrated amplification rate, so-called N factor can be numerically calculated by using a special integrant shown in the figure. The derivation process of the special integrant is summarized in Figure D-6.

Figure D-7 shows another candidate of integral path in JAXA's e^N method. This second candidate is an external streamline at boundary layer edge. In this model, the N factor can be numerically calculated by using another special integrant

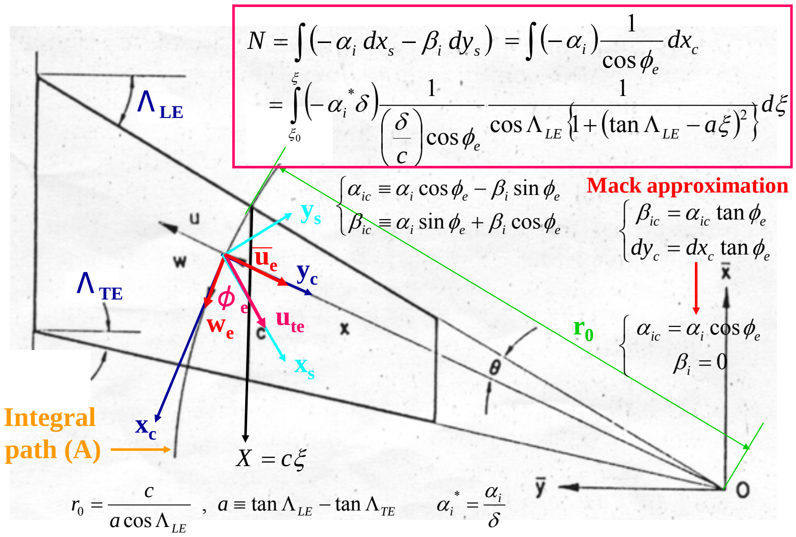

Figure D-5. Formulation of integral path (A)

$$N=\int(-\alpha_i\,dx_s-\beta_i\,dy_s)$$ **: definition based on streamline coordinate**

$$=\int(-\alpha_{ic}\,dx_c-\beta_{ic}\,dy_c)\longleftarrow\textbf{Transformation :}\begin{cases}\alpha_{ic}\equiv\alpha_i\cos\phi_e-\beta_i\sin\phi_e\\ \beta_{ic}\equiv\alpha_i\sin\phi_e+\beta_i\cos\phi_e\end{cases}$$

$$=\int\{-\alpha_{ic}(1+\tan^2\phi_e)\}dx_c\longleftarrow\textbf{Mack approx.:}\begin{cases}\beta_{ic}=\alpha_{ic}\tan\phi_e\\ dy_c=dx_c\tan\phi_e\end{cases}$$

$$=\int(-\alpha_{ic})\frac{1}{\cos^2\phi_e}dx_c$$

$$=\int(-\alpha_i)\frac{1}{\cos\phi_e}dx_c\longleftarrow\begin{cases}\alpha_{ic}=\alpha_i\cos\phi_e\\ \beta_i=0\end{cases}$$

$$dx_c=r_0d\theta=c\frac{\cos^2(\Lambda_{LE}-\theta)}{\cos\Lambda_{LE}}d\xi\longleftarrow d\theta=a\cos^2(\Lambda_{LE}-\theta)\,d\xi\ ,\ \xi\equiv\frac{X}{c}$$

$$\tan(\Lambda_{LE}-\theta)=\tan\Lambda_{LE}-a\xi$$

$$\therefore\ N=\int_{\xi_0}^{\xi}(-\alpha_i^*\delta)\frac{1}{\left(\frac{\delta}{c}\right)\cos\phi_e}\frac{1}{\cos\Lambda_{LE}\{1+(\tan\Lambda_{LE}-a\xi)^2\}}d\xi\ ,\quad \alpha_i^*=\frac{\alpha_i}{\delta}$$

modification term

Figure D-6. Derivation of integral form on integral path (A)

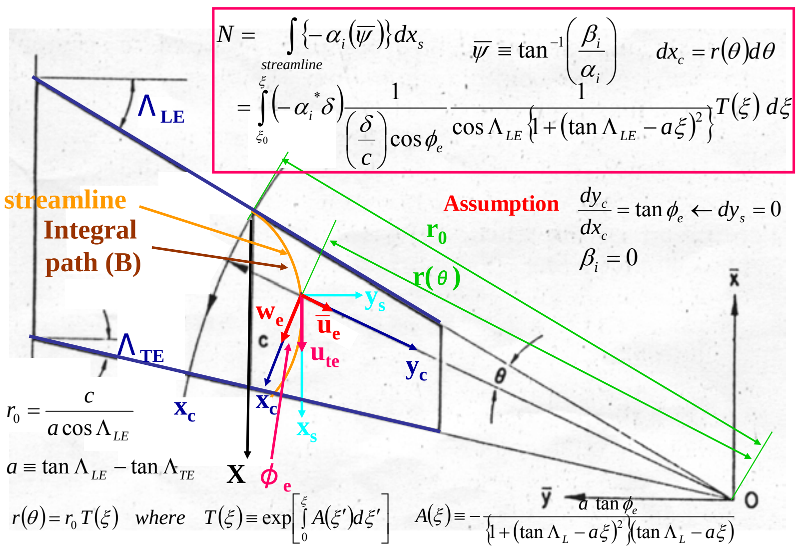

Figure D-7. Formulation of integral path (B)

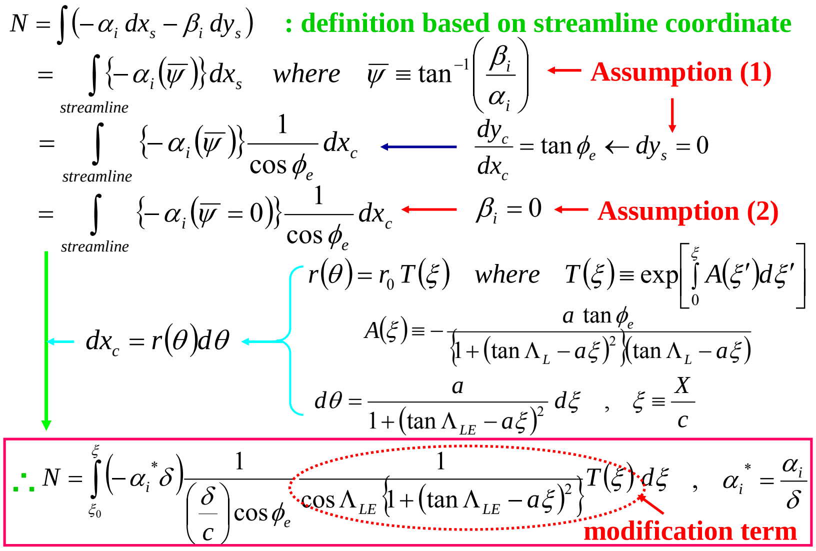

Figure D-8. Derivation of integral form on integral path (B)

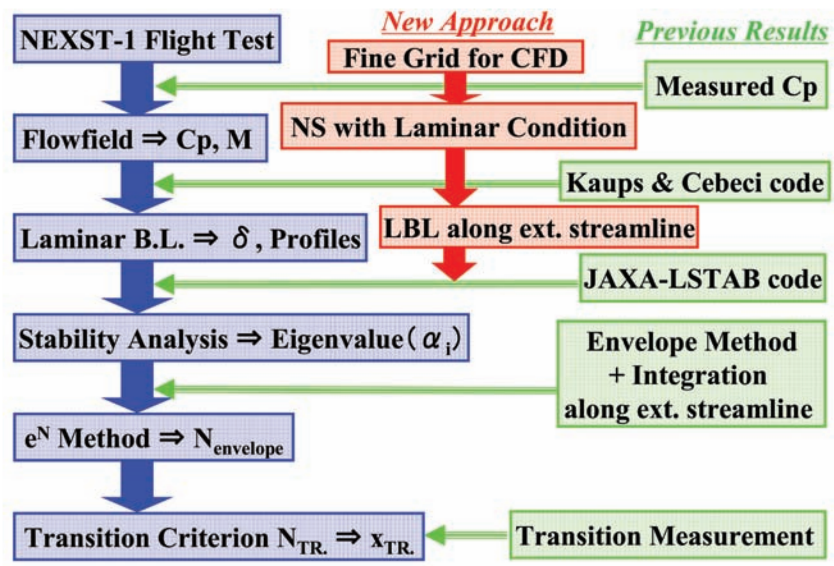

Figure D-9. New approach for transition analysis

shown in the figure. The derivation process of that integrant is summarized in Figure D-8.

Finally, as the Kaups and Cebeci method is based on the conical flow approximation which is well valid for relatively higher aspect ratio wing cases, it is considered that the precision of computing boundary layer is a little lower for low aspect ratio wing cases. Therefore, three dimensional approach is required for those cases. But since JAXA did not have a practical and effective code in the NEXST-1 project, Navier-Stokes computation at laminar condition was applied. This is a new approach by JAXA. A structure of this new approach is demonstrated in Figure D-9. This approach was mainly applied into the transition analysis on the NEXST-1 nose cone and 5-degree half-angle sharp cone at nonzero AOA condition and on the NEXST-1 wing at the design condition in flight test[37].

D-2. Transition analysis on the NEXST-1 nose cone at zero AOA and ONERA-S2MA test condition

First of all, present transition analysis was

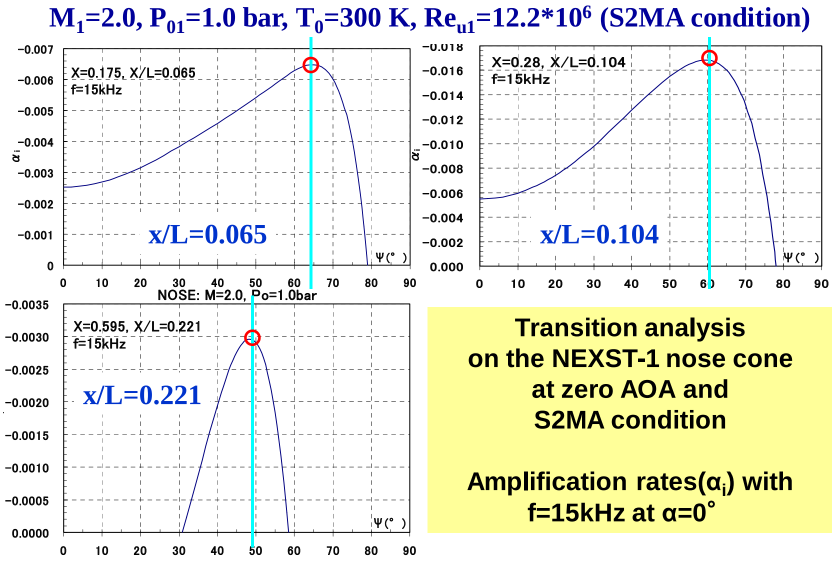

Figure D-10. Amplification rates on the NEXST-1 nose cone at M=2 and $\alpha = 0^{\circ}$

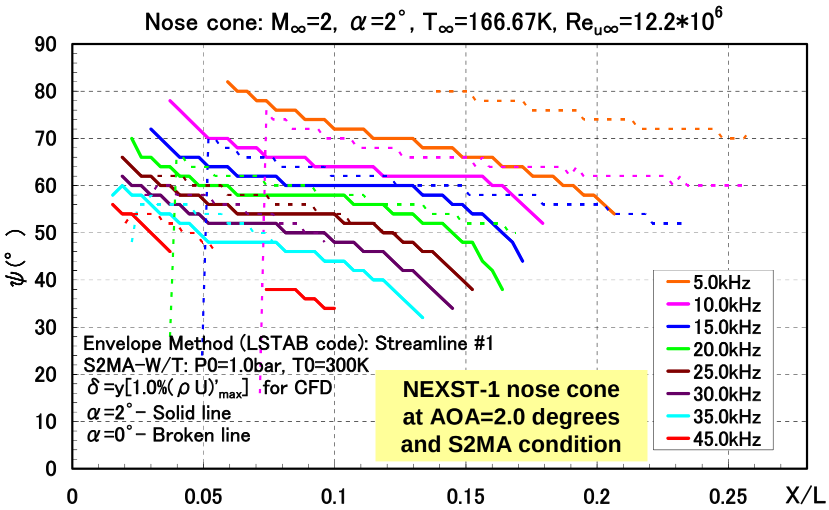

(a) External streamline #1

Figure D-11. Propagation direction of small disturbances on the NEXST-1 nose cone

conducted under the conditions summarized in Figure 6. Figure D-10 shows typical amplification rates with frequency of 15kHz. In the computation, JAXA used an axisymmetric boundary layer code called "TUF code[12]". This figure also demonstrates envelope strategy[30]. This strategy requires to select the most suitable amplification rate with the maximum absolute value in the range of propagation direction angle (Ψ). And according to such envelope strategy, N curves were computed and summarized in Figure 8.

D-3. Transition analysis on the NEXST-1 nose cone at nonzero AOA and ONERA-S2MA test condition

This analysis needs to compute complete three dimensional boundary layer characteristics. So JAXA decided to apply JAXA's Navier-Stokes code called "UPACS" to perform it because JAXA did not have any practical and effective boundary layer codes during the NEXTS-1 project. First of all, JAXA computed flowfield and laminar boundary layer characteristics of the NEXST-1 nose cone only at AOA=2 degrees using the UPACS code with all laminar flow condition. Then, edge of the boundary layer was estimated with an assumption

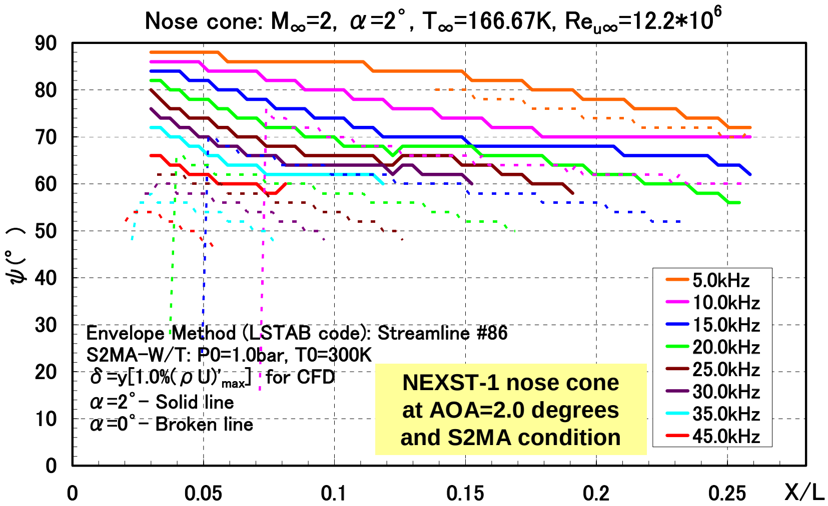

(b) External streamline #86

Figure D-11. Propagation direction of small disturbances on the NEXST-1 nose cone

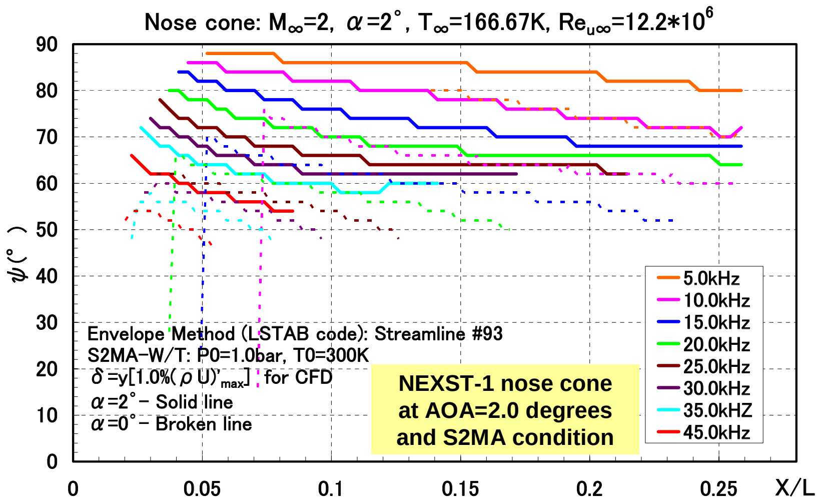

(c) External streamline #93

Figure D-11. Propagation direction of small disturbances on the NEXST-1 nose cone

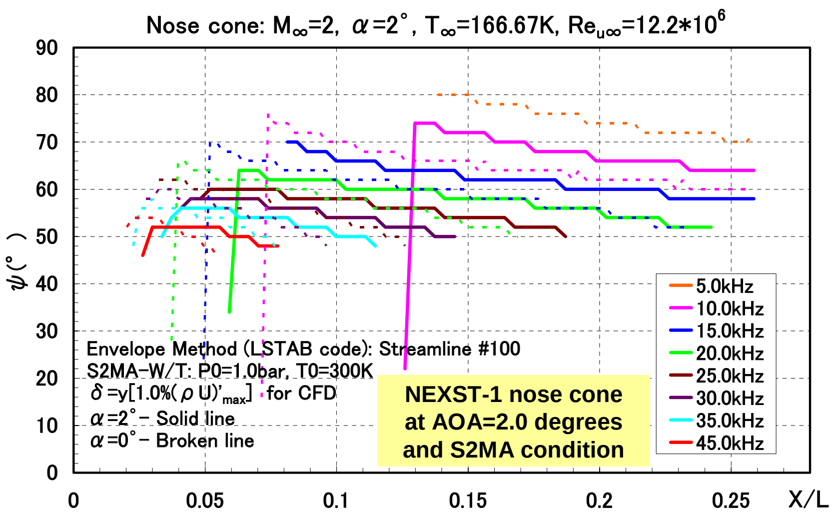

(d) External streamline #100

Figure D-11. Propagation direction of small disturbances on the NEXST-1 nose cone

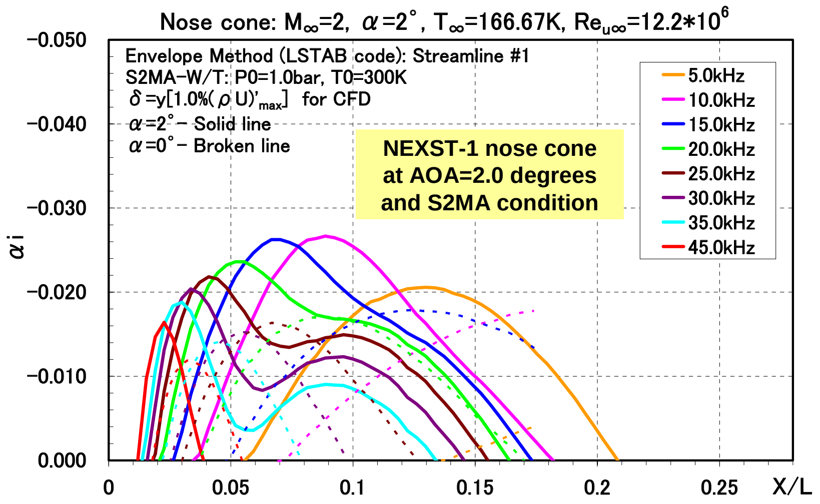

(a) External streamline #1

Figure D-12. Amplification rates (eigenvalues) on the NEXST-1 nose cone

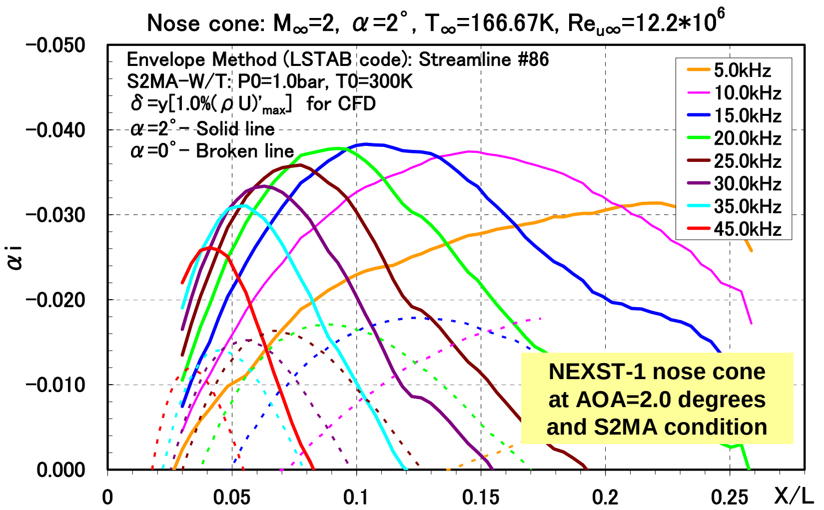

(b) External streamline #86

Figure D-12. Amplification rates (eigenvalues) on the NEXST-1 nose cone

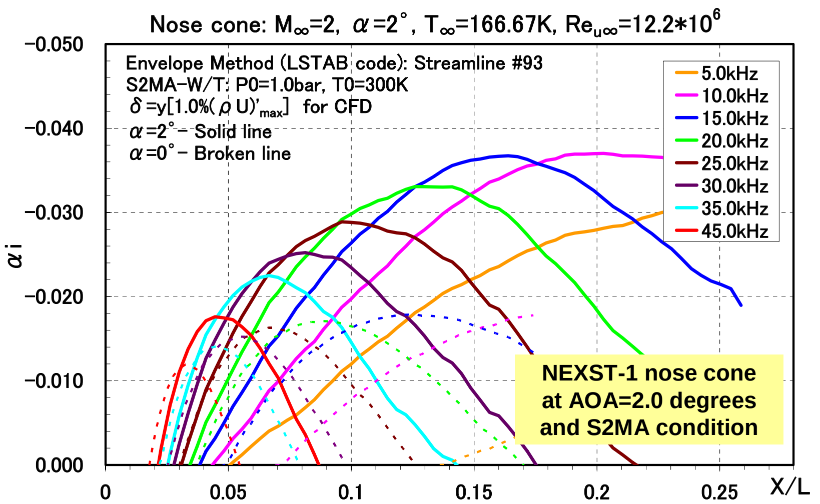

(c) External streamline #93

Figure D-12. Amplification rates (eigenvalues) on the NEXST-1 nose cone

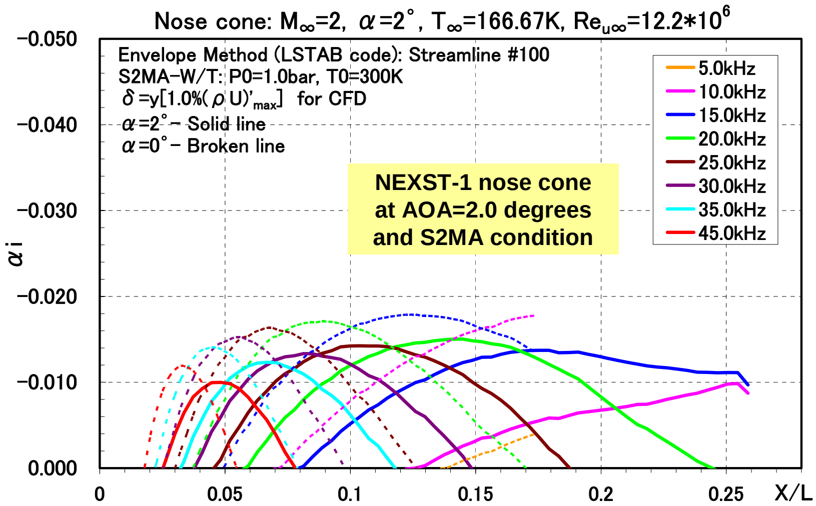

(d) External streamline #100

Figure D-12. Amplification rates (eigenvalues) on the NEXST-1 nose cone

of the following rule;

$$\delta = y \ \ at \ \ \frac{d(\rho U)}{dy} = 1.0\% \ of \left|\frac{d(\rho U)}{dy}\right|_{MAX}$$

This rule was already validated in the boundary layer analysis of the NEXST-1 nose cone at zero AOA condition, comparing the NS-based profiles with the results by the axisymmetic boundary layer code “TUF” .

To apply the JAXA's stability code to this analysis, external streamlines must be estimated with selecting the edge of boundary layer. Representative external streamlines are demonstrated in Figure 13.

Figures D-11 (a), (b), (c), and (d) show computed propagation direction for the streamlines according to a stability analysis result by JAXA. Figures D-12 (a), (b), (c), and (d) show computed amplification rates as eigenvalues of the stability equation. Under the assumption of selecting external streamline as an effective integral path for amplification rate, N characteristics and contours are shown in Figures 15 and 16.

D-4. Transition analysis on the NEXST-1 nose cone at non-zero AOA and FHI-W/T test condition

Figures D-13 (a), (b), (c), and (d) show a comparison of measured transition data with computed N contours. From those comparisons, any universal constant of the transition criterion for the N value has not been found. JAXA thinks further transition analysis on the NEXST-1 nose cone at nonzero AOA condition is necessary numerically and experimentally.

D-5. Transition analysis on the 5-degree half-angle sharp cone at non-zero AOA and FHI-W/T test condition

Figures D-14 shows a result of flowfield around the 5-degree half-angle sharp cone computed by JAXA's NS code with all laminar condition.

Figures D-15 (a), (b), (c), and (d) show a comparison of measured transition data with computed N contours. From those comparisons, any universal constant of the transition criterion for the N value has not been found; JAXA also needs to investigate the transition problem. However, Figure D-15(a) qualitatively shows a similar pattern, comparing with the experimental result at M=3.5 conducted by King[20].

Figure D-16 shows a comparison of measured transition location with the predicted transition location based on the N=6 transition criterion in side view. A qualitatively good agreement was

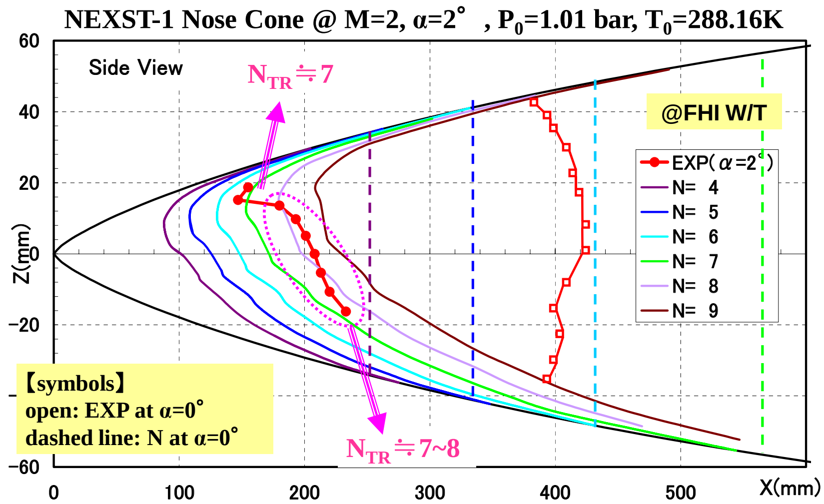

(a) Side view

Figure D-13. Comparison of N contours with transition measurement results at FHI W/T test condition

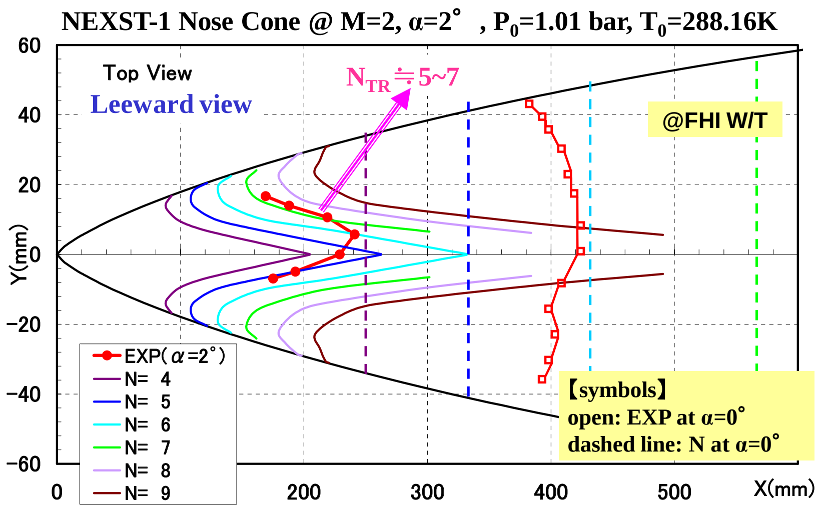

(b) Top view

Figure D-13. Comparison of N contours with transition measurement results at FHI W/T test condition

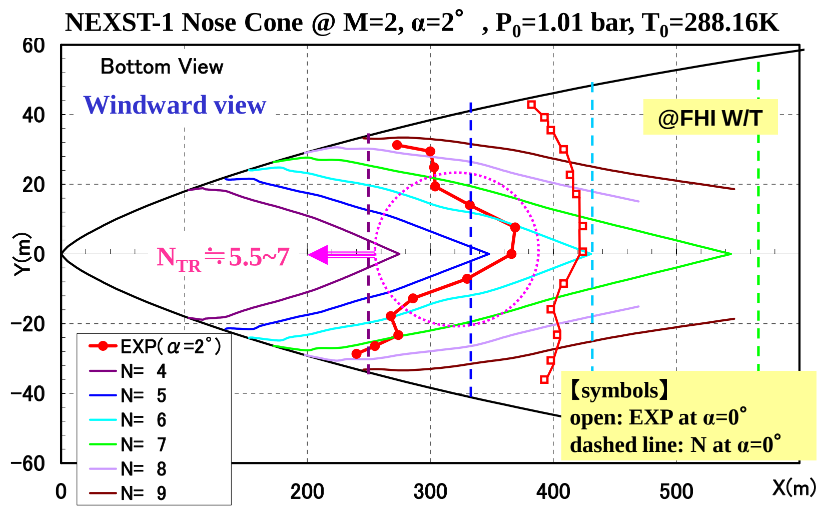

(c) Bottom view

Figure D-13. Comparison of N contours with transition measurement results at FHI W/T test condition

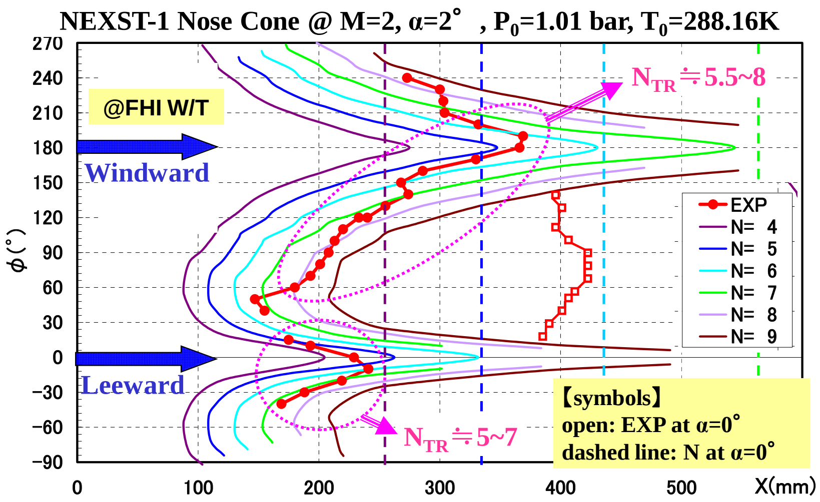

(d) Circumferential view

Figure D-13. Comparison of N contours with transition measurement results at FHI W/T test condition

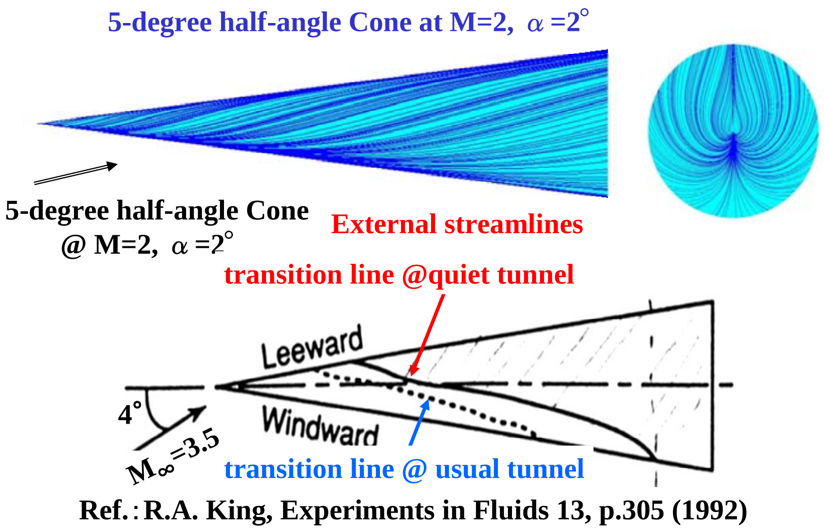

Figure D-14. NS analysis on the 5-degree half-angle sharp cone with all laminar condition

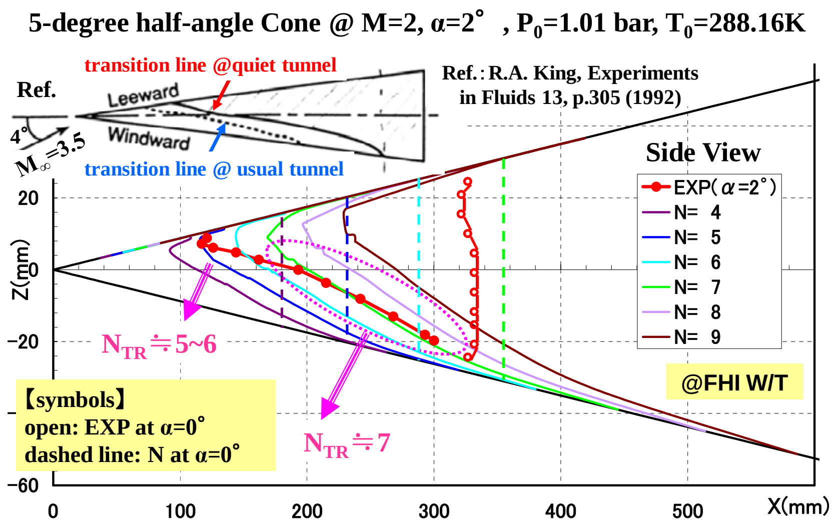

(a) Side view

Figure D-15. Comparison of N contours with transition measurement results at FHI W/T test condition

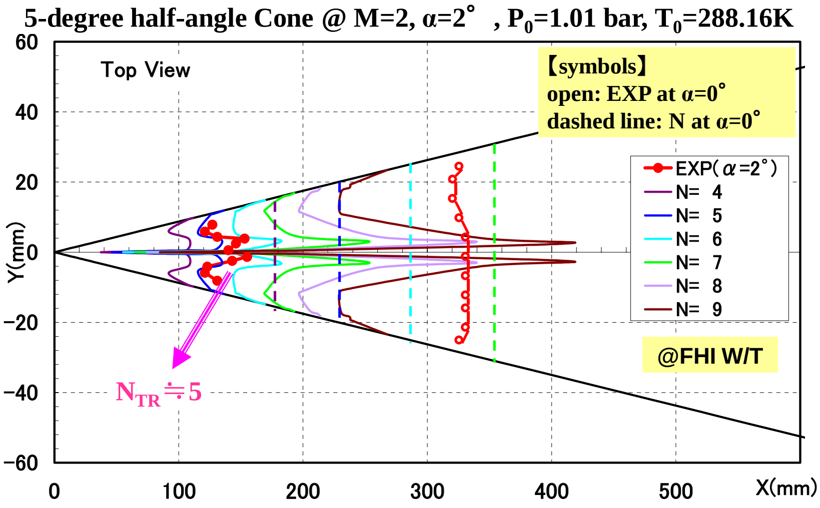

(b) Top view

Figure D-15. Comparison of N contours with transition measurement results at FHI W/T test condition

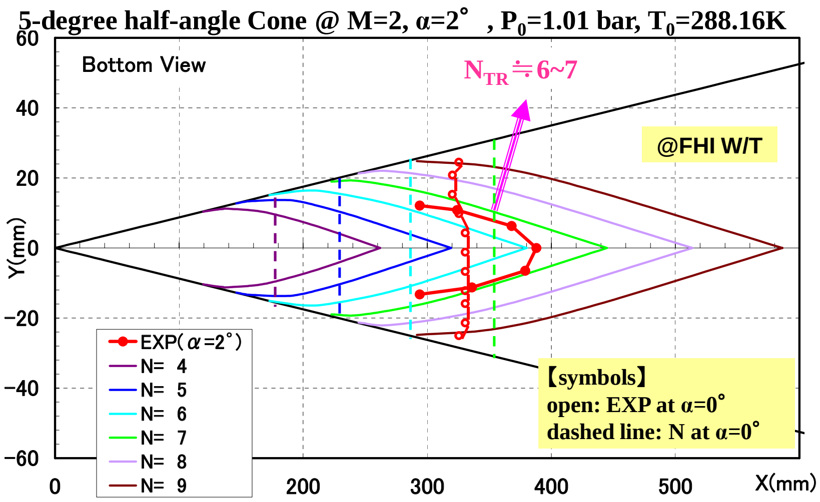

(c) Bottom view

Figure D-15. Comparison of N contours with transition measurement results at FHI W/T test condition

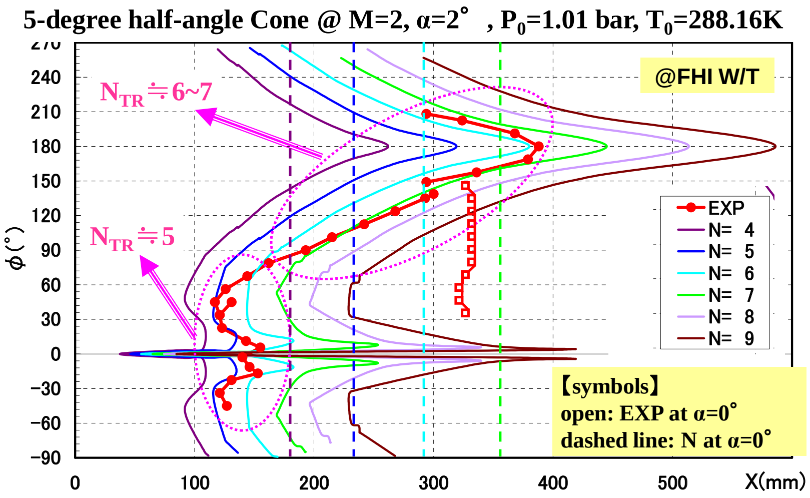

(d) Circumferential view

Figure D-15. Comparison of N contours with transition measurement results at FHI W/T test condition

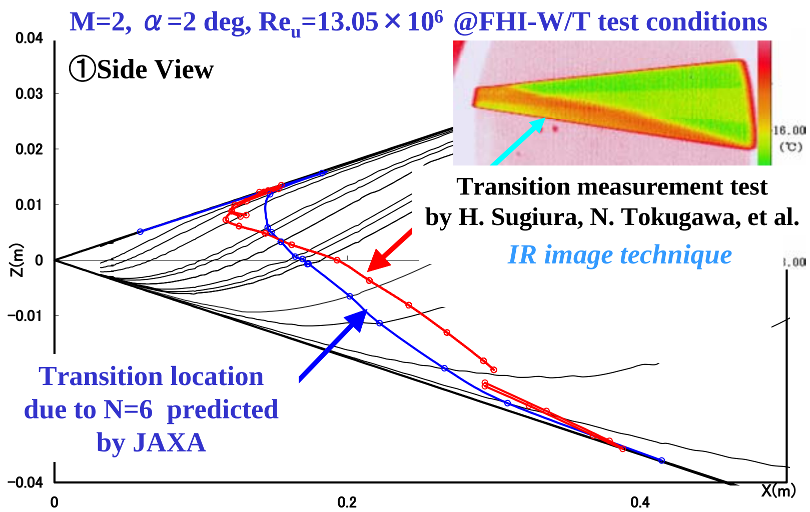

Figure D-16. Comparison of N=6 line with transition measurement results on the 5-degree half-angle sharp cone at FHI W/T test condition

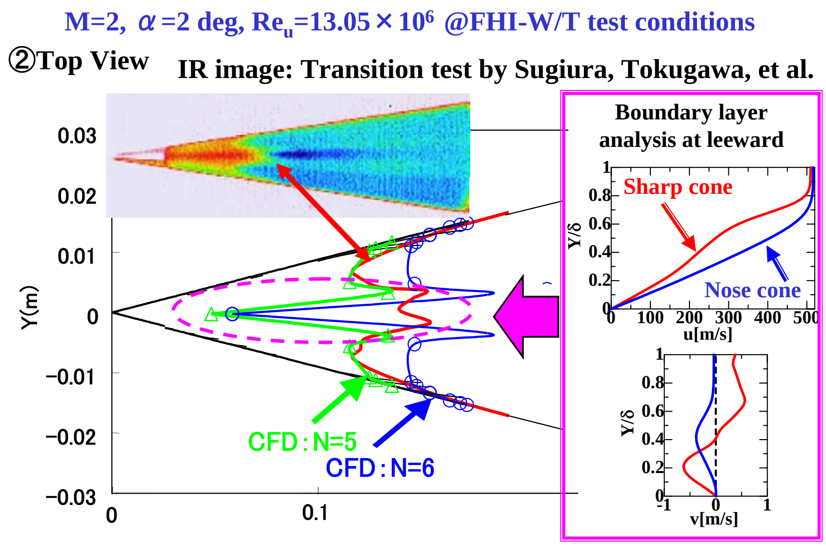

Figure D-17. Comparison of N=5 & 6 lines with transition measurement results on the 5-degree half-angle sharp cone at FHI W/T test condition

confirmed.

Figure D-17 shows a comparison of measured transition location with the predicted transition location based on the N=5 and 6 transition criteria in top view. In the top view, remarkable feature such as a W-shape pattern was obtained. It originates in deformation of streamwise velocity profile, compared with the NEXST-1 nose cone case.

Figure D-18 also shows comparisons for velocity profiles and N contours. Figure D-19 shows a comparison of crossflow velocity profiles near the top line. The 5-degeree half-angle sharp cone has inflow towards the symmetrical plane, so the inflow must escape in the direction normal to the symmetrical plane. It generates deformation of the boundary layer profile. On the other hand, the NEXST-1 nose cone has no inflow across the symmetrical plane because of the existence of streamwise strong acceleration. Therefore, it generates no deformation of the boundary layer profile. This is JAXA's explanation of the reason why the 5-degree half-angle sharp cone has the W-pattern on the transition location near the

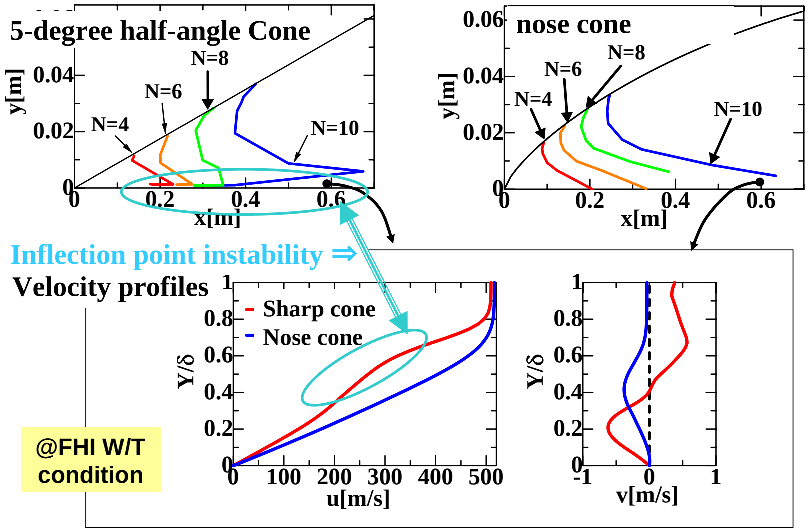

Figure D-18. Comparison of velocity profiles on leeward on the 5-degree half-angle sharp cone at M=2, α=2°

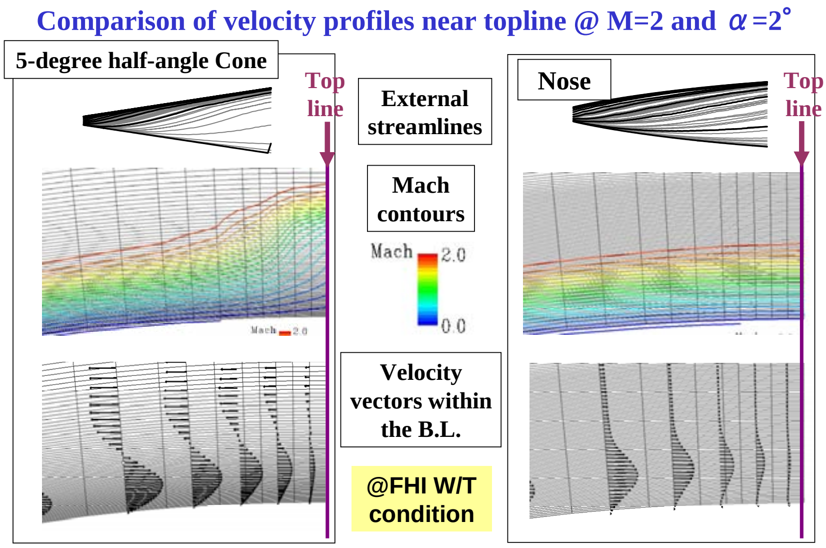

Figure D-19. Comparison of crossflow velocity profiles and Mach contours near leeward on the 5-degre half-angle sharp cone at M=2, α=2°

top region and the NEXST-1 nose cone has no W-pattern.

D-6. Transition analysis with new approach on the NEXST-1 NLF wing at flight test condition

In order to analyze transition characteristics of the NEXST-1 wing at flight test condition in detail, the conical flow approximation of the Kaups and Cebeci method must be corrected because of a possibility of existence of remarkable pressure gradient in the radial direction in polar coordinate system. Therefore, JAXA applied NS analysis for computing flowfield and boundary layer characteristics of the NEXST-1 NLF wing.

If NS computation with all laminar condition is conducted, there might be a possibility of unexpected laminar separation. Therefore, in order to obtain a stable and reliable solution, an artificial transition needs to be forced after the predicted

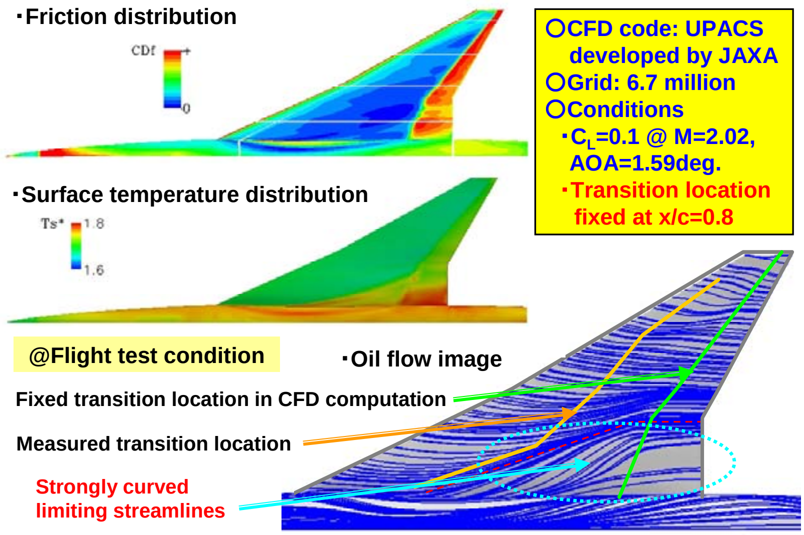

Figure D-20. NS result on the NEXST-1 wing at flight test condition with prescribed transition location $(x/c)_{TR.}$=0.8

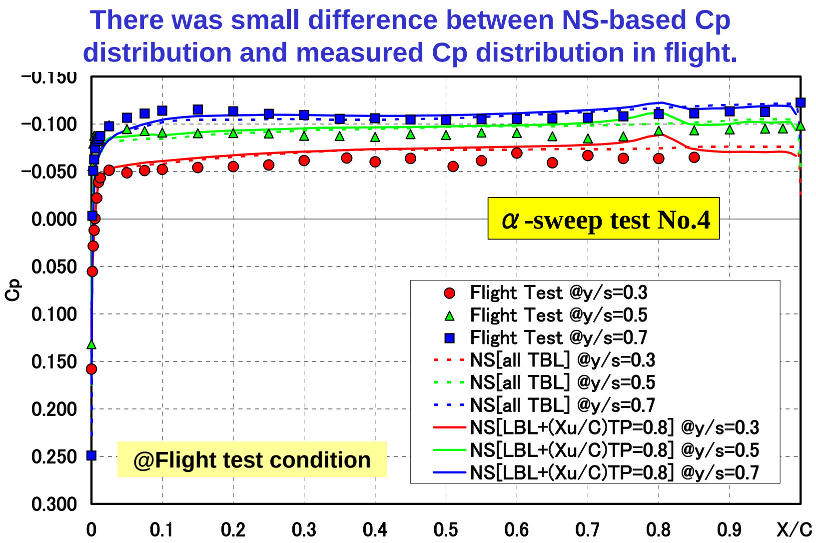

Figure D-21. Comparison of Cp distributions on the NEXST-1 wing at flight test condition

transition location. And JAXA tried to coerce the artificial transition at x/c=0.8 position. Figure D-20 shows results of NS-based flowfield.

Figure D-21 shows pressure distributions at representative spanwise stations, comparing NS results with measured data in flight test. The NS results include the numerical results computed at partially laminar condition (LBL) and all turbulent condition (TBL). Although a slight difference between NS-based and measured pressure distributions was found, JAXA judged that the difference had little influence on transition analysis because of the small amount of the difference.

In order to investigate behavior of laminar boundary layer velocity profiles in detail, first of all, three coordinates were defined as shown in Figures D-22 and D-23. Figure D-24 shows pressure distributions at representative spanwise stations again, including pressure distributions extremely near the spanwise stations. Figure D-25 shows pressure gradient at y/s=0.3 station in the radial direction using those pressure distributions. It was found that conical flow approximation was not valid. Therefore, the Kaups and Cebeci method

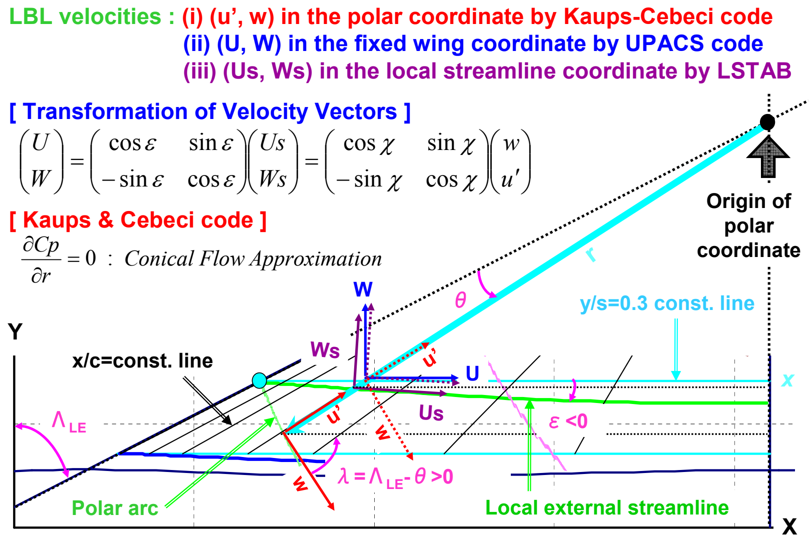

Figure D-22. Definition of each coordinate (part I)

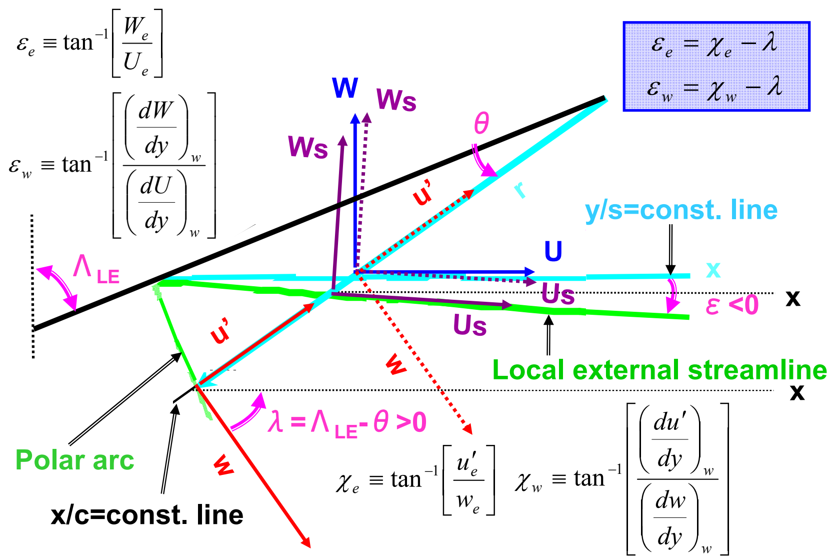

Figure D-23. Definition of each coordinate (part II)

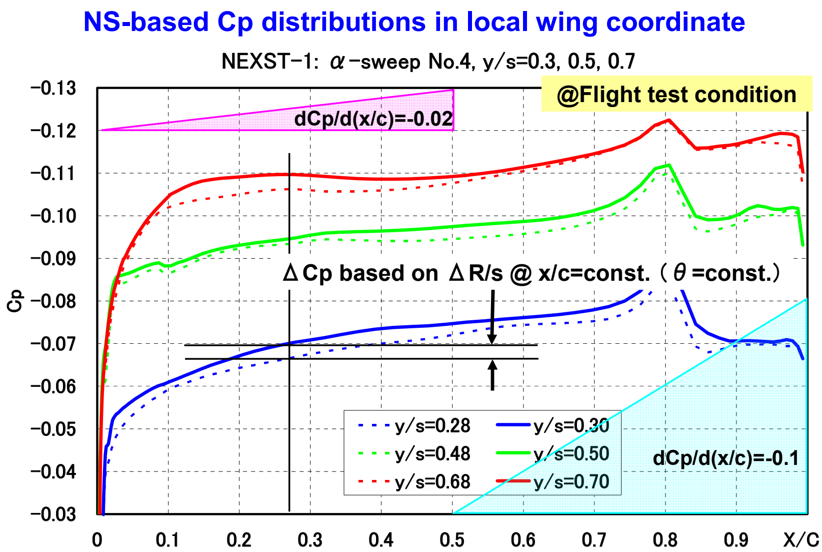

Figure D-24. Pressure distributions on the NEXST-1 wing at flight test condition

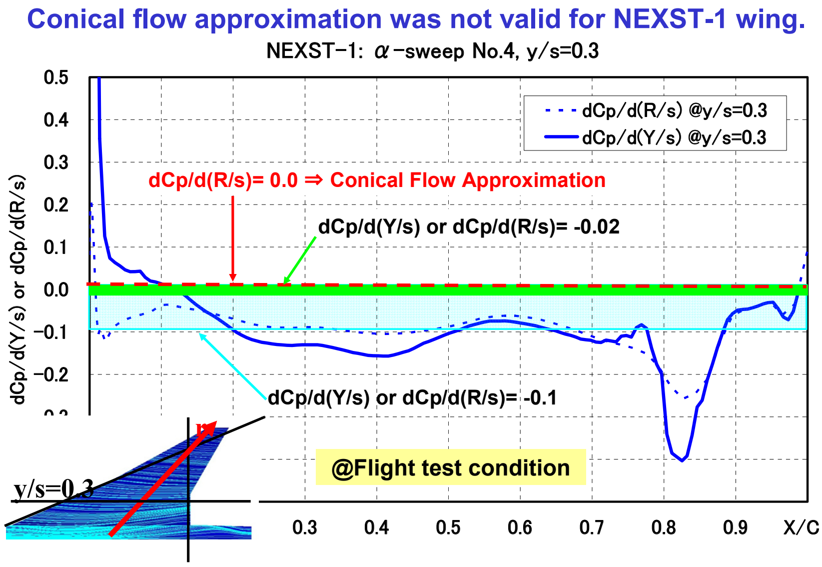

Figure D-25. Spanwise pressure gradient distributions on the NEXST-1 wing at flight test condition

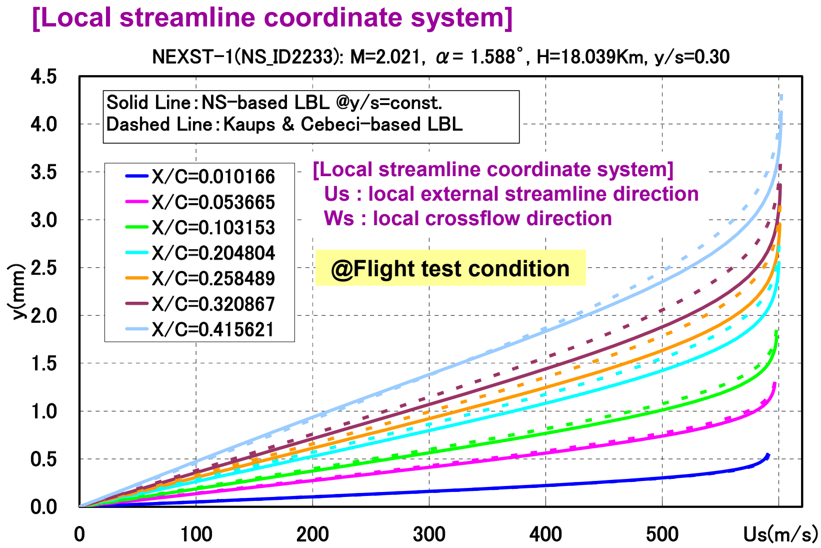

Figure D-26. Streamwise velocity profiles on the NEXST-1 wing at flight test condition

was not applied for detailed transition analysis on the NEXST-1 wing.

Figures D-26 and D-27 show computed boundary layer velocity profiles at several streamwise locations and y/c=0.3 spanwise station. Figure D-27 clearly indicates that the Kaups and Cebeci method does not estimate true feature on crossflow velocity profiles qualitatively, compared with the NS-based solutions. However, there are small differences in the boundary layer thickness distributions as shown in Figure D-28.

Figures D-29 and D-30 show eigenvalue distributions for amplification rate (α_i) and propagation direction (Ψ) at y/s=0.3 spanwise station. Figure D-31 shows N factors for different frequencies. Figure D-32 shows the envelopes of N factor curves, compared with the result based on the Kaups and Cebeci method.

Table D-1 shows a summary of transition analysis cases A~E on the NEXST-1 wing at flight test condition conducted by JAXA.

Figures D-33 to D-35 show computed N contours at the Cases C, D, and E described in Table D-1,

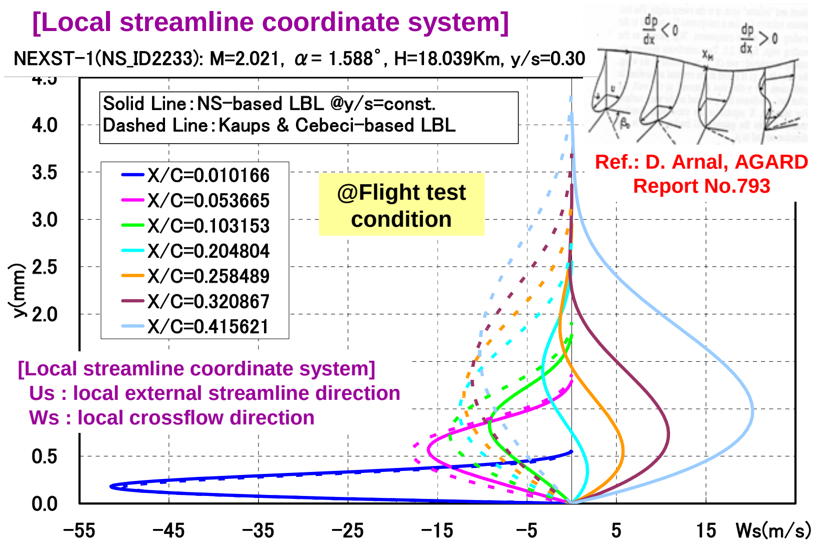

Figure D-27. Crossflow velocity profiles on the NEXST-1 wing at flight test condition

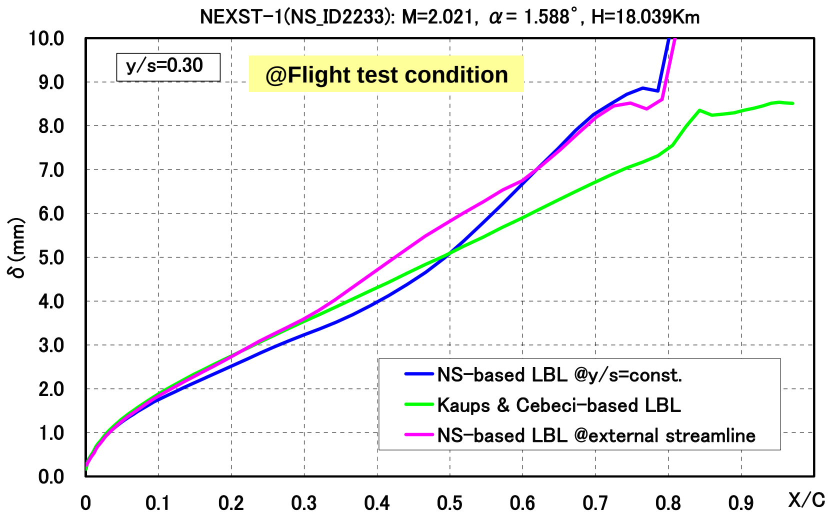

Figure D-28. Estimated boundary layer thickness on the NEXST-1 wing at flight test condition

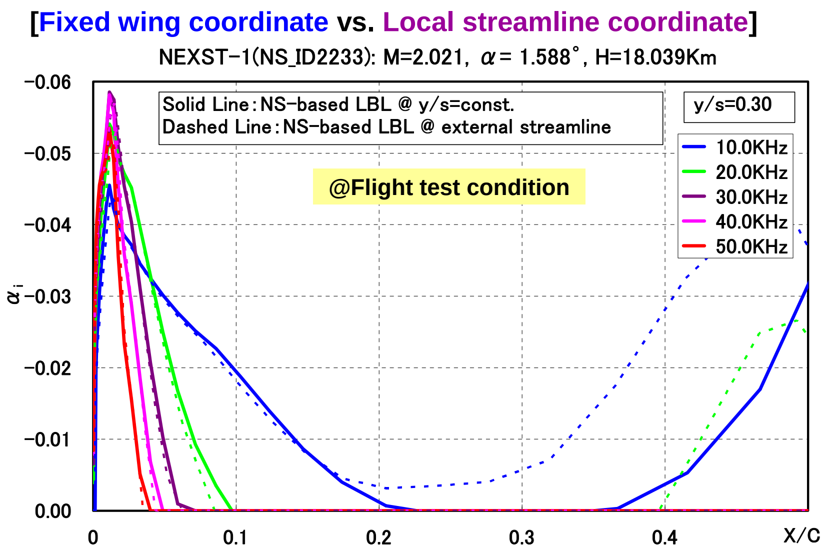

Figure D-29. Amplification rates (α_i) distributions on the NEXST-1 wing at flight test condition

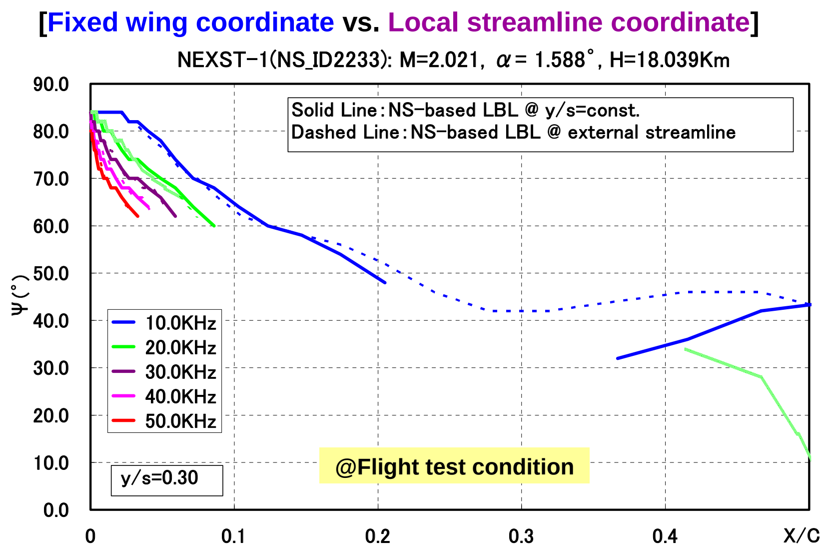

Figure D-30. Propagation direction angle (ψ) distributions on the NEXST-1 wing at flight test condition

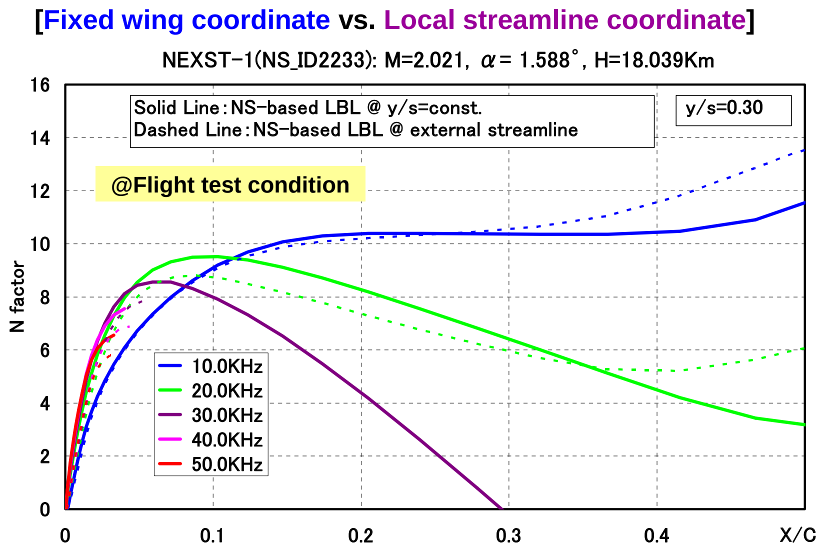

Figure D-31. N factor distributions on the NEXST-1 wing at flight test condition

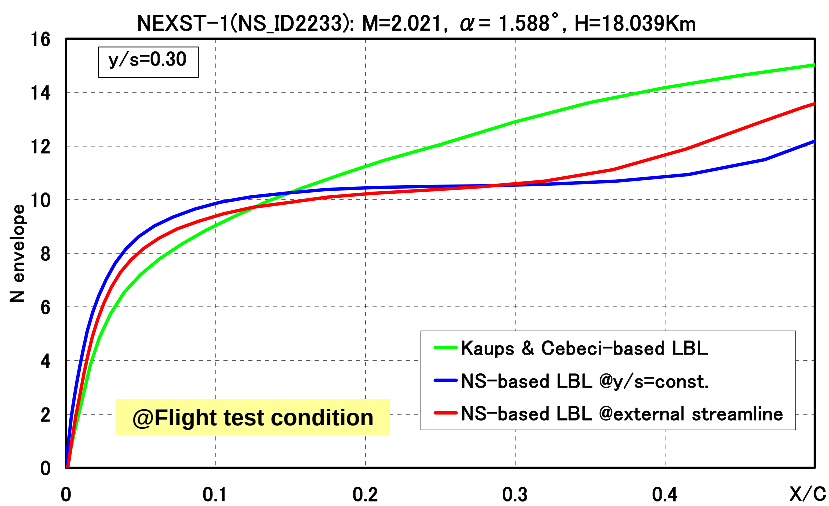

Figure D-32. $N_{envelope}$ distributions on the NEXST-1 wing at flight test condition comparing with the flight test data. In contrast with the Case C based on the Kaups and Cebeci method, so-called zigzag N patterns were obtained in the Case D and E.

In order to investigate an origin of the zigzag N pattern, each envelope curve of the N factor was focused at the Case D and summarized in Figures D-36 to D-38. Figure D-36 shows several envelopes of N factors at inner wing region. Almost flat distributions from x/c=0.1 to 0.4 were found. This implies a possibility of zigzag N pattern by specifying a certain transition N value. On the other hand, since Figures D-37 and D-38 show that several envelope curves have non-flat distributions, no zigzag N pattern is almost appeared. A mechanism of appearance of the zigzag N pattern is schematically demonstrated in Figure D-39. However, more detailed analysis is necessary to understand transition analysis on the NEXST-1 wing in comparing with the flight test data.

Finally, Figures D-40(a) ~ D-40(c) show comparisons of stability analysis results calculated using the fixed β method between ONERA and JAXA. The fixed β method gives smaller N values than the envelope method as demonstrated when compared with the Figures 40 (a) ~ 40(c). Although ONERA

Table D-1. Summary of new transition analysis cases

NEXST-1 wing @Flight test condition

・AOA-sweep No.4 (C_L=0.1 @ M=2.02, AOA=1.59deg. Rec=14.0 million)

Case	Flowfiled Computation				Transition Analysis	
	Cp			LBL	eN (LSTAB code)	
	method	transition loation	Cp position	method	Integral path	Integral Method
A	Flight Data	FLT@y/s	y/s=const.	Kaups & Cebeci	external streamline	analytical formulation
B	CFD(NS)	All Turbulent	y/s=const.	Kaups & Cebeci	external streamline	analytical formulation
C	CFD(NS)	$(x/c)_{TR}$=0.8	y/s=const.	Kaups & Cebeci	external streamline	analytical formulation
D	CFD(NS)	$(x/c)_{TR}$=0.8	y/s=const.	CFD(NS) results	external streamline	analytical formulation
E	CFD(NS)	$(x/c)_{TR}$=0.8	external streamline	CFD(NS) results	external streamline	numerical integration

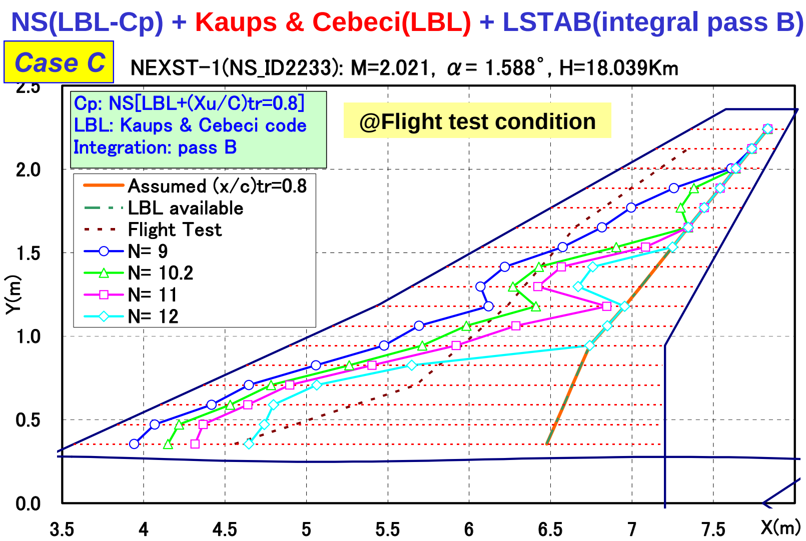

Figure D-33. N contours of "Analysis Case C" on the NEXST-1 wing at flight test condition

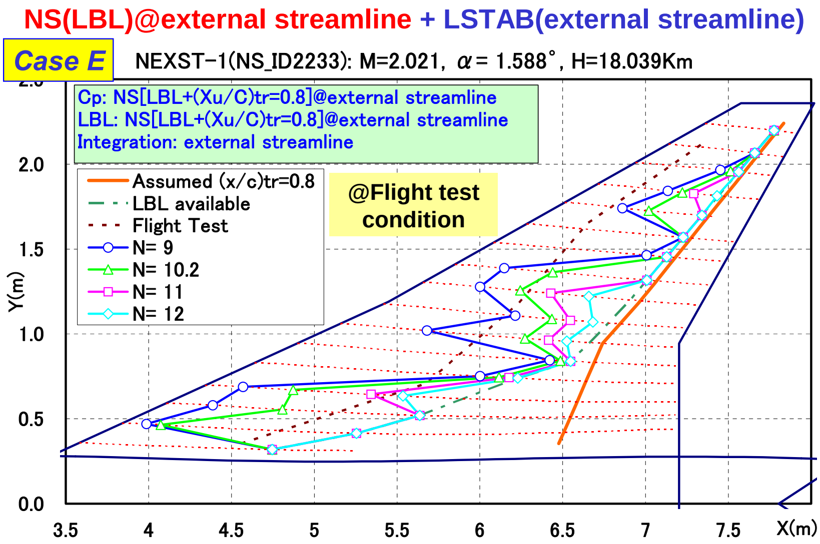

Figure D-34. N contours of "Analysis Case E" on the NEXST-1 wing at flight test condition

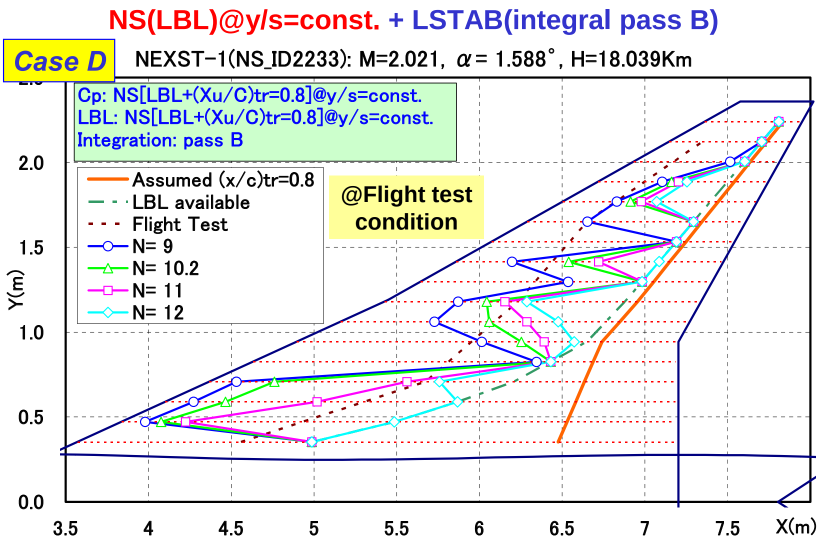

Figure D-35. N contours of "Analysis Case D" on the NEXST-1 wing at flight test condition

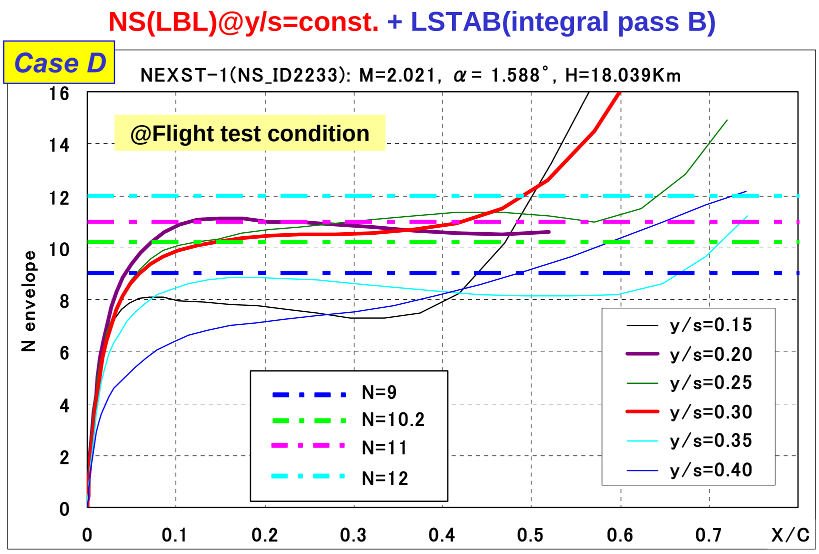

Figure D-36. $N_{envelope}$ distribution on the inner wing of the NEXST-1 airplane at flight test condition

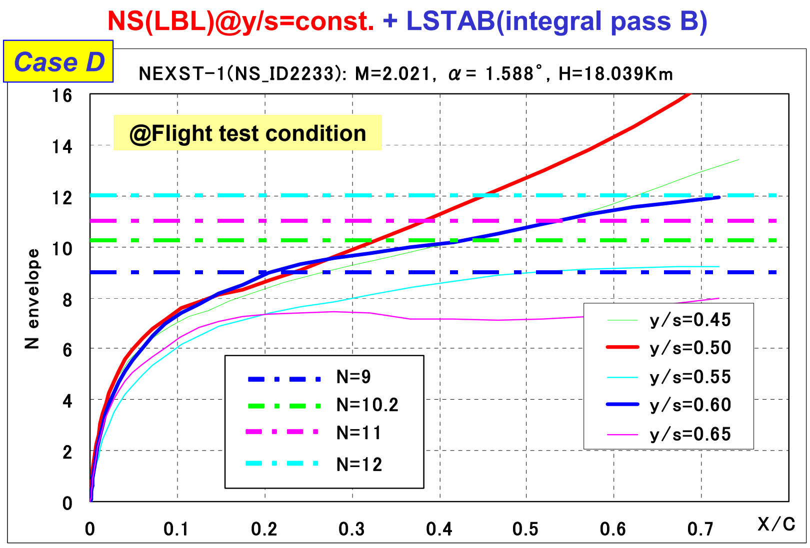

Figure D-37. $N_{envelope}$ distribution on the mid-wing of the NEXST-1 airplane at flight test condition

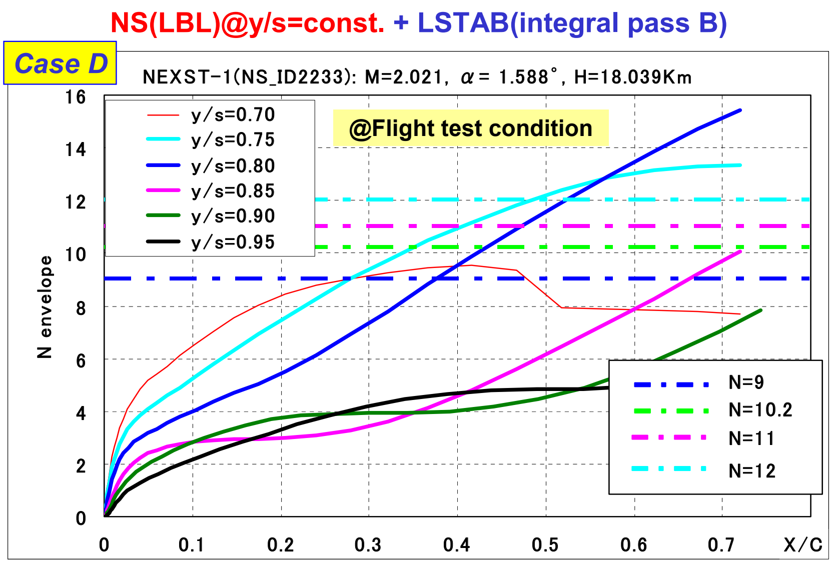

Figure D-38. $N_{envelope}$ distribution on the outer wing of the NEXST-1 airplane at flight test condition

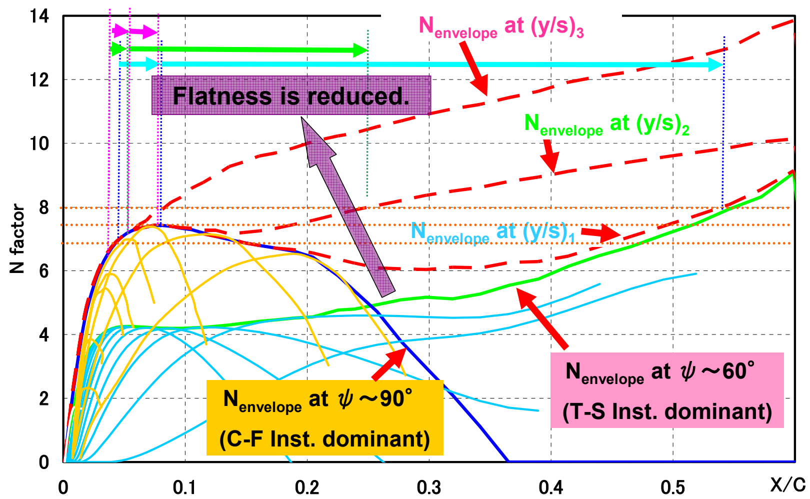

Figure D-39. An illustration of cause of "zigzag" N pattern proposes that the fixed β method is more effective to understand physics of transition mechanism, namely to separate the most instability mode, any detailed consideration has not been performed yet. However, the present good agreement between ONERA's and JAXA's results indicates both laboratories have a potential to analyze such physical mechanism.

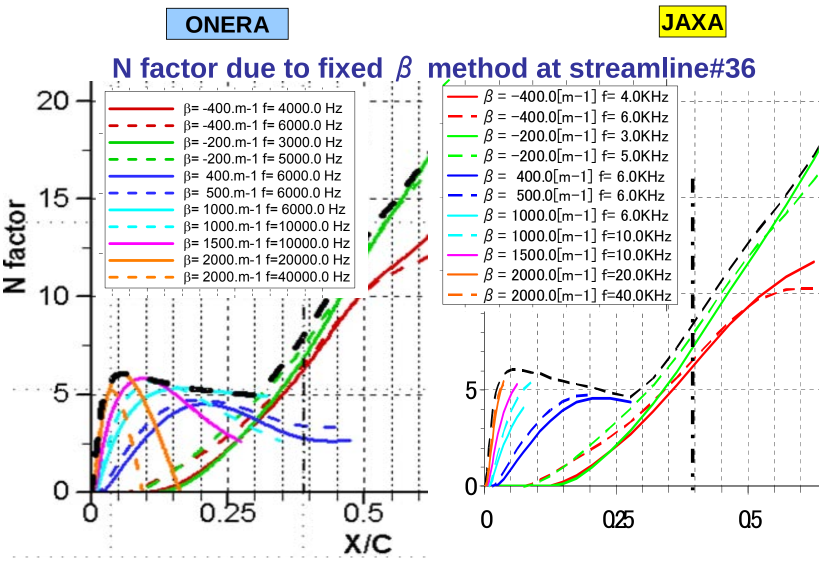

(a) Streamline #36

Figure D-40. Comparison of stability results based on fixed β model

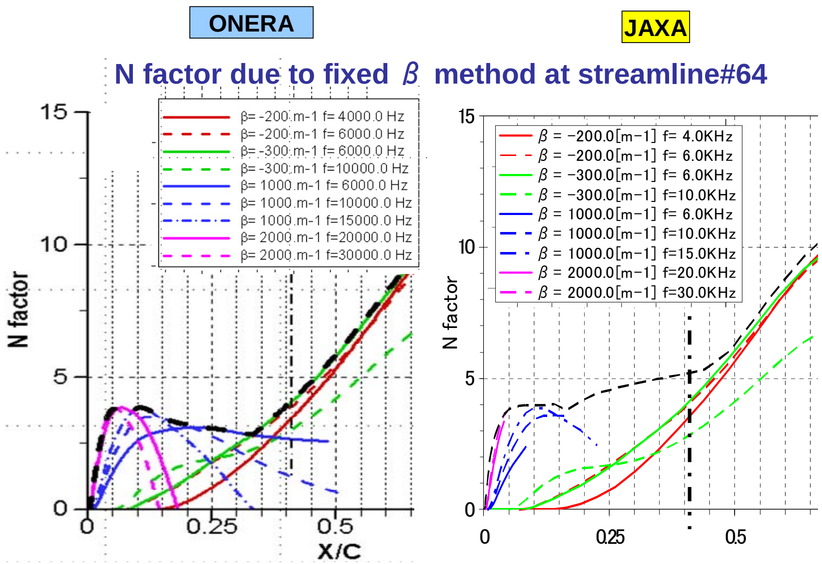

(b) Streamline #64

Figure D-40. Comparison of stability results based on fixed β model

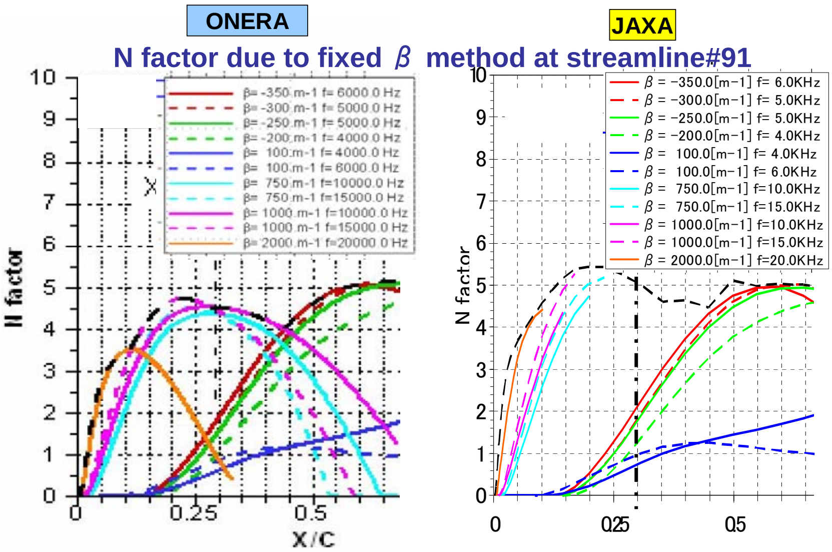

(c) Streamline #91

Figure D-40. Comparison of stability results based on fixed β model